Alma Mater Studiorum – Università di Bologna

DOTTORATO DI RICERCA IN

SCIENZE DELLA TERRA, DELLA VITA E DELL'AMBIENTE

Ciclo XXXII

Settore Concorsuale: 04/A2

Settore Scientifico Disciplinare: GEO/02

DEFORMED STRATIGRAPHIC MARKERS IN THE SHALLOW SUBSURFACE OF THE PO PLAIN: POSSIBLE INDICATORS OF RECENT TECTONIC ACTIVITY?

Presentata da: **Bianca Costagli**

Coordinatore Dottorato

Giulio Viola

Supervisore

Alessandro Amorosi

Co-Supervisore

Luigi Bruno

Esame finale anno 2020

Summary

ABSTRACT 3

1. INTRODUCTION 5

2. THE PO BASIN: GEOLOGICAL SETTING 12

2.1 Tectonic setting 12

2.2 Stratigraphic architecture 15

3. DATABASE AND METHODS 22

3.1 Geologic database 23

3.2 Seismic analysis 29

3.3 Geochemical analysis 29

3.4 Geotechnical analysis 31

3.5 Petrel data processing 33

4. MANUSCRIPTS 35

4.1 Paper 1 35

4.2 Paper 2 63

4.3 Paper 3 83

4.4 Paper 4 101

5. CONCLUSIONS 119

REFERENCES 125

ABSTRACT

The Po Basin is a wedge-top basin developed atop a system of blind thrusts that represent the most external structures of the Apenninic chain. These structures were originally considered to be inactive. Geomorphological and geophysical studies have supported the hypothesis of a recent activation of several blind thrusts. This hypothesis has been confirmed for some areas (e.g., the "Mirandola anticline") by two M=6 earthquakes that struck Emilia-Romagna in 2012.

This research program is an attempt to use Late Pleistocene and Holocene stratigraphic markers as possible indicators of recent tectonic activity. Through accurate identification and high-resolution mapping of deformed stratigraphic markers, the aim of the research is to understand the extent to which tectonics may influence Quaternary stratigraphy on short (millennial to centennial) temporal scales and explore the possible use of high-resolution Quaternary stratigraphy to help predict the likely spatial distribution of future damaging earthquakes in the study area.

The detailed chronostratigraphic framework reconstructed in the study area was built through distinct highly effective stratigraphic markers of different type. These markers were accurately selected on the basis of their sedimentological characteristics, and were typified for their fossil content.

Distinct types of stratigraphic markers include:

(i) Paleosols. Pedogenically modified horizons on flat floodplain surfaces represent key markers for high-resolution stratigraphic analysis, because of their high correlation potential. Two weakly developed paleosols were mapped in the Po Plain: the paleosol formed at the onset of the Last Glacial Maximum (29-24 ky) and the paleosol related to the Yonger Dryas cooling event (12.9-11.7 ky).

(ii) Peat layers (swamp deposits) and lagoonal horizons (9-6 ky). Brackish deposits, in particular, are the most reliable stratigraphic markers, as they represent horizontal layers at time of deposition.

(iii) Fossiliferous sand body that extends continuously in S-N direction, parallel to the shoreline. A wedge-shaped sediment body formed in response to coastal progradation, during the MIS 5e highstand was mapped in the Po Plain. The notable landward migration of the shoreline during the Last Interglacial makes this sand body as a stratigraphic marker of regional significance.

Geological cross-sections across key stratigraphic areas and 3D mapping outline remarkable deformation of late Quaternary deposits above the main buried tectonic structures, with dislocations

of several meters. To this purpose, we reconstructed in detail the deep and shallow stratigraphy of a wide portion of the Po coastal plain through seismic analysis and sediment-core correlation.

In this work we demonstrate that areas of maximum deformation of Late Pleistocene-Middle Holocene stratigraphic markers are strikingly coincident with the epicenters of historic and instrumental seismicity dating back to the last five centuries and that the offset of marker horizons across the Argenta-Longastrino ridge coincides with the location of major thrust fronts inferred indipendently from prior geophysical investigations.

In this respect, the deformation of stratigraphic markers is interpreted to reflect the combined effect of recent tectonic activity along the buried thrust fronts and differential subsidence due to sediment compaction.

This research shows that the accurate sedimentological and stratigraphic analysis of shallow buried depositional systems used in conjunction with conventional seismic stratigraphy can help assess a decipherable record of near-surface tectonic deformation.

1. INTRODUCTION

Over the past decades, the scientific community has developed an increasing interest towards facies characterization and reconstruction of stratigraphic architecture of late Quaternary successions (Demarest and Kraft, 1987; Nummedal and Swift, 1987; Saito, 1994; Morton and Suter, 1996; Marcucci, 2000; Bender et al., 2005). These studies have mostly focused on the sedimentary evolution in response to relative sea-level change.

Late Quaternary successions provide a fundamental basis for high-resolution sequence statigraphic analysis, for a number of reasons: eustatic fluctuations for the Late Pleistocene-Holocene period are well established; the influence of other factors on sedimentation is more easily detected than in older successions; radiocarbon dating, although restricted to the last 40 ky, enables the construction of a reliable chronostratigraphic framework; and diagnostic tests (geochemical and geotechnical) may further characterize the successions. Quaternary systems, especially in close temporal proximity to the Holocene, can be used to develop reliable predictive models in ancient rocks (Blum et al., 2013).

Since the late Eighties, the Geological Survey of Emilia-Romagna carried out an extensive interdisciplinary research attempt, aimed at understanding these complex successions, within the framework of the Geological Mapping Protocol of Italy, at the 1:50,000 scale. The research integrates outcrop and subsurface studies, both in the northern Apennines foothills and in the adjacent subsurface, in order to reconstruct the Po Basin depositional history during Pliocene and Quaternary times.

The Po Plain, a 46,000 km^2 wide alluvial plain of northern Italy, represents one of the most intensively investigated late Quaternary successions. The stratigraphic interpretation of the depositional units cropping out at the Po Basin margin is based upon recent field work and previously published papers (Ricci Lucchi et al., 1981, 1982; Gasperi et al., 1986; Vai and Castellarin, 1992; Pini, 1999).

Subsurface research at the basin scale has been carried out for hydrocarbon and water research (AGIP Mineraria, 1959; AGIP, 1977; Aquater-ENEL, 1981), for structural analysis (Castellarin et al., 1985; Dondi and D'Andrea, 1986; Pieri and Groppi, 1975; Ori, 1993; Regione Emilia-Romagna and ENI-AGIP, 1998; Amorosi et al., 1999b; Regione Lombardia and ENI Divisione AGIP, 2002; Amorosi, 2008), and for stratigraphic and sedimentological investigations (Amorosi et al., 1996; 1999a; 2003; 2008a; 2008b; 2014; 2015; 2017a; 2017b; 2019; Amorosi and Colalongo, 2005; Campo et al., 2016; Bruno et al., 2017a; b; 2019).

These studies include the analysis of 30,000 km of seismic reflection profiles provided by ENI-AGIP, along with the sedimentological-stratigraphic interpretation of over 11,000 km of continuously cored boreholes, and logging measurements (electric logs, spontaneous potential, and, where available, sonic logs) from approximately 600 boreholes.

Few delta plains worldwide have the same wide availability of data as the Po Plain. These areas include: (i) Mississipi Delta (Törnqvist et al., 2006, 2008; Chamberlain et al., 2018); (ii) Mekong Delta (Proske et al., 2011; Hoang, et al., 2016; Tjallingii et al., 2010; Tamura et al., 2009; Tanabe at al., 2003, 2012; Zoccarato et al., 2018); (iii) Ebro Delta (Somoza et al., 1998); and Changjiang (Yangtze) delta (Hori et al., 2002). The Rhine-Meuse system shares many similarities with the Po Plain: a detailed knowledge of the Holocene stratigraphy has been achieved by the University of Utrecht over the last decades (Berendsen and Stouthamer, 2000; Cohen et al., 2002; 2003; Hijma et al., 2009; Stouthamer et al. 2011), along with recent advances in the quantification of peat distribution and compaction (van Asselen et al., 2009; 2018; Koster et al., 2018a).

In Italy, the Tevere delta plain has a considerable data set with an abundance of core data, seismic sections an radiocarbon dates (Bellotti et al., 1994; 1995; Milli et al., 2013, 2016 with references therein).

The Po Plain–Adriatic Sea system, within the Alpine–Apennine foreland basin, is a peculiar setting, influenced by high and laterally variable subsidence and sediment supply rates under rapid high-magnitude relative sea-level change.

A high-resolution research has been conducted since the Nineties, both offshore (Trincardi et al., 1991; 1994; 1996; 2004; Correggiari et al., 1992; 2001; 2005a; b; Cattaneo and Trincardi, 1999; Trincardi and Correggiari, 2000; Roveri et al., 2001; Ridente and Trincardi, 2002; 2005; 2006; Cattaneo et al., 2003; 2007; Ridente et al., 2008; 2009; Maselli et al., 2010; 2011; Maselli and Trincardi, 2013; Pellegrini et al., 2015, 2016, 2017, 2018 and onshore (Amorosi et al., 1999a; b; 2003; 204; 2005; 2008a; b; 2014; 2017a; b; 2019; Scarponi and Kowalewski, 2004; Scarponi et al., 2013; Bruno et al.m 2017a; b; Campo et al., 2017)

The integration of seismic profiles and cored boreholes with geochemical (Amorosi, 2012; Amorosi et al., 2019), mineralogical (Amorosi et al., 2002), petrographic (Marchesini et al., 2000), paleontological (Amorosi et al., 1999; 2003; 2004; Fiorini, 2004), and pollen (Amorosi et al., 2004; 2008; Amorosi, 2008) analyses has led to the detailed reconstruction of the Po Basin stratigraphic architecture.

The Po Plain–Adriatic Sea system, thus, represents a uniquely suited natural laboratory, where complementary offshore and onshore research provides a modern analog of source-to-sink analysis, with remarkable implications for hydrocarbon exploration. It represents one of the most

intensively investigated late Quaternary successions where paleoenvironmental evolution has been tracked for the first time from the fluvial to deep-marine realms, over 1000 km in length (Amorosi et al., 2016b).

Dynamics of Po Delta progradation have been outlined in detail and in basin systems with strongly heterogeneous compositional signatures. The combination of geochemistry and paleoecology helped to build a linkage between onshore research (Amorosi et al., 2017a) and offshore studies (Correggiari et al., 2005a; 2005b; Pellegrini et al., 2016; 2018). Stratigraphic correlations based on sediment provenance and paleoecological indicators may help to trace distinct delta lobes within homogeneous lithosomes, as a function of sedimental provenance (Amorosi et al., 2019).

The Po Plain is located in a tectonically active area that is experiencing crustal shortening due to the convergence between Africa and Eurasia (Serpelloni et al., 2007); due to a lack of geomorphological evidence of recent tectonic activity, the Po Plain has long been considered a low seismic-risk area.

Nevertheless, in May 2012, an earthquake sequence hit the central Po Plain (Anzidei et al., 2012; Govoni et al., 2014), including two mainshocks of Mw 6.1 (May 20, 02:03:53 UTC) and 6.0 (May 29, 07:00:03 UTC). After the 2012 events, a marked uplift of the ground (up to 17 cm) was measured around the epicentral area through DInSAR technique and high precision levelling (Bignami et al., 2012; Salvi et al., 2012; Caputo et al., 2015). Before the 2012 sequence, earthquakes of low-to-medium intensity have been recorded in the Po Plain (Fig. 1a) in 1234 (Mw 5.1, Ferrara), 1285 (Mw 5.1 Ferrara) 1346, 1411 (Mw 5.1 Ferrara) 1570-1574 (Mw 5.5 Ferrara), 1591 (Mw 5.1 Bagnacavallo), 1624 (Mw 5.4 Argenta), 1639 (Mw 5.3 Finale Emilia), 1688 (Mw 5.9 Bagnacavallo), 1796 (Mw 5.6 Molinella), 1909 (Mw 5.5 Molinella), 1963 (Mw 5.2 Bagnacavallo) and 1967 (Mw 5.4 Longastrino), with moderate to heavy damage (Macroseismic Intensity, IMCS > VII) (Iside Working Group, 2010; Rovida et al., 2011). The 2012 seismic events were generated by the most external thrusts of the Northern Apennines, which are buried beneath the southern Po Plain.

Recent stratigraphic studies have been carried out deliberately far from tectonically active areas, in order to assess sedimentary evolution in response to relative sea-level change. Following the 2012 Po Plain earthquakes, few studies focused on the possible use of stratigraphic criteria to assess the deformation of Quaternary strata. These works used paleosurfaces that were far from being horizontal at the time of formation (for example, paleosols and fluvial channel-belts).

By contrast, this project aims at understanding the extent to which tectonics may influence Quaternary stratigraphy on short (millennial to centennial) temporal scales analysing also the deformation of stratigraphic markers that approximate paleohorizontal surfaces (brackish horizons).

The use of soil horizons in mapping Quaternary deposits is a well-established methodology (Morrison, 1978). Quaternary pedostratigraphy, however, has focused predominantly on paleosols developed on fluvial terraces (Bestland, 1997; Ufnar, 2007; Eppes et al., 2008) or parts of loess-paleosol sequences (Kemp et al., 1995; Zhisheng and Porter, 1997; Berger et al., 2002), with the aim to reconstruct pedosedimentary processes, climate change, or landscape evolution (Mahaney et al., 1993; Feng and Wang, 2005; Kemp et al., 2006; Schellenberger and Veit, 2006; Sheldon and Tabor, 2009).

Paleosols can be read as regional stratigraphic markers in alluvial plain deposits, where they represent a powerful tool to subdivide monotonous alluvial clay-rich succession (Bown and Kraus, 1981; 1987; Wright and Marriott, 1993; Kraus, 1999; Trendell et al., 2012). Paleosols have been commonly used as a mapping tool in pre-Quaternary successions, but recent studies (Wallinga et al., 2004; Srivastava et al., 2010; Amorosi et al., 2014; 2016a; 2017; Tsatskin et al., 2015) have started considering the importance of Quaternary paleosols not only for pedostratigraphic analysis, but also as stratigraphic tools for correlating alluvial deposits.

Pedogenically modified horizons represent effective key markers for high-resolution stratigraphic analysis in continental sequence stratigraphy, because of their high correlation potential. The main limitation on their use is that they may have had a complex morphology at the time of their formation. Thus, only qualitative evaluation of their post-burial deformation is possible. Holocene peat/lagoonal horizons are, instead, much more reliable indicators of post-burial deformation, as they represent approximately horizontal surfaces (Törnqvist, 2008). The disadvantage of this type of markers is their relatively limited areal extent (Bruno et al., 2019). In specific areas of the Ferrara and Ravenna coastal plains, just above the culmination of the buried anticlines, all these stratigraphic markers appear to be significantly deformed.

The first part of this Ph.D. thesis focuses on an accurate reconstruction of the Late Pleistocene-Holocene stratigraphic architecture across a wide portion of the Po Plain, close to the Argenta and Longastrino areas. The stratigraphic analysis, based on thousands of cores/borehole data and hundreds of radiocarbon dates, uses distinct types of stratigraphic markers, including weakly developed paleosols, lagoon and peat horizons, tops of fluvial channel-belt sand bodies, marine flooding surfaces and their lateral equivalents. These markers were identified, traced and mapped in the subsurface for tens of kilometers.

In Paper 1, we show that high-resolution Quaternary stratigraphy used in conjunction with conventional seismic stratigraphy can represent an interesting technique to assess a comprehensible record of near-surface tectonic deformation, in areas where such markers can hardly be imaged in seismic lines due to the generally insufficient resolution at very shallow depths. Prominent stratigraphic markers were used from a 110-m-thick cored succession of the Argenta-Longastrino area to reconstruct a coherent, high-resolution record of Last Interglacial to Middle Holocene deformation supported by 102 radiocarbon dates.

Five deformed marker horizons, above the culmination of the buried Longastrino anticline, were traced through accurate high-resolution mapping: (i) a fossiliferous sand body associated to the isotope stage MIS5e (ii) the Late Pleistocene paleosol dated to the Marine Isotope Stage 3/2 transition (24-29 cal ky BP); (iii) the Pleistocene-Holocene paleosol dated around the Younger Dryas cold event, (11-13 cal ky BP,YD paleosol of Amorosi et al., 2017a; (iv) a lagoon horizon dated to 8.3-8.6 ky BP; and (v) a younger lagoon horizon dated to 5.6-6.2 ky BP.

In Paper 2, we provide for the first time a 3D picture of the stratigraphic deformation documented in detail in Paper 1, over an area of 1500 km^2. This paper is focused, in particular, on the accurate high-resolution mapping of three deformed stratigraphic markers, with the aim to demonstrate the relations between deformed stratigraphic markers and tectonic activity along the buried structures above the Ferrara Arc, with a particular focus on the Longastrino thrust front. The 3D-mapping, carried out using the software package Petrel 2014, was based on 506 stratigraphic data (core logs and cone penetration profiles), chronologically constrained by 140 radiocarbon dates. This part of the study aimed to identify and characterize from a geometric point of view paleosols and flooding surfaces into a chronologically constrained stratigraphic model. Specifically, the maps depict the spatial distribution of two weakly developed paleosols, dated to the Marine Isotope Stage 3/2 transition (24-29 cal ky BP) and the Younger Dryas cold event (11-13 cal ky BP), respectively, as well as a peat horizon dated to 6.1 cal kyr BP.

Our working hypothesis is that very recent deformation of Late Pleistocene and Holocene markers may have been driven by a combination of tectonic activity along the buried thrust fronts, and differential subsidence due to compaction of underlying sediments.

In order to estimate the tectonic component we analyzed unpublished seismic profiles from the Argenta-Longastrino area to investigate the seismic stratigraphy below the areas of maximum deformation highlighted in this study. The tectonic component by removing the isostatic effects of the sediment load, was estimated adopting the Airy backstripping technique, through the freely available Backstrip software from Hunt Mountain Software.

In order to assess the contribution of sediment compaction to natural subsidence, in Paper 3, a finite-element 1D decompaction model and geotechnical analysis were applied to the Quaternary succession of the Argenta-Longastrino area. The mechanical characterization of the main lithofacies associations was based on oedometer tests bulk-density and loss on ignition tests carried out at Utrecht University, where I spent my three-months abroad period. Ten undisturbed samples recovered from the Argenta area were analyzed performing (i) dry bulk density analyses, (ii) oedometer tests in the laboratory, and (iii) calculating the amount of compaction based on CPTU-data (Koster et al., 2018a). Two laterally extensive lagoon horizons, from the Present and Last Interglacials, respectively, were used as reference marker beds: (i) a lagoon horizon dated to 5.6 ky B.P. which accumulated in a lower delta plain environment (~ 0 m above coeval sea level); (ii) the lagoon horizon broadly assigned to the MIS 5e highstand (120-116 cal ky BP). Stratal architecture down to 3 km through seismic analysis was reconstructed to discuss the relations between subsidence and structural setting.

The high-resolution stratigraphic framework that forms the basis of Papers 1-3 was constructed using an integrated approach that combines facies analysis, sediment composition and palaeontology. An example of this technique is shown in Paper 4, where the combination of bulk sediment geochemistry and benthic foraminiferal distribution was used to (i) delineate the boundaries of deltaic lobes with a homogeneous lithology, (ii) identify clinothem architecture, and (iii) generate a realistic model of 3D deltaic upbuilding and evolution. To this purpose, we used well-established geochemical markers, such as: (i) chromium, which has been used as a reliable indicator of Po River provenance from ophiolite successions of the Western Alps (Amorosi et al., 2002; Amorosi and Sammartino, 2018; Curzi et al., 2006; Greggio et al., 2018); and (ii) magnesium, which is an indicator of Eastern (and Central) Alps provenance from dolostones (Amorosi et al., 2002, 2007; Amorosi and Sammartino, 2018; Curzi et al., 2006; Greggio et al., 2018).

As regards my contribution to the papers, I analyzed a wide spectrum of stratigraphic and radiocarbon data, building geological cross-sections throughout the study area. I collected samples for radiocarbon dating and geochemical analysis. I analyzed the samples for texture, color, organic-matter content, plant remains and other noteworthy soil characteristics. I determined accurately the depositional facies, on the basis of lithology, accessory components, compositional attributes, and their macrofaunal content. As regards the geochemical analysis, I prepared samples for XRF analysis, loss on ignition tests and dry bulk density analyses. I carried out also geotechnical laboratory analysis at the University of Utrecht, in particular oedometer tests and I calculated the amount of compaction based on CPTU-data. I used the software Petrel to build a grid of

stratigraphic cross-sections and generate maps of deformed stratigraphic markers. I devoted several months to incorporate new data in the Petrel project and to trace surfaces to obtain a 3D stratigraphic scheme. Furthermore I analyzed unpublished seismic profiles from the Argenta-Longastrino area.

This three-year research project is the result of collaborative projects between the University of Bologna and:

- Geological, Seismic and Soil Survey of Regione Emilia-Romagna which made available its database with more than 2,000 data, including stratigraphic descriptions from continuously drilled cores and water-well logs, cone penetration tests, radiocarbon dating, pollen profiles and geotechnical data;
- KIGAM laboratory (Republic of Korea), where 128 radiocarbon dates from organic matter-rich samples and shells were carried out.
- Schlumberger, which supported the project providing the 3D software package Petrel.

2. THE PO BASIN: GEOLOGICAL SETTING

2.1 Tectonic setting

The Po Plain is one of the largest alluvial plains in Europe. Nowadays, it represents 15% of the Italian peninsula and a large part of Italian industrial activities are concentrated in this region. The overall basin stratigraphy has been thoroughly depicted in the last three decades through integrated seismic analysis (Pieri and Groppi, 1981), magnetostratigraphic studies (Muttoni et al., 2003; Scardia et al., 2006), and well-log interpretation (Ori, 1993). These studies, characterized by seismic profiles interpretation, aimed first at hydrocarbon research (AGIP Mineraria, 1959; AGIP, 1977) and then at depicting structural architecture and aquifer distribution in the Po Basin (Pieri and Groppi, 1975; Bartolini et al., 1982; Cremonini and Ricci Lucchi, 1982; Castellarin et al., 1985; Boccaletti et al., 1987; Doglioni, 1993; Regione Emilia-Romagna and ENI-AGIP, 1998; Amorosi et al., 1999; Regione Lombardia and ENI Divisione AGIP, 2002; Amorosi and Colalongo, 2005; Molinari et al., 2007; Amorosi, 2008).

The Po Plain is a ~48,000 km^2 wide alluvial plain bounded by the S-verging Alpine fold-and-thrust belt to the North, and by the N-NE verging Apennines to the South (Ricci Lucchi, 1986; Doglioni, 1993). These two mountain chains with opposite structural vergence represent distinct sources of sediment for the Po Basin.

With a total length of 652 km, the Po River is the longest river in Italy and it flows from the western Alps eastward into the Adriatic Sea (Fig. 1). It receives a number of transverse tributaries from both mountain chains. The Po River subdivides the Po Plain in two areas: to the North it is characterized by coarser and more sandy-rich deposits, while to the South a finer stratigraphic succession is present (Astori et al., 2002).

The Po Plain can be described as the superficial expression of the Po Basin, a rapidly subsiding foreland basin developed atop a system of blind thrusts (Pieri and Groppi, 1981).

The two mountain chains formed as a consequence of the convergence between Africa and Eurasia, which started in the Cretaceous (Carminati and Doglioni, 2012), with an ongoing motion of 3-8 mm/y (Serpelloni et al., 2007). The northern limit of the Po Basin is represented by the Southern Alps, with an extension of 700 km, related to the Apulian-Adriatic margin deformation (Kearey and Vine, 1990). The Southern Alps are a post-collisional mountain chain connected to the southward subduction of the European plate underneath the Adriatic plate (Vannoli et al., 2015). It is characterized by a S-verging fold-and-thrust belt, where non-metamorphosed Permian-Mesozoic

and Tertiary deposits have been folded in various phases from the Eocene to the Plio-Quaternary (Castellarin, 2001).

The southern margin of the Po Basin is represented by the buried Apenninic northern margin (AGIP, 1977; Boccaletti et al., 1985; Castellarin et al., 1992; Argnani et al., 2003). The Po Basin represents the most external structure of the Apenninic chain and the Apennines formation is related to the WSW-dipping subduction of the Adria plate beneath the European crust, which started after the post-collisional phase of the Alpine orogenesis (Vai and Martini, 2001). The Apennine thrust fronts, foredeep basins and extensional back arcs migrated progressively to the East as a consequence of the radial retreat of the subduction process (Doglioni et al., 1999), as confirmed by deep tomographic profiles (Castellarin et al., 1994).

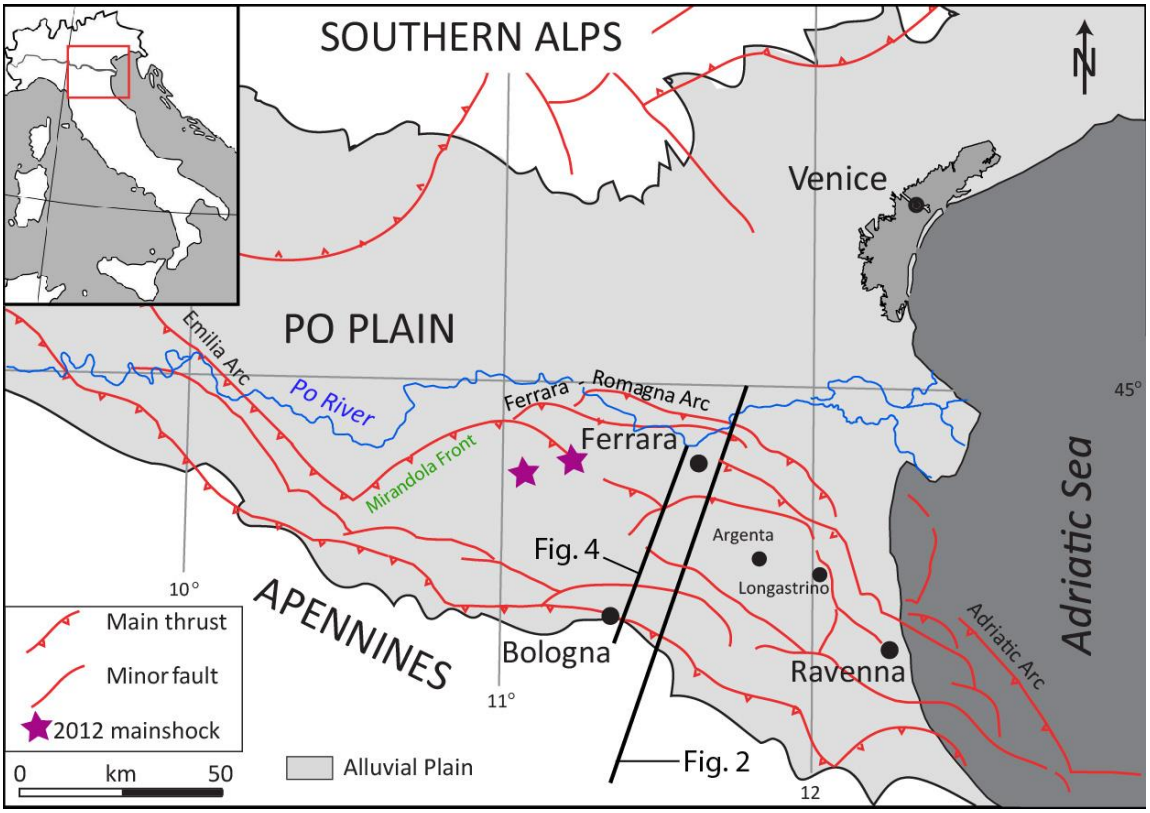

Fig. 1. Structural map of the Po Basin with indication of the buried Alpine and Apenninic structures. Modified from Burrato et al. (2003).

The N-verging fold-and-thrust belt Apenninic structure (Fig. 2) involves Mesozoic to Neogene deposits of Adria and the older basement (Picotti and Pazzaglia, 2008). Its buried structure beneath the Po Plain was clearly shown by Pieri and Groppi (1981). The buried Apennines thrust front is composed of north-verging thrusts arranged in four asymmetric arcs: from west to east, Monferrato Arc, Emilia Arc, Ferrara-Romagna Arc, and Adriatic Arc (Pieri and Groppi, 1981; Mazzoli et al., 2015). These arcs are characterized, in the western portion, by W-verging fold-and-

thrusts, while to the East they are composed by *en-echelon* folds and NE-verging high-angle reverse faults (Fig. 3; Costa, 2003).

The Ferrara-Romagna Arc, buried beneath the modern coastal plain, is in turn subdivided into three main fold-and-thrust systems: (i) the external Ferrara-Casaglia thrust front; and, in a more internal position, (ii) the Mirandola thrust system to the SW, and (iii) the Longastrino thrust front to the SE. The main phase of tectonic activity of these structures has been dated to the Late Miocene-Early Pliocene (Picotti et al., 2009), based on seismic data. In contrast, Late Pliocene-Holocene tectonic activity has been considered negligible.

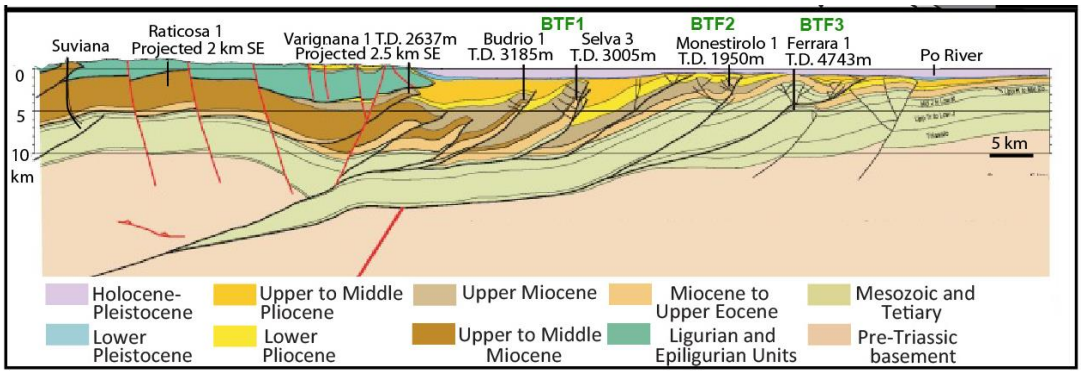

Fig. 2. Fold-and-thrust belt buried structures beneath the Po Plain (see Fig. 1 for location). Modified from Picotti and Pazzaglia (2008).

The Pliocene–Quaternary sedimentary fill of the Po Basin may exceed 7000 m in the thickest depocenters (Pieri and Groppi, 1981; Castellarin et al., 1985). The apparently non-deformed geometry of the buried structures firstly led to the wrong assumption that these folds and thrusts were inactive.

Geomorphological and geophysical studies (Burrato et al., 2003; Carminati and Vadacca, 2010; Picotti and Pazzaglia, 2008) have supported the hypothesis of a recent reactivation of the external thrusts (Ferrara arc and Mirandola anticline) that led to the M 6.0 2012 earthquake (Bonini et al., 2014; Caputo et al., 2012; Carannante et al.,2015; Chiarabba et al., 2014; Govoni et al., 2014). A marked uplift of the ground (up to 17 cm) was measured around the epicentral area of the 2012 events (maximum magnitude Mw ~ 6.1 on May 20; Anzidei et al., 2012; Carannante et al., 2015) through DInSAR technique and high-precision levelling (Bignami et al., 2012; Caputo et al., 2015; Salvi et al., 2012).

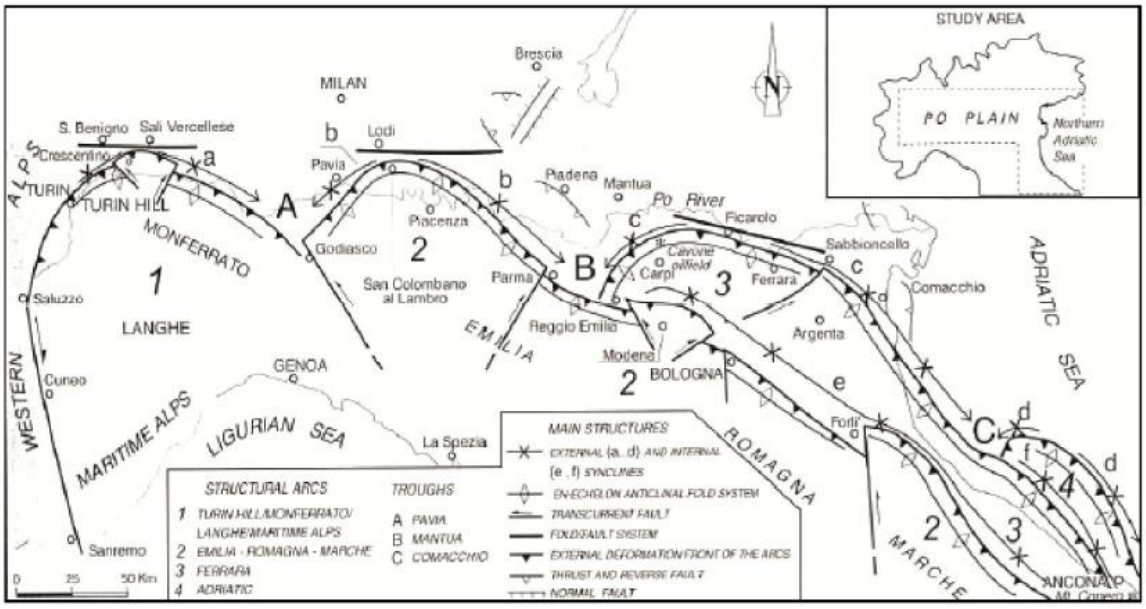

Fig. 3. The buried Apenninic outer fronts From Costa (2003).

Nevertheless, the entire Po Basin presents a natural component of subsidence related to the crustal flexure generated by the Apennines growth (Carminati et al., 2005), with long-term subsidence rates, controlled by tectonics and geodynamics, between 0.4 and 2.4 mm/y, where the highest values are registered in the modern Po Delta (Antonioli et al., 2009).

2.2 Stratigraphic architecture

The Pliocene-Quaternary sedimentary fill of the Po Basin has been thoroughly investigated through seismic data for hydrocarbon exploration (Pieri and Groppi, 1981) and stratigraphic cross-sections (Regione Emilia-Romagna and ENI-AGIP, 1998; Regione Lombardia and ENI-Divisione AGIP, 2002).

These studies revealed a progressive decrease in the degree of tectonic deformation from base to top (Fig. 4) and led to the subdivision of the basin fill into third-order depositional sequences separated by regional stratigraphic unconformities (Regione Emilia-Romagna and ENI-AGIP, 1998). Every stratigraphic units (UBSU), indicating a phase of significant basin geometry modification.

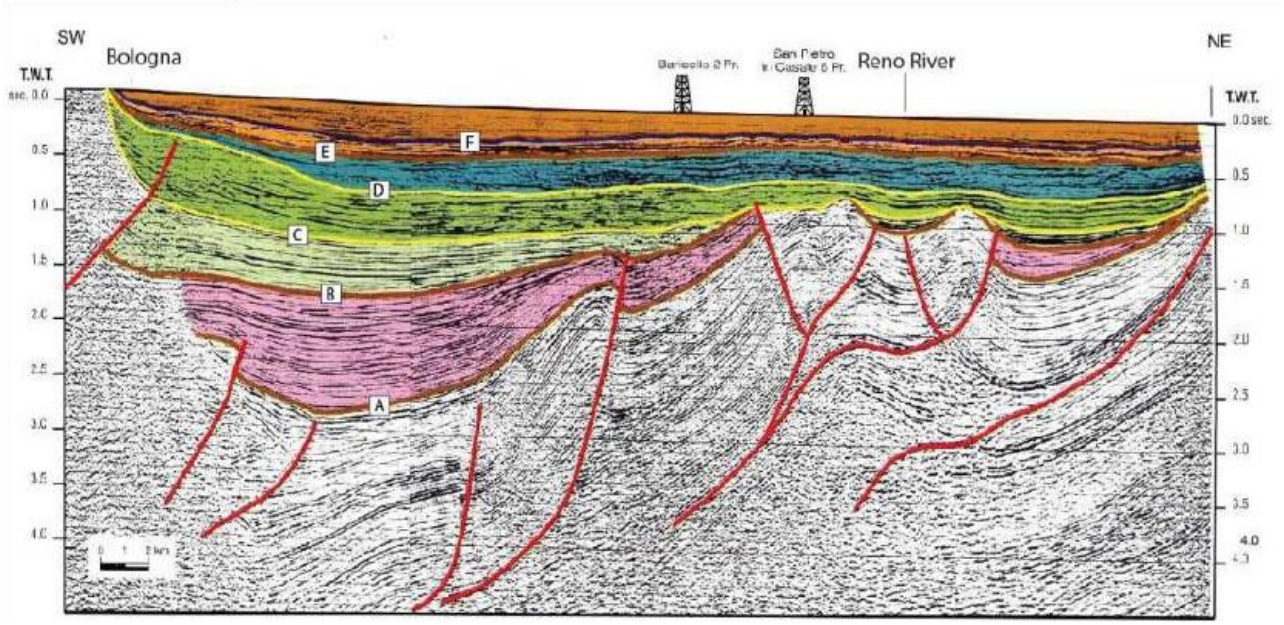

Fig. 4. Seismic profile interpretation between Bologna and Ferrara: Plio-Quaternary Po Basin fill subdivision into six depositional sequences. From Regione Emilia-Romagna & Eni-Agip (1998).

Four main Quaternary unconformities (Fig. 5) were used for the stratigraphic subdivision of the Po Basin succession in depositional sequences, representing important phases in the basin evolution history:

- 1.6 Ma BP unconformity, linked to a regional tectonic uplifting event in the southern part of the Po Basin, which resulted in the shifting of sedimentation towards the basin center;
- 1.24 Ma BP unconformity (green line in Fig. 5), mainly caused by tectonic activity;
- 0.87 Ma BP unconformity surface (red line in Fig. 5, the "R Surface" of Muttoni et al., 2003, coinciding with the E surface of Fig. 4). It is linked to the first great Pleistocene alpine glaciation. According to Muttoni et al. (2003) and Pini et al. (2004), the Red Surface does not appear to have tectonic origin, as it is not associated with angular unconformities in seismic profiles;
- 0.45 Ma BP unconformity (yellow line in Fig. 5, coinciding with the F surface of Fig. 4), probably caused by a minor uplifting event of the compressive Apenninic structures (Regione Lombardia and ENI-Divisione AGIP, 2002).

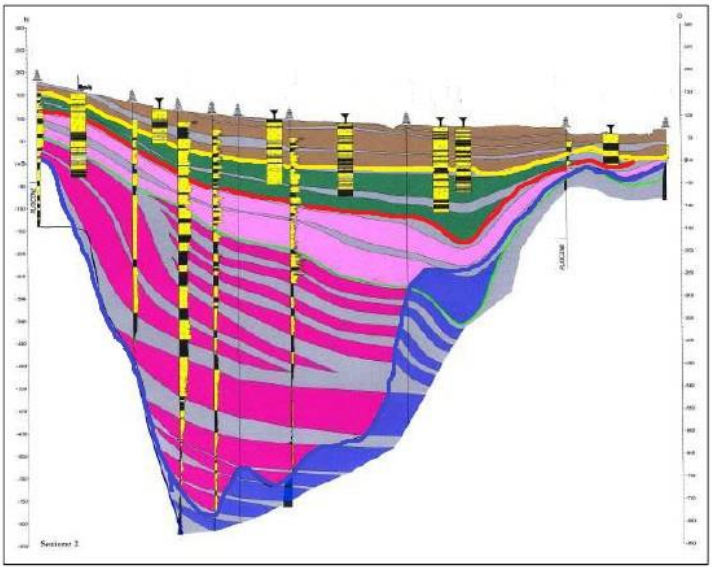

Fig. 5. Subsurface stratigraphy of the upper Po Basin fill. The yellow line corresponds to the "F" unconformity of Fig. 4, and the red one to the "E" unconformity. From Regione Lombardia and ENI-Divisione AGIP (2002).

The post-0.87 Ma Quaternary succession represents the Po Supersynthem of Amorosi et al. (2008) and includes deposits of middle-late Pleistocene to Holocene age (Fig. 6). The lower boundary of the Po Supersynthem (red line in Fig. 5, E surface of Fig. 4) has been seismically mapped throughout the basin (Regione Emilia-Romagna and ENI-AGIP, 1998; Regione Lombardia and Eni Divisione Agip, 2002).

Identification and lateral tracing within the Po Supersynthem of a lower-rank regional unconformity (0.45 Ma unconformity; yellow line in Fig. 5, F surface of Fig. 4) has led to its subdivision into two sub-units, namely Lower and Upper Po Synthems (Fig. 6). Each synthem has been partitioned into four sub-units (sub-synthems), which define geologically and hydraulically distinct aquifers, each one with a mean thickness of a few tens of meters. Thickness variations may be linked locally to tectonic activity.

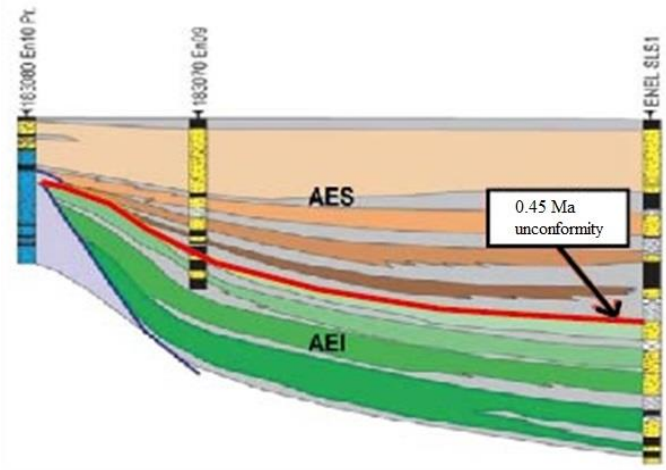

Fig. 6. Po Supersynthem subdivided into Lower and Upper Po Synthems by the ca. 0.45 Ma unconformity (modified from Regione Emilia-Romagna & ENI-AGIP, 1998).

The youngest sequence, the lower boundary of which has an estimated age of ca. 0.87 Ma, is subdivided into a number of lower rank (fourth-order), transgressive-regressive (T-R) cycles, produced by glacio-eustatic variations. These T-R cycles represent the sedimentary response to 4^{th}-order sea-level fluctuations linked to the Milankovitch-scale (100 ky) cyclicity. Each depositional cycle is characterized by a recurring alternation of coastal and alluvial deposits (Amorosi et al., 2004; 2005; 2008): close to the basin margin, at the Apennines foothills, and beneath the modern Po River, the stratigraphic architecture is dominated by gravelly amalgamated alluvial fan bodies, with lateral transition to alternating gravelly/sandy fluvial-channel and muddy overbank deposits (Ori, 1993; Amorosi et al., 1996). Distal areas are, instead, characterized by an alternation of alluvial plain and swamp deposits rich in organic matter with coastal deposits in transgressive-regressive (T-R) cycles (Amorosi, 2008).

The youngest T-R cycle has been extensively studied over the last decades (Rizzini, 1974; Bondesan et al., 1995; Amorosi et al., 1999a; 2003; 2008; 2017a; Bruno et al., 2017; 2019; Campo et al., 2017). This cycle shows a Holocene succession, a few meters thick, separated from the underlying Last Glacial Maximum alluvial deposits by a subaerial unconformity surface. The sequence-stratigraphic interpretation of the 4^{th}-order depositional sequences reflects the classic subdivision into systems tract:

- The lower unit is composed by a thick alluvial succession that accumulated between 125,000 and 20,000 years BP, during the long phase of sea-level drop, i.e. falling-stage systems tract (FSST), and the subsequent lowstand systems tract (LST). These systems tracts are characterized by channel incision and paleosol development in the interfluves;
- The overlying unit corresponds to the lower transgressive portion of the Holocene transgressive-regressive sequence, recording an increase in accommodation space and the landward migration of depositional environments, from purely marine to brackish and freshwater ones, as a result of rising sea-level (transgressive systems tract, TST). In the subsurface of modern coastal plains, early TST sedimentation is commonly lacking, generating an important hiatus that divides LST from the overlying TST, including the Pleistocene-Holocene boundary. The lower TST is commonly registered only within incised-valley fill (Posamentier and Allen, 1999);
- The upper unit records delta and strandplain progradation, which characterizes the following highstand systems tract (HST), when fluvial processes are intensified in response to the lowering of sea-level rise (Stanley and Warne, 1994).

During the long phase of sea-level fall and the subsequent lowstand phase, proximal areas are characterized by the deposition of thick, sand fluvial bodies with seaward migration of alluvial systems and an increase in erosion (Amorosi and Colalongo, 2005). The rapid sea-level rise and the following highstand are instead dominated by fine-grained alluvial sedimentation, representing the landward equivalent of transgressive-regressive coastal successions (Fig. 7).

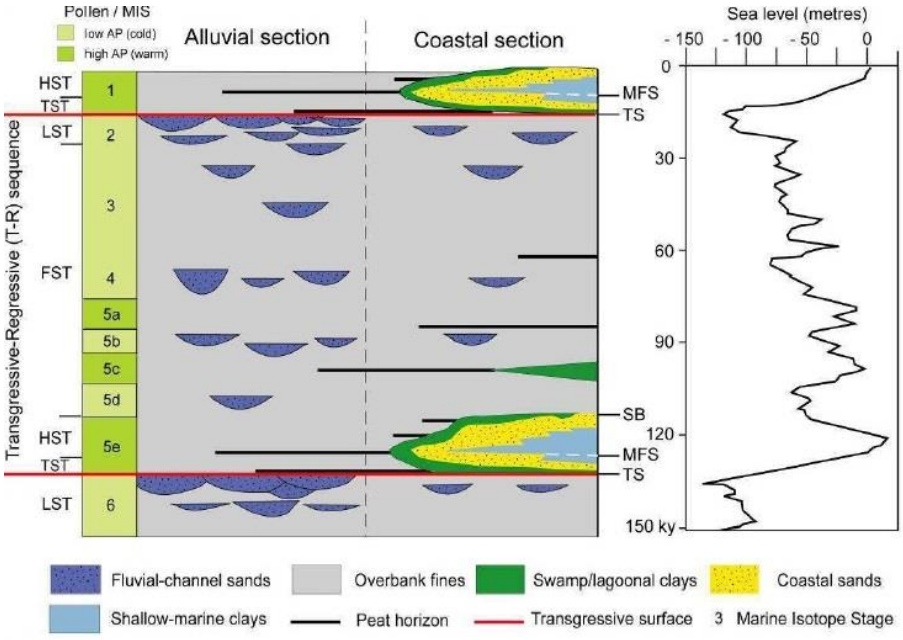

Fig. 7. Schematic stratigraphic representation of the post-125 ky Po Basin succession showing the relationships between climate change, stratigraphic architecture, sequence stratigraphic interpretation and sea-level change within T-R sequences. From Amorosi and Colalongo (2005)

T-R cycles are laterally persistent and bounded by transgressive surfaces (TS) that are physically traceable at the basin scale. Transgressive surfaces are directly traceable in coastal areas at the continental-coastal transition (Fig. 8), whereas in more proximal portions of the basin they are located at the top of laterally-extensive fluvial-channel bodies (Amorosi and Colalongo, 2005). Amorosi (2008) documented that transgressive surfaces are characterized by a peculiar pollen signal that marks the transition from glacial to interglacial periods. In relatively proximal positions, the lower portions of T-R cycles are characterized by thick floodplain sedimentary bodies with high concentration of *Quercus, Betula, Corylus, Tilia* and *Ulmus* pollen, and with low concentrations of *Pinus;* the first ones represent thermophilous taxa indicating the development of forests and suggesting that the lower parts of each T-R cycle accumulated at the onset of warm-temperature interglacial phases (Amorosi et al., 2004). Fluvial-channel sand bodies in the upper portion of the T-R cycles are instead characterized by high concentrations of *Pinus* and NAP (non-arboreal pollen), indicating their development under glacial conditions.

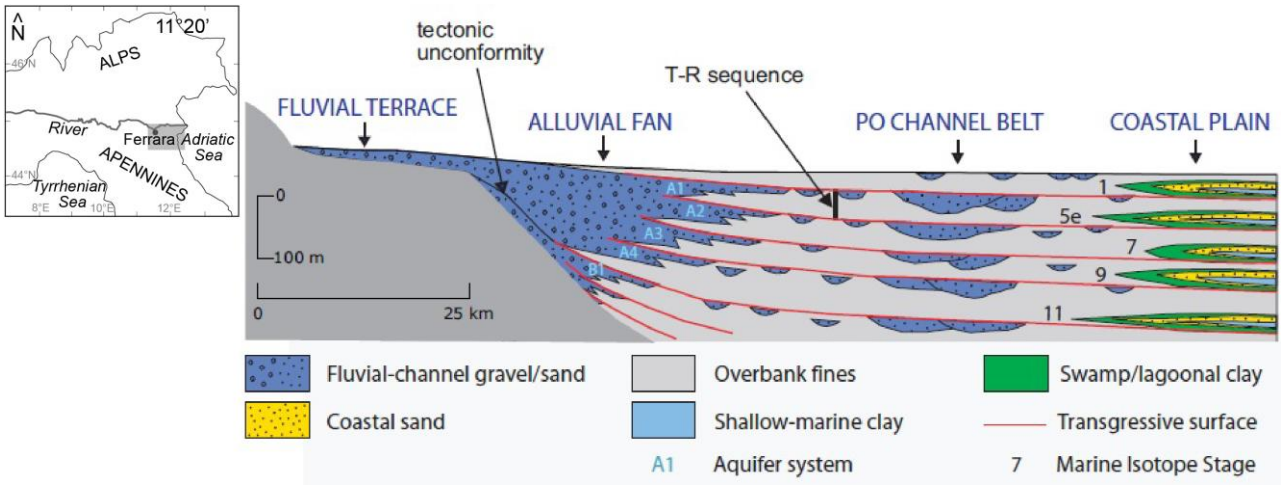

Fig. 8. Schematic cross-section from the Apennines to the Adriatic Sea, showing the basin-scale linkage between alluvial and coastal systems. From Amorosi (2008).

Depositional systems also show a sedimentary response at sub-Milankovitch (millennial) scales (Lowrie and Hamiter, 1995; Somoza et al., 1998; Amorosi et al., 2004; Amorosi et al., 2008; Amorosi et al., 2017a).

The Quaternary portion of the Po Basin fill is composed mainly of continental units (Regione Emilia Romagna, 1998; Amorosi et al., 2008a), and shallow-marine deposits occur only in the eastern Po Plain at distinct stratigraphic levels. Particularly, marine sediments dated to the Marine Isotope Stage (MIS) 5e with ESR (Electronic Spin Resonance) or based on pollen curves, have been encountered in cores at depth > 100 m (Amorosi et al., 1999; 2004; Ferranti et al., 2006). The post-MIS 5e stage of falling sea level is represented by an exceptionally expanded (~ 80 m) alluvial succession (Amorosi et al., 2004) composed of: (i) fluvial-channel sand bodies arranged in an aggradational stacking pattern (Amorosi et al., 2016a; Campo et al., 2017) and (ii) floodplain muds with vertically stacked paleosols (Amorosi et al., 2016a).

Pedogenically modified horizons represent regional stratigraphic markers in alluvial plain deposits, where they represent a powerful tool to subdivide monotonous alluvial clay-rich successions (Bown and Kraus, 1987; Wright and Marriott, 1993; Kraus, 1999; Trendell et al., 2012), effective key markers for high-resolution stratigraphic analysis in continental sequence stratigraphy.

Pedogenically modified horizons within thick floodplain deposits show a high correlation potential (Amorosi et al., 2015; 2017b; Morelli et al., 2017). In particular, two weakly developed paleosols exhibit the highest correlation potential: (1) the Last Glacial Maximum paleosol (LGM), assigned to the Marine Isotope Stage 3/2 transition and dated to 30-24 cal ky BP (onset of the Last

Glacial Maximum), and the Younger Dryas paleosol, dated to 12.9-11.7 cal ky BP (Fig. 9). This latter is a laterally extensive paleosol that marks the boundary between the Late Pleistocene and the Holocene successions (YD paleosol, Amorosi et al., 2016a, 2017b). Holocene deposits, up to 30 m thick, consist in their lower part of estuarine and lagoonal facies arranged in a retrogradational stacking pattern (Amorosi et al., 2003; 2017a; Bruno et al., 2017). Late Holocene deposits record the progradation of the Po Delta and of its associated strandplains (Amorosi et al., 2003; 2017a; Stefani and Vincenzi, 2005). Due to their high lateral extent and to high concentration of organic carbon for radiometric dating, Holocene peat layers are reliable stratigraphic markers within subsurface coastal plain successions.

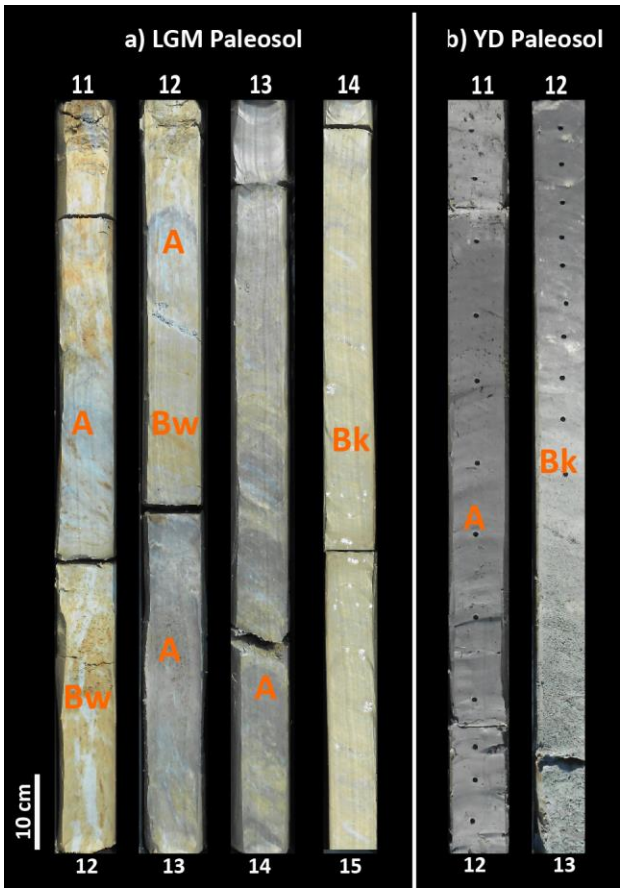

Fig .9. Representative core photographs of: (a) the Last Glacial Maximum paleosol (LGM), assigned to the Marine Isotope Stage 3/2 transition and dated to 30-24 cal ky BP (onset of the Last Glacial Maximum; from core B2, a continuous core drilled specifically for this project); and (b) the Younger Dryas paleosol dated to 12.9-11.7 cal ky BPA (from core EM 13, recovered as part of coring program initiated by ExxonMobil Upstream Research Company).

In the sedimentological literature, stratigraphic studies have also investigated 5th-and 6th-order cycles as seen in the Mississippi delta (Lowrie and Hamiter, 1995) and in the Ebro delta in Spain (Somoza et al., 1998). The stratigraphic architecture is characterized here by a series of parasequences piled up, where each parasequence represents a shallowing-upward successions bounded by flooding surfaces or minor transgressive surfaces (Van Wagoner et al., 1990; Kamola and Van Wagoner, 1995).

The stratigraphy of the Holocene Po Basin fill coastal succession is characterized by a similar parasequence architecture (Amorosi and Milli, 2001; Amorosi et al., 2005; Correggiari et al., 2005; Stefani and Vincenzi, 2005; Bruno et al., 2019), that suggests a step-wise sea-level rise with intermittent phases of landward shift in facies followed by a generalized progradation (Fig. 10).

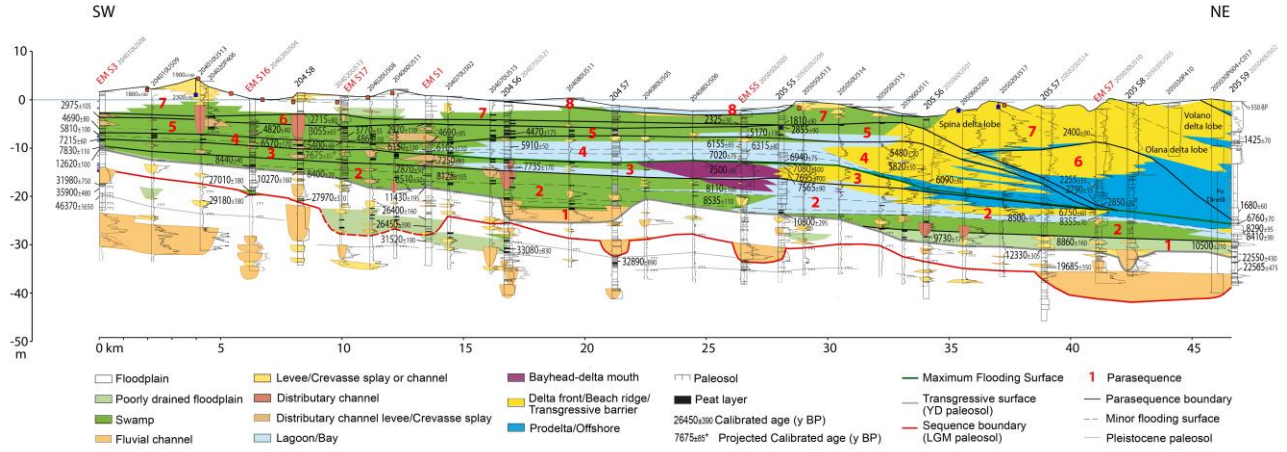

Fig. 10. Parasequence architecture of the Holocene succession in the Emilia-Romagna coastal plain. From Amorosi et al. (2017a).

Three main flooding surfaces and their landward equivalents were recognized within the early Holocene succession and dated to about 11.5, 9,2 and 7,7 kyr BP. These surfaces mark the base of three transgressive parasequences that developed in response to the eustatic rise (Bruno et al., 2017b).

3. DATABASE AND METHODS

The high-resolution stratigraphic analysis of the Late Quaternary deposits from the Po Basin and mapping of stratigraphic markers were carried out through:

- Stratigraphic correlations based on the Regione Emilia-Romagna (RER) database, where borehole and water-well log descriptions were supported by geotechnical tests and radiocarbon dating;
- Two dimensional cross-sections and three dimensional analysis across an area about 2,000 km^2 wide;
- Additional cores drilled during the 2017-2019 period;

- New radiocarbon dates to implement the chronostratigraphic framework;
- Seismic profiles;
- Geochemical and geotechnical analyses;
- Petrel package, Schlumberger's software platform used in the exploration and production sector of the petroleum industry, that brought stratigraphic correlations from a classic 2-D view to a 3-D perspective.

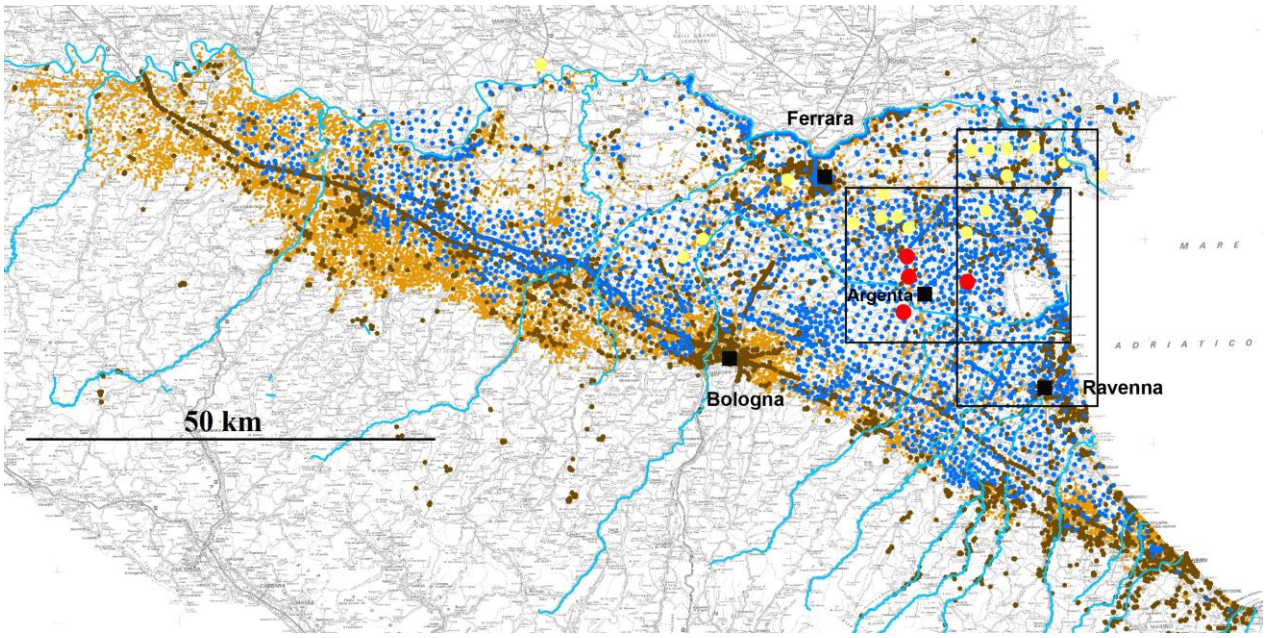

Fig. 11. The Emilia-Romagna Geological Survey database (in brown, continuous core descriptions; in blue, CPT/CPTU tests; in orange, water wells). Continuous cores drilled specifically for this project are in red; Continuous cores drilled in collaboration with ExxonMobil Upstream Research Company between 2014 and 2016 are in yellow. The investigated areas are bordered by black boxes.

3.1 Geologic database

During the last 20 years the Geologic Mapping Project (CARG project) of Regione Emilia-Romagna at 1:50,000 scale led to the collection of hundreds of new stratigraphic information through a massive drilling campaign. More than 2,500 data were used for this work.

The RER database (Fig. 11) was implemented between 2014 and 2016 by 19 boreholes in the framework of a scientific collaboration between Bologna University and ExxonMobil (yellow dots in Fig. 11) and by 4 new cores drilled between May and September 2018 specifically for this project (red dots in Fig. 11).

The geologic database analyzed for this study is composed of different types of stratigraphic data, with particular vertical resolution, range of depth and quality of the description.

• *Continuously cored boreholes* (17-30 m deep; B1-B4 in red color in Fig. 11), specifically drilled for this project in the area between Argenta and Longastrino. Boreholes were drilled with a continuous perforating system to assure a non-disturbed stratigraphy (Fig. 12) and to collect undisturbed samples. The cores were opened with a lengthwise cut and lithofacies characteristics, sediment texture, grain size, color and accessory materials (fossils, plant and wood fragments) were examined. Pocket penetrometer values were collected from fine-grained deposits. These cores represent the most efficient tool for stratigraphic correlation, as they enable direct observation of lithofacies characteristics, grain size and sediment textures. Accessory material (i.e. shells, roots, wood and plant fragments, carbonates concretions, Fe and Mg oxides etc.) were described, along with organic matter for radiocarbon dating. Samples were collected for geochemical and geotechnical analyses, paleontological investigations and radiocarbon dating.

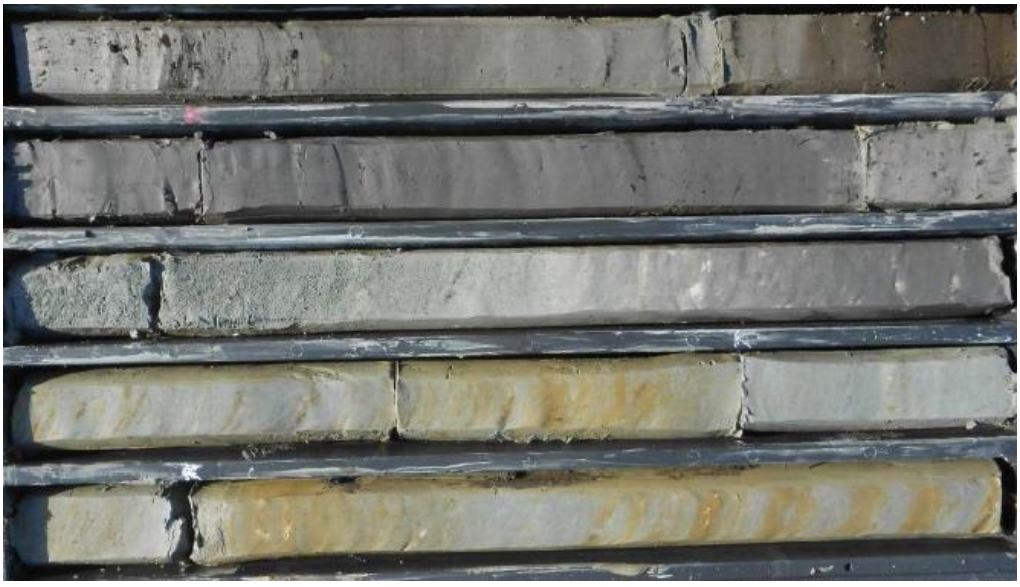

Fig. 12. Example of a newly-drilled core recovered during this study in the Argenta area.

• *Continuously cored boreholes* (20-53 m deep; in yellow color in Fig. 11), recovered as part of an extensive research and coring program initiated by ExxonMobil Upstream Research Company. These cores are associated with high-resolution core descriptions, including information about lithology, color, consistency, contacts, accessory material, pocket penetrometer and environment of deposition. Calibrated radiocarbon dates are associated to these stratigraphic data.

• *Core descriptions* (20-200 m deep; in brown color in Fig.11) from the RER database, include two distinct types of data: (i) stratigraphic descriptions carried out specifically in the frame of the

CARG Project (Fig. 13a), which are associated with several sedimentological information, including lithology, color, consistency, contacts, accessory material, pocket penetrometer and torvane values, pedologic information and environment of deposition. Uncalibrated radiocarbon dates are locally available; (ii) stratigraphic descriptions (Fig. 13b) collected from hydrogeological and geotechnical surveys, which commonly lack information such as accessory material, consistency and environment of deposition.

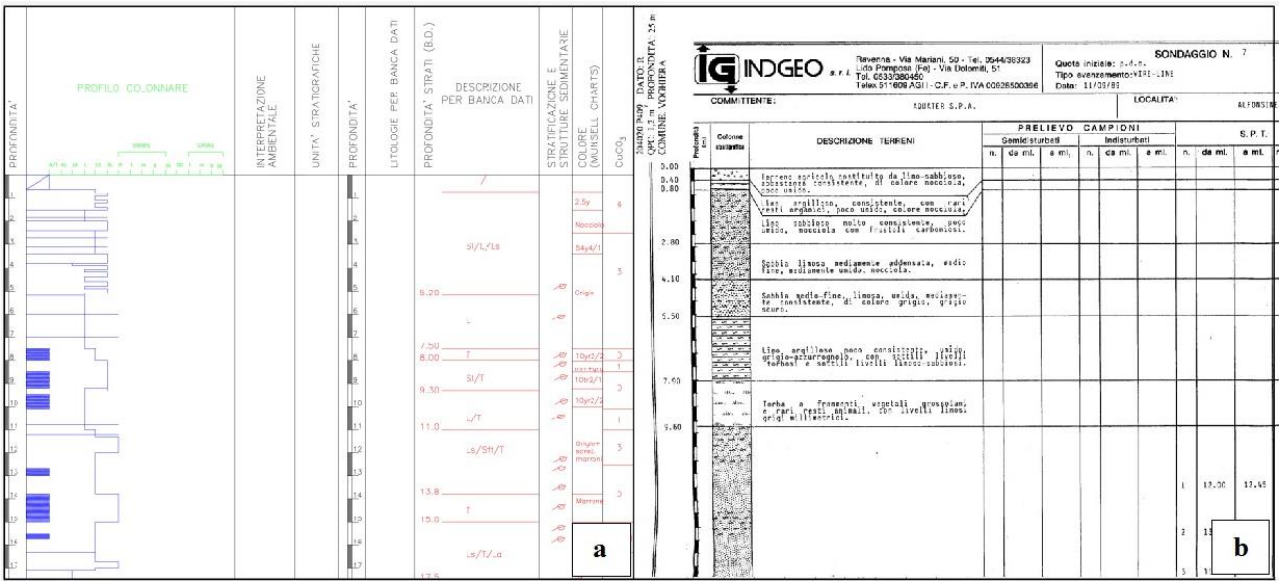

Fig. 13. (a) Example of detailed stratigraphic core description from the CARG Project; (b) Example of conventional stratigraphic core description from the RER Geological Survey database.

• *Water wells* (15-450 m deep; in orange color in Fig. 11), drilled for hydrogeological purposes, commonly have scarce vertical resolution (Fig. 14): only thick sedimentary bodies are recorded, with basic grain-size or aquifer/aquitard information. Additional annotations on color, grain size tendencies and organic matter content are rarely available. This kind of data was utilized for the identification of thick fluvial-channel sand bodies, and for their correlation throughout the study area.

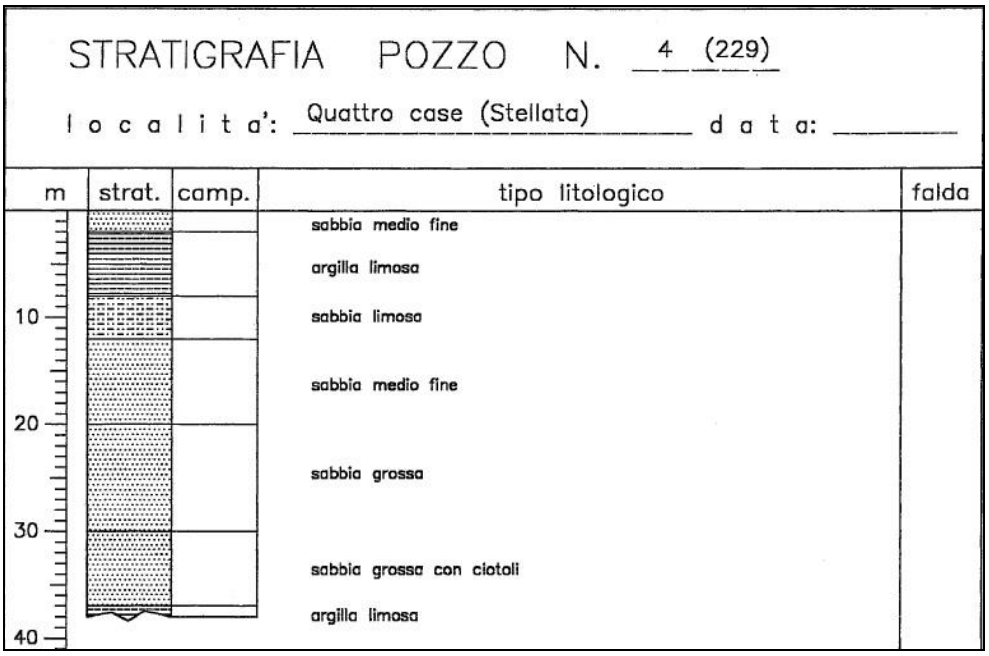

Fig. 14. Example of poor-quality stratigraphic description (water-well log from the RER database).

• *Piezocone penetration tests (CPTU)* (30-36 m deep; in blu color in Fig. 11) are a powerful, though indirect, tool for high-resolution stratigraphic correlations that is commonly used for geotechnical studies. These tests attest soil resistance to penetration providing cone resistance (Q_c) and sleeve friction (f_s) values, and also pore water pressure (u) values. These tests are relatively low-cost and display high vertical resolution (Fig. 15), with a mean investigation depth of 35 m. The efficiency of CPTU tests for facies characterization and stratigraphic correlation of late Quaternary deposits, following stratigraphic calibration with adjacent cores, has been investigated by Amorosi and Marchi (1999), Styllas (2014), and Amorosi et al. (2015). The reader is referred to these works for detailed information about their use in stratigraphy.

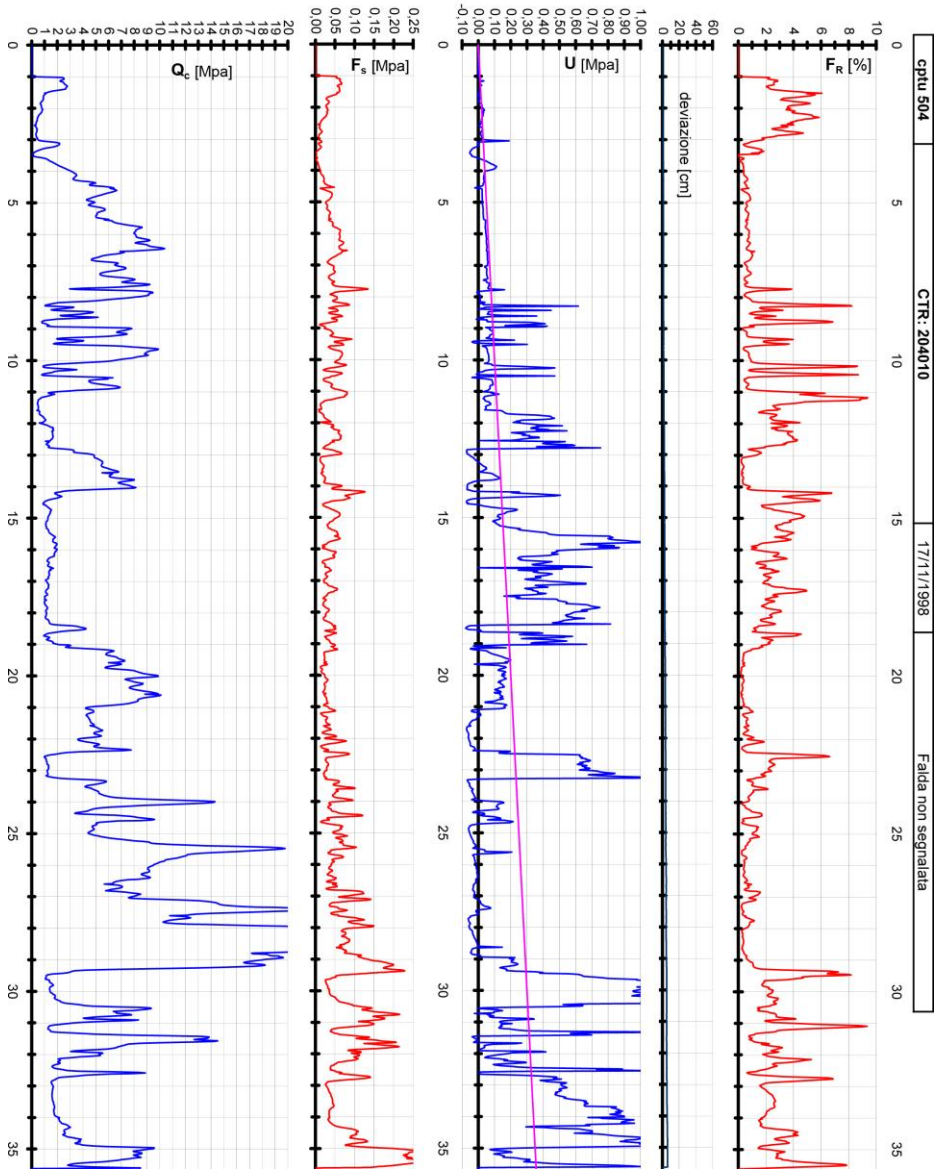

Fig. 15. Example of piezocone penetration test (from the RER database).

Facies associations and depositional environments were reconstructed, with specific attention paid to lithology, accessory components, compositional attributes, and faunal content. We particularly focused on elements that could lead to the identification of stratigraphic markers: (i) paleosols, characterized by high consistency, gray/dark gray colors, reaction to HCl, presence of carbonate concretions and high pocket penetrometer values; (ii) peat layers, dominated by high organic-matter content, plant remains and woods; (iii) fossiliferous brackish horizons, clay layers characterized by the presence of shell fragments and plant remains (Fig. 16).

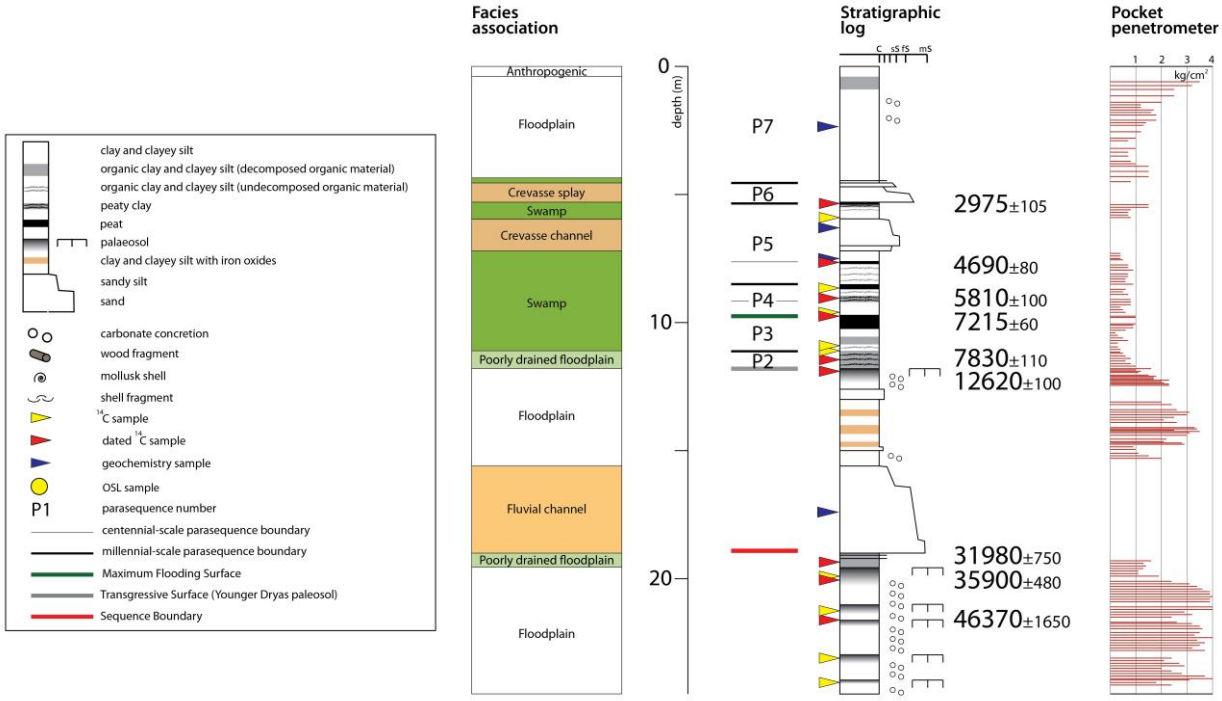

Fig. 16. Stratigraphic log and facies interpretations of one of the borehole drilled as part of an extensive research and coring program initiated by ExxonMobil Upstream Research Company.

The chronologic framework was ensured by (i) radiocarbon dates from the RER database; (ii) radiocarbon dates from 20 cores drilled in collaboration with ExxonMobil (iii) radiocarbon dates from organic-rich samples from the four new cores specifically drilled for this study. Samples were dated at KIGAM laboratory (Korea Institute of Geoscience and Mineral Resources, Daejeon, Republic of Korea). Uncalibrated dates were then calibrated using Oxcal 4.2 (Ramsey and Lee, 2013), with the Intcal13 calibration curve and Marine13 dataset (Reimer et al., 2013), as shown in Figure 17.

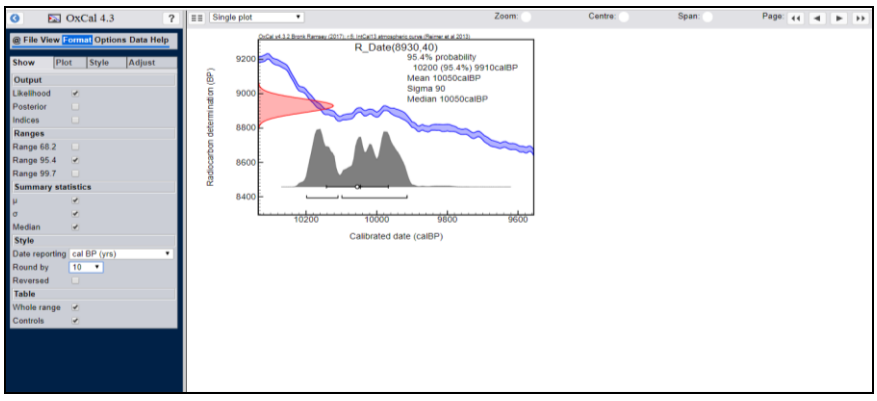

Fig. 17. Oxcal 4.2 radiocarbon dating example. Free online source at https://c14.arch.ox.acuk/oxcal/OxCal.html.

Before AMS counting, organic samples (e.g. wood) were pre-treated with acid-alkali-acid method in order to remove $CaCO_3$ and humic-acids contamination. Shell samples were subjected to HCl etches to eliminate secondary carbonate component. Soil and peat samples were treated with 0.5M NaOH at 80°C for 2 hours to extract humic acid without extraction of the humin-acid portion. Humic acids were then collected by adding conc. HCl to the solution.

Optically-stimulated luminescence (OSL) dating from bottom core B1 was carried out at the Luminescence Dating Laboratory of the University of Oxford, UK. The sample destined for OSL dating was recovered during drilling operations with an Oesterberg cell. A 60 cm core segment was removed and the exposed top and bottom parts were then sealed with paraffin. Subsequently, the paraffin caps were removed in a dark room and the upper and lowermost 5 cm of the sample were discarded. The innermost part of the core segment was stored in lightproof containers.

3.2 Seismic analysis

- *Seismic profiles*

The detailed reconstruction of deep stratal architecture in the study area was carried out through the interpretation of 95 2D seismic profiles from the Eni s.p.a. database, after calibration with 45 well logs (depth of 300-5000 m) available online at https://unmig.mise.gov.it/. Seismic interpretation relied on the identification and tracking of the main unconformities and their correlative conformities. Cross-sectional stratal geometries and seismic reflection terminations were used to isolate stratal discontinuities in the study area.

3.3 Geochemical analysis

- *Dry bulk density and Loss on ignition tests*

Each sample was dried at 105 °C and weighed on an electronic scale (accuracy of 0.01 g) to determine dry bulk density (δ_{dry}=dried weight/5cm^3). Samples were subsequently heated at 550 °C for 4 hours to determine loss on ignition. For determining dry bulk density, the greatest error was introduced by the use of a 5 cm^3 field sampler. It is estimated that the error in volume calculations may be up to 10% (5±0.5 cm^3). According to standard rules of error propagation, the fractional uncertainty in the bulk density calculations is 10%. The preparation of samples for Loss on ignition tests was carried out in the laboratories of the University of Bologna and the University of Utrecht.

Ten undisturbed sampled from cores B1-B4 were collected to quantify the amount of compaction by comparing the dry bulk density of compacted and uncompacted peat samples and measuring changes in dry bulk density with depth (van Asselen and Roosendaal, 2009). During compaction, the pore volume decreases and dry bulk density increases. Hence, changes in dry bulk density of buried peat, compared to the dry bulk density of surface peat, which is generally in an uncompacted state, can be used to estimate the relative amount of compaction. Peat samples were taken at 5-cm intervals from the undisturbed samples using a 1 cm x 1 cm x 5 cm sampler (Fig. 18). The δ_{dry} and LOI data of uncompacted peat samples were used to establish an equation to calculate the uncompacted dry bulk density ($\delta_{dry,uncomp}$) of each 5 cm^3 compacted peat samples, based on its LOI. The $\delta_{dry,uncomp}$ ($\delta_{dry,uncomp}= a\text{-}ce^{-(b7LOI}$) was used to calculate the decompacted thickness of each 5 cm^3 compacted sample, ignoring lateral strain ($h_{decomp}=(\delta_{dry,\ comp/}\ \delta_{dry,uncomp})*5$). In this equation the parameters *a,b* and *c* are fitted parameters (*a*=1.5, *b*=6 and *c*=1.53), obtained from samples of uncompacted peat from the Biebrza in Poland; peat samples from the Po Delta plain have similar plant species composition and organic matter-content (Van Asselen, 2011). The percentage of compaction was expressed as the ratio of volume reduction ($v_{red}=1*1*(h_{decomp})-1*1*5$) to the calculated decompacted volume in a 5 cm^3 peat sample ($v_{decom}=1*1*h_{decomp}$): compaction=(v_{red}/v_{decomp})*100.

Fig. 18. Example of an undisturbed sample; peat samples were taken at 5-cm intervals from the undisturbed samples using a 1 cm x 1 cm x 5 cm sampler.

• *X-ray fluorescence analysis*

X-ray fluorescence is a non-destructive analytical technique used to determine the elemental composition of materials. XRF analyzers determine the chemistry of a sample by measuring the fluorescent (or secondary) X-ray emitted from a sample when it is excited by a primary X-ray source. Each of the elements present in a sample produces a set of characteristic fluorescent X-ray that is unique for that specific element. It is an excellent technology for qualitative and quantitative analysis of material composition.

The preparation of samples for XRF analysis took place in the laboratories of the University of Bologna. The analysis of powdered material requires that the sample be placed into a boric acid support (Fig. 20). The process includes grinding a sample into a fine powder, ideally to a grain size of <75um, than pressing the powder with the acid boric support in a die, in order to produce a homogenous sample. Samples, pressed into tablets, were analyzed for 10 major and 16 trace elements in a Philips PW1480 spectrometry with a Rh tube (Fig. 19).

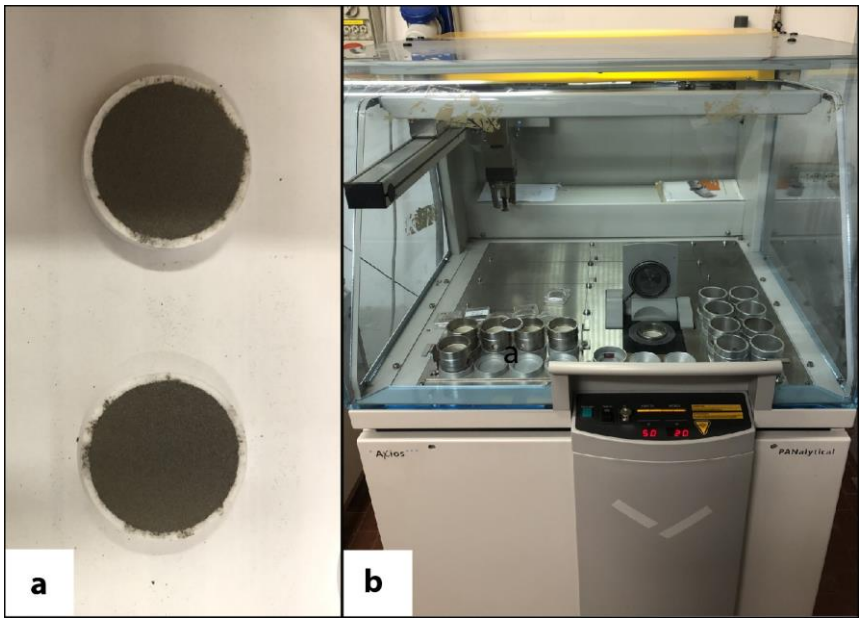

Fig. 19. (a) Example of sample for XRF test placed into a boric acid support; (b) XRF of the University of Bologna; PW1480 wavelength sequential dispersion spectrometer with Rh tube.

3.4 Geotechnical analysis

• *Cone penetration test*

Cone penetration testing (CPTU) can be used to determine the void ratio and compressibility of Holocene peat in the Po Plain. To parametrize the relation between soil compression and CPT measurements, a simple regression analysis was performed between the void ratio measured in the laboratory and *qn* ($qn = qt - \sigma_{v)}$ derived from CPT logs ($qt = qc + u\,(1-an)$). The void ratio decreases in peat samples from layers that have been exposed to increasing vertical effective stress (Koster et al., 2018a). The compression percentage is expressed as the ratio between void ratio of a single peat layer and the void ratio of natural peat ($100-(e/e_0)*100$). The void ratio for the different organic matter content classes ($e= (3.64 + 0.86 * \text{N organic matter content})qn^{-(0.28+0.33N)}$) relates the organic matter content measured in the laboratory with the *qn* derived from CPT logs. The numerical values were determined by trend fitting (Koster et al., 2018b).

In the Po Plain, it has been observed that cone resistance increases with deeper burial of Holocene peat, owing to increasing compression. According to Landva (2006), the void ratio of natural peat (e_0= (2.27 + 27.55 * N organic matter content)$\sigma'_v{}^{-(0.12+0.34N)}$) was determined using a vertical effective stress of 3.7 KPa and a value of organic matter content of 0.7.

• *Oedometer test*

The oedometer test was used to investigate the 1-D consolidation behavior of fine samples. An undisturbed soil sample 20.5 mm in height and 60 mm in diameter was confined in a steel confining ring and immersed in a water bath. The top and bottom of the specimen were placed in contact with porous discs, so that drainage of the specimen took place in the vertical direction when vertical stress was applied (Fig. 20). In particular, twelve undisturbed samples were analyzed: they were subjected to a series of pre-selected vertical stresses, each of which was held constant, while dial gauge measurements of vertical deformation of the top of the specimen were made, and until movements ceased (24h). Dial gauge readings were taken at standard intervals (1 min.) of time after the start of the test. For each increment, the final settlement of the soil sample, as well as the time taken to reach the final settlement were recorded. The results of each loading stage of the oedometer test were normally plotted as the dial gauge readings either as a function of square root of elapsed time, or as a function of the logarithm of elapsed time. The increment of vertical strain Δε v was determined for each loading increment. The coefficient of volume compressibility (mv) was defined as the ratio of volumetric strain over change in effective stress.

Fig. 20. Example of the oedometer cell used in the tests presented in this study.

• *Decompaction model*

Decompacted thickness H_0 of a soil column presently comprised between depth z_1 and z_2 has been computed as (Gambolati et al., 1998):

$$H_0 = (1 + e_0) \int_{z_1}^{z_2} \frac{dz}{1 + e(z)}$$

where e_0 initial void index and $e(z)$ is the void index at depth z. The behavior of $e(z)$ in virgin loading conditions is given by $e(z) = e_0 - C_c \log \sigma_z$, with C_c the compression index and σ_z the intergranular effective stress.

The deformation of each unit is computed as $(H_0 - H)/H_0$, with H the actual thickness of the unit (Paper 3).

3.5 Petrel data processing

In addition to classic two-dimensional cross-sections, a 3D software, Petrel, was also used to analyze data and reconstruct three-dimensional maps of stratigraphic markers. The first necessary step was the preliminary 2D stratigraphic analysis of boreholes and CPTU tests, which were added to the software and examined through a series of NW-SE and SW-NE cross-sections (Fig. 21). This step aims at tracing paleosols, peat layers, lagoon horizons and identifying fluvial-channel bodies.

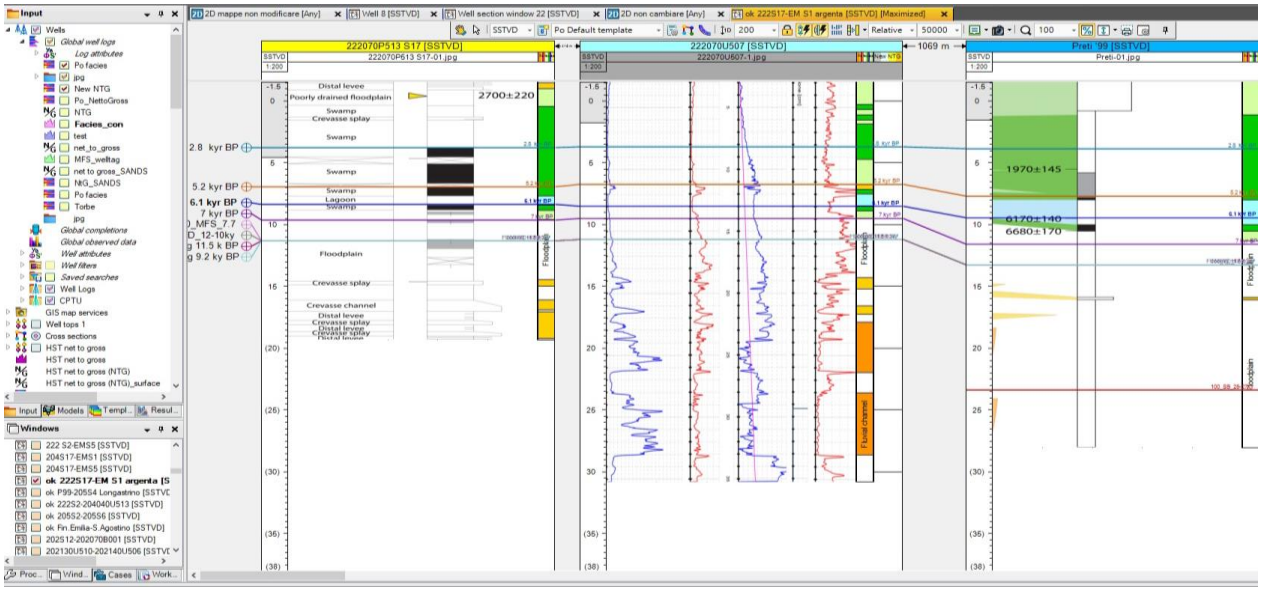

Fig. 21. Example of core and CPTU stratigraphic interpretations from a 2D cross-section on Petrel 2014.

When the 2D stratigraphic correlations were reliable, the convergent interpolation algorithm was used to recreate the 3D geometry of the picked surfaces. The convergent gridder (Fig. 22) takes a set of randomly distributed scattered points and computes an output grid showing a high-quality model representation of the input data. This type of algorithm adapts to a sparse or dense data distribution through converging iterations at finer grid resolution. Stratigraphic surfaces were then manually modified to better fit the geologic model.

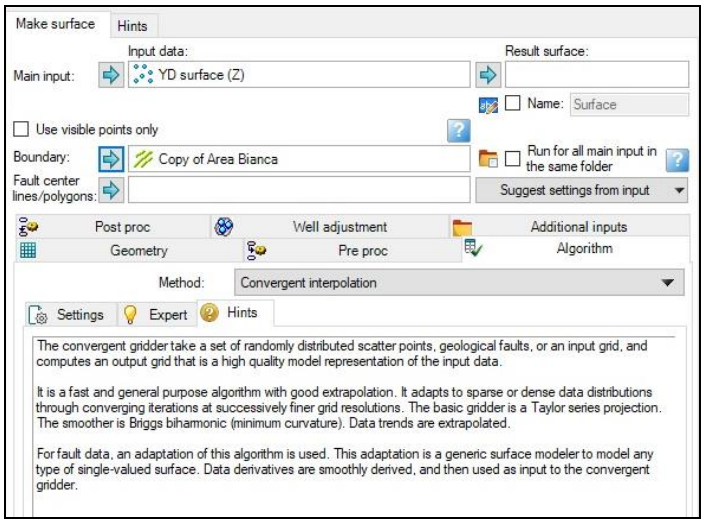

Fig. 22. Example of the gridder used for 3D reconstructions

Although Petrel is typically used for seismic interpretation, in this work it was adapted to our specific needs, such as correlation and interpretation of sparse stratigraphic data. Its application goes beyond 3D modelling, as it was found very useful for classic 2D correlations too, to ensure reliable facies correlations in cross-sections that can be rapidly generated.

4. MANUSCRIPTS

4.1 Paper 1

Deformation patters of Late Quaternary strata and their relation to active tectonics, Po Basin, Italy

Alessandro Amorosi, Luigi Bruno, Bruno Campo, **Bianca Costagli**, Wan Hong, Vincenzo Picotti, Stefano Claudio Vaiani.

Sedimentology

Submitted in Jenuary 2020

Deformation patters of Late Quaternary strata and their relation to active tectonics, Po Basin, Italy

Alessandro Amorosi[1], Luigi Bruno[2], Bruno Campo[1], Bianca Costagli[1], Wan Hong[3], Vincenzo Picotti[4], Stefano Claudio Vaiani[1]

[1]Department of Biological, Geological and Environmental Sciences, University of Bologna, Via Zamboni 67, 40126, Bologna, Italy.

[2]Department of Chemical and Geological Sciences, University of Modena and Reggio Emilia, Via Campi 103, 41125 Modena, Italy

[3]KIGAM Korea Institute of Geoscience and Mineral Resources, 92 Gwahangro, Yuseong-gu, Daejeon Metropolitan City, South Korea.

[4]ETH, Department of Earth Sciences, Sonneggstrasse 5, 8092 Zurich, Switzerland

Abstract

Despite increased application of subsurface datasets below the limits of seismic resolution, reconstructing near-surface deformation of key stratigraphic markers in modern alluvial and coastal plains through sediment core analysis has received little attention. Highly resolved stratigraphy of Late Pleistocene-Holocene deposits, down to 10-150 m depth, across a wide portion of the southern Po Plain provides an unambiguous documentation on the deformation of previously flat-lying strata that goes back in time beyond the limits of morphological, historical and paleoseismic records. Five prominent key horizons, accurately selected on the basis of their sedimentological characteristics and typified for their fossil content, were used as synchronous, highly effective stratigraphic markers (M1-M5) that can be traced for tens of kilometers across the basin. A facies-controlled approach in the Argenta-Longastrino region tied to a robust chronology (102 radiocarbon dates) reveals considerable stratigraphic offset of laterally extensive nearshore (M1) and lagoon (M4-M5) marker beds originally deposited in a horizontal position and assigned to the Last Interglacial and Early-Middle Holocene, respectively, as well as of two weakly developed paleosols (M2-M3) of

latest Pleistocene age. The location of more intense deformation of these marker horizons is remarkably coincident with the axes of the buried ramp anticlines, across which new seismic images reveal substantially warped stratal geometries of Early Pleistocene strata, previously thought to be undeformed. The striking spatial coincidence with the epicenters of historic and instrumental seismicity suggests that deformation of marker beds M1-M5 might reflect, in part at least, syntectonically generated relief and, possibly, active tectonism. Delineating a geologic scenario of Late Pleistocene-Holocene tectonic deformation through a combined stratigraphic and sedimentological approach may represent the missing link between the analysis of long-term (basin-scale), steady-state tectonics, acting on 10^6-10^7-year time periods and short-term deformation, primarily developed on 10^0-10^2-year time scales.

Keywords: Stratigraphic marker, Near-surface deformation, Sediment core analysis, Po Plain, Quaternary, Holocene

1. Introduction

Conventional seismic analysis in onshore regions provides insufficient resolution into the identification of low-throw, late Quaternary blind faults. In such areas, geomorphic and paleoseismic data of Quaternary age are routinely used for detecting active tectonics. Geomorphic data include uplifted fluvial or marine terraces, changes in stream gradients, vegetation lineaments, topographic scarps, and aligned drainages (Azor et al., 2002; Keller et al., 2002; Picotti and Pazzaglia, 2008; Matsu'ura and Sugaya, 2017). Paleoseismic investigations comprise excavation of trenches and surficial coring surveys (Barka et al., 2002; Prentice et al., 2010; Audemard and Michetti, 2011). However, in modern alluvial and coastal plains developed on top of actively subsiding basins, tectonics can have no significant or persistent geomorphic expression. Far from the basin margins, in particular, tectonically-generated accommodation is systematically counterbalanced by depositional filling, and the record of past seismic events is no longer prominent in the resulting flat morphology. On the other hand, shallow coring or trenching datasets are spatially limited and provide highly fragmentary point data that are typically focused on very short temporal scales that can be poorly representative of the past seismic activity. In particular, large earthquakes with long recurrence intervals can be missed by the use of temporally short datasets. As a consequence, geological records on longer (millennial) temporal scales and high-

resolution near-surface stratigraphic studies are crucial to understand the occurrence of large, but infrequent seismic events (Sinha et al., 2005; Dura et al., 2016).

The Po Plain (northern Italy), a region historically with rare earthquakes greater than magnitude 5, experienced two larger than expected (M_w~6.0) damaging earthquakes in 2012, close to the village of Mirandola (Fig 1A). Coseismic surface ruptures in the central sector of the buried Ferrara arc resulted in ground fractures associated with widespread soil liquefaction phenomena and a 15-20 cm anticlinal crest growth (Caputo et al., 2015; Carannante et al., 2015).

The Po Plain has been the object of intensive geophysical surveys and drillings by oil companies, aimed at an improved characterization of the petroleum systems active in the area (Pieri and Groppi, 1981; Ghielmi et al., 2010; 2013; Amadori et al., 2019). Previous stratigraphic studies have focused largely on the deformation of the Pliocene to Middle Pleistocene syntectonic basin fill and prominent basin-scale unconformities have been tracked in the subsurface (Regione Emilia-Romagna & ENI-AGIP, 1998; Regione Lombardia & ENI-Divisione Agip, 2002; Muttoni et al., 2003; Ghielmi et al., 2010, 2013; Garzanti et al., 2011; Amadori et al., 2019). In contrast, deformation of Late Pleistocene-Holocene deposits over the past 125 ky has received very little study. Few researchers have addressed some aspects of the possible use of stratigraphic criteria to assess the deformation of near-surface Pleistocene strata in the Po Basin. These studies, however, suffered from a lack of paleotopographic accuracy, as they focused on paleosurfaces that were far from being horizontal at the time of formation: for example, paleosols (Amorosi et al., 2017b) and fluvial channel-belts (Stefani et al., 2018).

This paper explores the deformation of targeted stratigraphic markers that approximate paleohorizontal surfaces through accurate facies analysis of a relatively shallow (< 150 m), Late Pleistocene-Holocene sedimentary succession. The south-eastern Po Plain serves as a very useful location for high-resolution Quaternary records, as it has received intensive study, and a comprehensive sequence stratigraphic, sedimentological, and paleontological framework, chronologically constrained by over 200 radiocarbon dates, is available (Amorosi et al., 2017a, b; Bruno et al., 2017; Campo et al., 2017).

In order to enhance stratigraphic interpretation, a coring survey was carried out in the Argenta-Longastrino area (Fig. 1A), between May and October 2018, and four continuous cores (B1-B4 in Fig. 1A), 17 m to 35 m long, were recovered. Depositional facies were determined accurately on the basis of lithology, accessory components, and their faunal content. Beyond the limits of radiocarbon dating, age determinations include one sample dated by optically stimulated luminescence (OSL), along with published electron spin resonance (ESR) data coupled with pollen profiles (Amorosi et al., 2004; Ferranti et al., 2006).

The approach taken here involves the high-resolution study of drill cores of Late Pleistocene-Holocene age from the shallow subsurface, coupled with the seismic stratigraphic analysis of the basin fill. The aim of this paper is to show that accurate sedimentological and stratigraphic analysis of shallow buried depositional systems can help assess patterns of active deformation below the resolution of conventional seismic stratigraphy and beyond the short temporal scales intrinsic to geomorphic and paleoseismic datasets. By comparing the recent deformation of key stratigraphic markers with the location of major tectonic structures and historical/instrumental records of seismic activity, specific objective of this study is to explore the possible use of high-resolution Quaternary stratigraphy to help predict the likely spatial distribution of future damaging earthquakes in the study area.

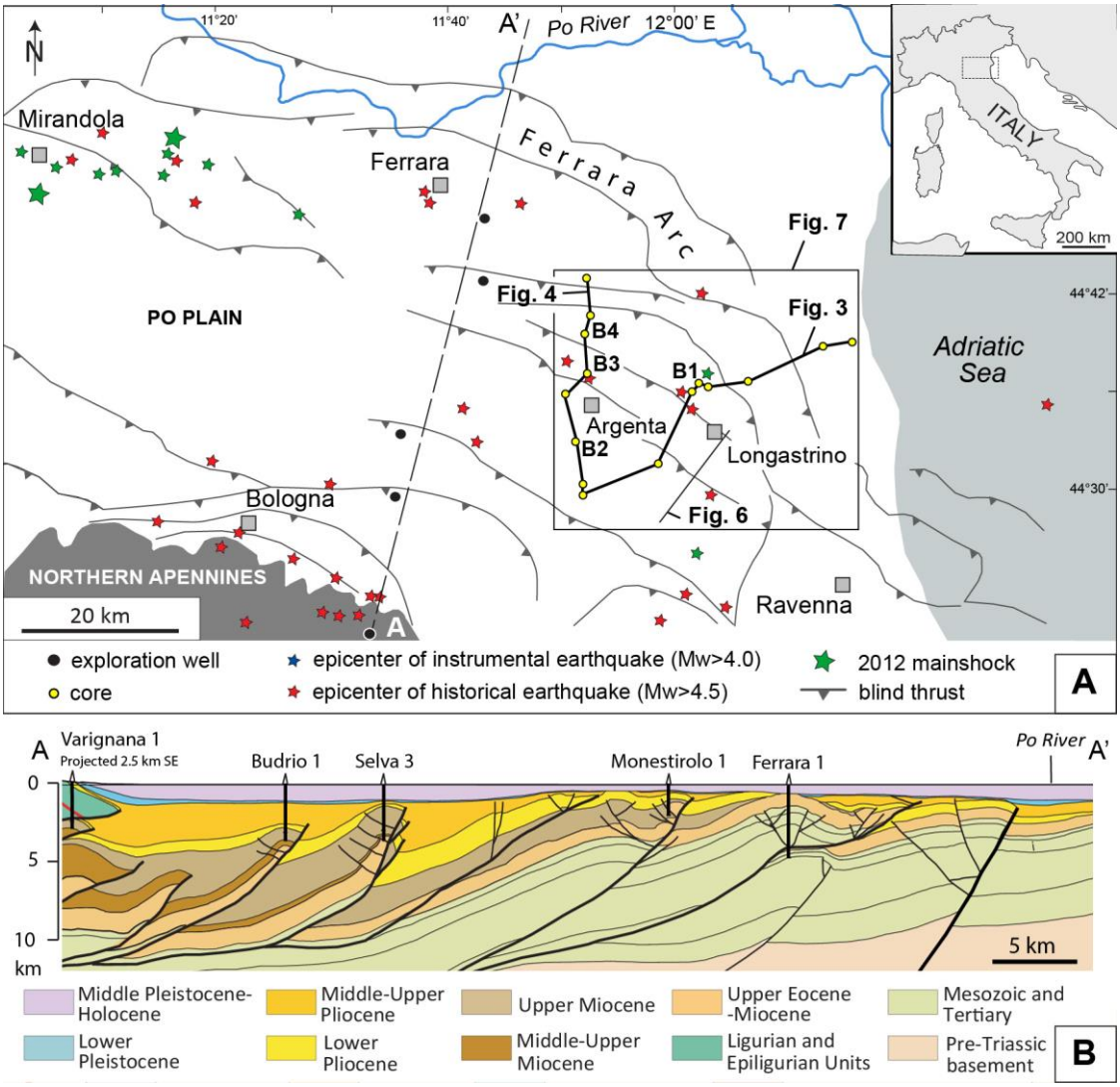

Fig. 1. A) Study area, structural setting, with location of the Ferrara arc and minor thrust fronts, and the earthquake catalog, with spatial distribution of historical and instrumental earthquakes >Mw 4.5 and >Mw 4.0, respectively. Section traces of Figures 4, 5, and 6 are also shown. B) Schematic profile showing the major fold-and-thrust belt structures buried beneath the Po Plain (modified after Picotti and Pazzaglia., 2008; see dashed line in Fig. 1A, for location).

2. Geological Setting

The northern Apennines thrust-and-fold belt developed since the Late Oligocene in the context of the collision between the European plate and the Adria plate. The development of the Apennines foredeep, in particular, has been related to the eastward rollback of the subducting Adria plate (Malinverno and Ryan, 1986; Royden et al., 1987; Doglioni, 1993). The northern Apennines foreland basin evolved through a series of successive regional tectonic phases that led to the progressive outward (NE) migration of the thrust-and-fold belt and related foredeeps (Ricci Lucchi, 1986). The Po Plain-Adriatic foredeep, bounded by the outermost thrust-propagation folds of the northern Apennines at its inner margin, and by the Adriatic foreland ramp at the outer margin, was affected by active synsedimentary compressional tectonics since the Late Miocene (Ghielmi et al., 2013). The Quaternary geodynamic evolution and the tectonic processes active along the northern Apennines thrust fronts and in the adjacent Po-Adriatic foredeep domains have been analysed and discussed at length by several authors (e.g. Picotti and Pazzaglia, 2008; Fantoni and Franciosi, 2010; Bresciani and Perotti, 2014; Gunderson et al., 2018).

The geometry of the northern Apennines accretionary prism consists of three main arcuate thrust systems (Monferrato, Emilia and Ferrara-Romagna-Adriatic arcs in Amadori et al., 2019). The buried thrusts and related fault-propagation folds beneath the modern Po Plain have been investigated through interpretation of a dense network of seismic lines and well logs (Pieri & Groppi, 1981; Picotti et al., 2007; Picotti and Pazzaglia, 2008; Toscani et al., 2009; Fantoni and Franciosi, 2010; Ghielmi et al., 2013; Martelli et al., 2017; Livani et al., 2018; Amadori et al., 2019). Anticline structures are associated with ramp overthrusts and are separated by large synclines (Fig. 1B) that record much larger subsidence rates (Carminati et al., 2003; Ghielmi et al., 2010; Martelli et al. 2017). The Ferrara arc represents one of the most external structures of the northern Apennines (Fig. 1A): it has been tectonically active since the Early Pliocene to present times (Scrocca et al., 2007; Valensise et al., 2009; Boccaletti et al., 2011; Maesano et al., 2015; DISS Working Group, 2018). Distinct thrust systems belong to the Ferrara arc (Fig. 1A, B): the Mirandola structure, at the western edge of the Ferrara arc (Fig. 1A), include active seismogenic faults (Boccaletti et al., 2004; Bonini et al., 2014; Govoni et al., 2014).

The major architectural components of the Pliocene-Quaternary Po Basin fill stack to form a two-fold, cyclic hierarchy of: (i) third-order depositional sequences, separated at the basin margin by tectonically formed angular unconformities (Regione Emilia-Romagna & ENI-AGIP, 1998; Regione Lombardia & ENI-Divisione Agip, 2002; Amadori et al., 2019); and (ii) fourth-order (100 ky), transgressive-regressive (T-R) sequences controlled by glacio-eustatic fluctuations (Amorosi et

al., 2004; 2008). The younger successions display progressively lower deformation than older deposits. Distinctive cyclic alternations of coastal and alluvial facies are the most prominent feature of T-R sequences. The uppermost two transgressive surfaces, recording the Last Interglacial and Holocene marine ingressions, respectively, are best recognized beneath the modern coastal plain (Amorosi et al., 2004), i.e. in the subsurface of the study area.

3. Methods

Cores B1-B4 (Fig. 1A) were recovered through a continuous perforating system that guaranteed an undisturbed stratigraphy and high recovery percentages (> 90%). Cores were split lengthwise and described for grain size, sedimentary structures, color, organic-matter content, type of stratigraphic contact, and accessory materials (Fe-Mn oxides, carbonate nodules, vegetation remains, woods etc.). Pocket penetration values supplied additional information about geotechnical characteristics of the study deposits.

Microfossil associations provide excellent paleoenvironmental resolution in core deposits, far greater that can be obtained from traditional sedimentologic analysis, especially in mud-prone sedimentary successions. In this study, paleontological data, mainly based on foraminifera and ostracoda, highlighted subtle changes in depth, salinity, degree of confinement, oxygen and food availability in the depositional environment (e.g. Debenay et al. 2000; Murray 2006; Barbieri and Vaiani 2018). Comparison with spatial distribution patterns of the modern meiofauna helped define the boundaries of individual facies assemblages and was useful to constrain and correlate sediment packages on a basin scale (Rossi and Vaiani, 2008; Campo et al., 2017; Amorosi et al., 2019). Thirty-three samples were analyzed for facies characterization of cores B1-B4 (Fig. 2). In addition, 89 samples were collected from Holocene (41 samples) and Last Interglacial (48 samples) coastal and paralic deposits of cores 204-S3 and 222-S2 (Fig. 3). These new data were integrated by a review of published paleontological analyses from cores 204-S5, 204-S17, 205-S1, 205-S2, 205-S4, 205-S10 and 222-S2 (Amorosi et al. 2003, 2004, 2005; Geological Map of Italy at 1:50,000 scale, Sheet 222 - Lugo).

Stratigraphic correlation relied upon a total of 102 radiocarbon dates (Supplementary Table S1). The ^{14}C database includes a set of 39 published dates (Preti et al., 1999; Amorosi et al., 2003; 2005; 2017a; 2019; Bruno et al., 2019; Geological Map of Italy Sheets 204 “Portomaggiore” and 222 “Lugo”) and 63 unpublished radiocarbon dates. Radiocarbon dating on 49 samples from cores B1-B4 (Fig. 2) was performed at KIGAM laboratory (Daejon City, Republic of Korea) on wood, plant fragments, peat and shells (Supplementary Table S1). The calibration of conventional radiocarbon

ages was based on the IntCal13 dataset (Reimer et al., 2013) using OxCal 4.3. (Bronk Ramsey, 2009). Before AMS counting, organic samples (e.g. wood) were pre-treated with acid-alkali-acid method in order to remove $CaCO_3$ and humic-acids contamination. Shell samples were subjected to HCl etches to eliminate secondary carbonate component. Soil and peat samples were treated with 0.5M NaOH at 80°C for 2 hours to extract humic acid without extraction of the humin-acid portion. Humic acids were then collected by adding conc. HCl to the solution.

Optically-stimulated luminescence (OSL) dating from bottom core B1 was carried out at the Luminescence Dating Laboratory of the University of Oxford, UK. The sample destined for OSL dating was recovered during drilling operations with an Oesterberg cell. A 60 cm core segment was removed and the exposed top and bottom parts were then sealed with paraffin. Subsequently, the paraffin caps were removed in a dark room and the upper and lowermost 5 cm of the sample were discarded. The innermost part of the core segment was stored in lightproof containers. Measurements were performed on small multigrain aliquots (n=30) with standard automated luminescence readers made by Risø and Freiberg Instruments using a double SAR post-IR blue or post-IR Green OSL measurement protocol. Dose rate calculations are based on Aitken (1985) and are derived from the concentrations of radioactive elements (potassium, rubidium, thorium and uranium) within the sediment sample(s). These were derived from elemental analysis by ICP-MS/AES using a fusion sample preparation technique. The final OSL age estimate includes an additional 4% systematic error to account for uncertainties in source calibration and measurement reproducibility. Dose rate calculations were obtained using dose rate conversion factors of Guerin et al. (2011) and calculated using the DRAC software (v1.02) developed by Durcan et al. (2015). The contribution of cosmic radiation to the total dose rate was calculated as a function of latitude, altitude, burial depth and an average over-burden density of 1.9 g/cm^3 based on data by Prescott and Hutton (1994).

Location, data of the event, and magnitude of hystorical earthquakes (Fig. 1A and Supplementary Table S2) are from the Parametric Catalogue of Italian Earthquakes 2015 (CPTI15 in Rovida et al., 2019). This catalog, produced by *Istituto Nazionale di Geofisica e Vulcanologia* (INGV), is available via its open-access website (*https://emidius.mi.ingv.it/CPTI15-DBMI15/index_en.htm*). CPTI15 includes homogeneous macroseismic and instrumental data and parameters for Italian earthquakes with maximum intensity ≥ 5 or magnitude ≥ 4.0 in the period 1000-2014 AD. Additional instrumental data were taken from ISIDe (ISIDe Working Group INGV, 2015). The focal mechanisms of instrumental events associated with the Ferrara arc are reported by Martelli et al. (2017).

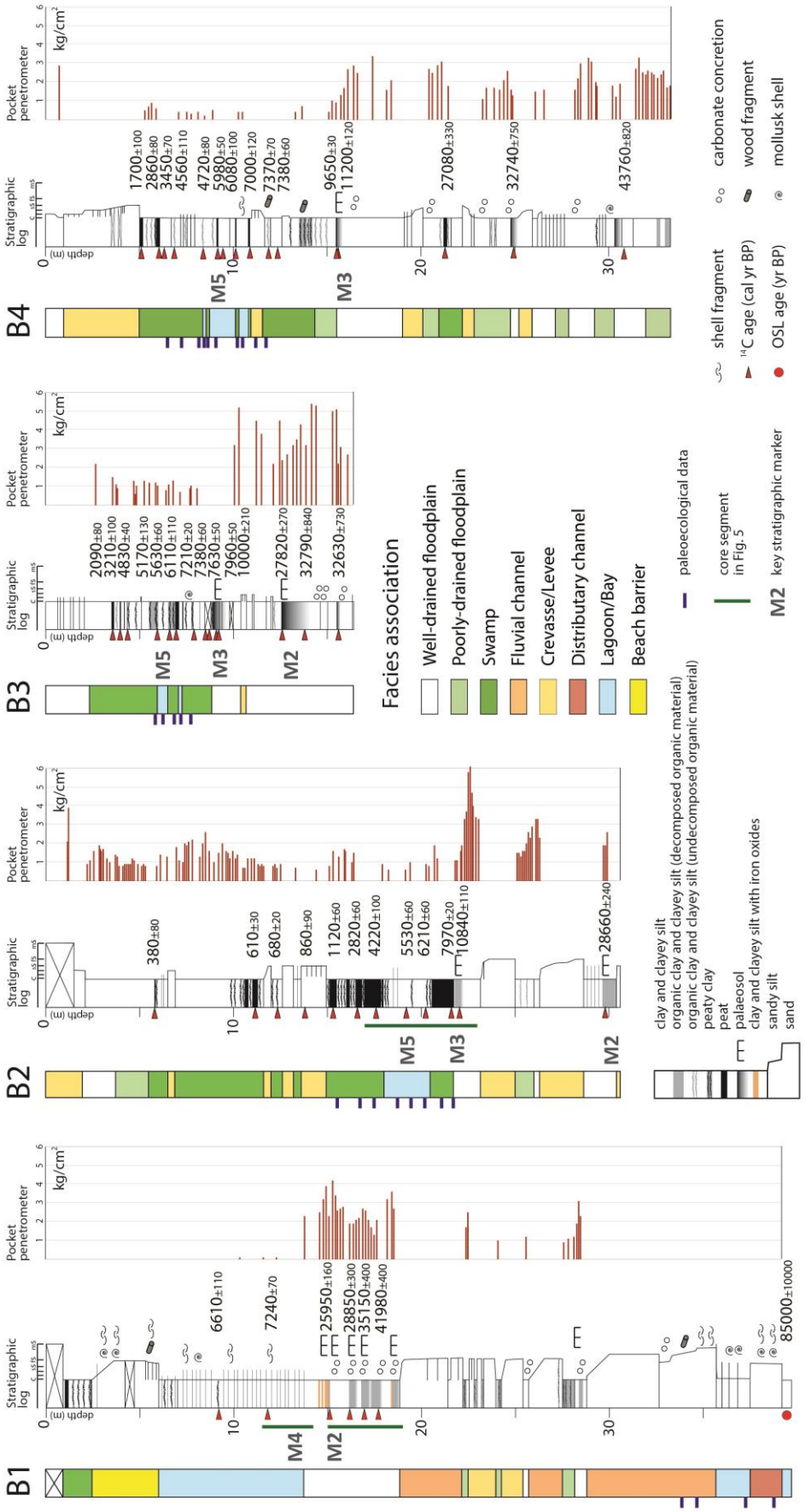

Fig. 2. Detailed stratigraphy and facies interpretation of cores B1-B4 (see Fig. 1, for location). Stratigraphic markers of Figures 3 and 4 are indicated.

4. Sedimentary Facies

As the focus of this paper lies on the deformation of selected key stratigraphic horizons, only diagnostic lithologic, sedimentological and paleontological features for the identification of such marker beds are illustrated in detail (see next section). Sedimentological characteristics of Late Pleistocene-Holocene deposits are summarized in the subsequent text: for comprehensive facies descriptions, the reader is referred to Amorosi et al. (2017a). Seven major facies associations were identified in cores B1-B4 (Fig. 2) to represent distinctive depositional settings:

i) The fluvial/distributary channel facies association consists of coarse to fine sand bodies, 2 to 10 m thick (Fig. 2), with erosional base and characteristic fining-upward trends. Individual channel bodies commonly amalgamate to form composite channel bodies. This can be seen especially in Late Pleistocene alluvial deposits (core B1 in Fig. 2), where thick sand bodies typically are part of laterally extensive fluvial channel-belts (Amorosi et al., 2017b). The meiofauna in this facies is generally absent. Occasionally, poorly-preserved specimens of reworked marine foraminifers are encountered; they can be accompanied by fragments of freshwater ostracods. Distributary-channel sands (core B1 in Fig. 2) were differentiated from fluvial-channel deposits based on distinctive depositional contexts and their host facies, that includes abundant shell fragments and mollusk shells.

ii) The crevasse/levee facies association, 0.5-3.5 m thick (Fig. 2), is composed largely of medium to fine sand and silt, and can be observed at various stratigraphic levels. Sand bodies with internal fining-up or coarsening-up trends, are interpreted to reflect crevasse channels or crevasse splays, respectively. Centimeter-thick alternations of very fine sand and silt, with abundant plant debris are considered, instead, natural levee deposits, laterally connected to the channel fill.

iii) The well-drained floodplain facies association, > 6 m thick (Fig. 2), consists predominantly of varicolored and locally hardened silt, as well as minor clay. Yellow, red and black mottles due to Fe and Mn oxides are common. Pedogenically modified horizons, with an abundance of carbonate nodules, are typically observed and represent clearly identifiable horizons (see next section). This facies association, which is inferred to reflect a floodplain with low groundwater table, is generally barren or may contain at most a few mollusk fragments and/or opercula of gastropods. Pocket penetration values range between 1.5 and 3.0 kg/cm^2 (up to 6.0 kg/cm^2 - Fig. 2).

iv) The poorly-drained floodplain facies association, up to 2.5 m thick (Fig. 2), consists of soft silt with subordinate clay. Compared to its well-drained counterpart, this lithofacies assemblage is thinner, displays uniform grey color due to a lack of oxidation, as well as lower consistency. Pocket penetration tests in this facies yielded values in the range of 0.9-2.3 kg/cm^2 (Fig. 2). This facies association is interpreted to have formed in a poorly drained flood basin, with a high water table.

v) The swamp facies association, up to 10 m thick (Fig. 2), is made up of very soft clay and peat with abundant plant fragments and wood. Freshwater-oligohaline mollusks are common. Three-dimensional facies architecture has shown that this lithofacies assemblage formed in semipermanently flooded wetlands, as part of an inner estuarine environment evolving into an upper delta plain during the Holocene (Amorosi et al., 2017a; Bruno et al., 2017; 2019). Pocket penetration values range between 0.2 and 1.5 kg/cm^2 (Fig. 2).

vi) Freshwater/hypohaline deposits transform seawards to a wide range of facies typical of brackish environments behind a barrier complex, as part of outer estuary to lower delta plain depositional systems (Amorosi et al., 2017a; 2019; Bruno et al., 2017). The lagoon/bay facies association, up to 6 m thick (Fig. 2), is mud-rich, and commonly dominated by very fossiliferous grey clay. Its brackish oligotypic fauna (*Cerastoderma glaucum* is the dominant species, followed by *Abra segmentum, Loripes orbiculatus,* and *Ecrobia ventrosa* - Amorosi et al., 2017a), able to tolerate frequent changes in salinity, indicates a depositional environment fed by mixed marine and fluvial water sources. Where the facies is heterolithic, it exhibits an abundance of shell-rich, graded sand beds (core B1 in Fig. 2) and is interpreted to reflect the distal fringe of a flood-tidal delta or a washover fan. Pocket penetration tests yielded values in the range of 0.2-1.0 kg/cm^2 (Fig. 2).

The beach-barrier facies association is poorly represented in the study cores. It was encountered only in core B1, where this facies assemblage is about 3 m thick (Fig. 2). It consists of fine to coarse sand, typified by an abundance of highly fragmented marine mollusks. Poor preservation of sedimentary structures precludes a clear differentiation between distinct sub-environments, though lower shoreface deposits are assumed to be finer-grained than upper shoreface or foreshore sediment bodies.

5. Key stratigraphic markers

High-resolution stratigraphic data for the study area are presented on two cross-sections in Figures 3 and 4, where 24 stratigraphic logs and 38 piezocone penetration tests have average spacing of ~1000 m. To identify diagnostic marker horizons in the study succession and track them in the subsurface, sediment core stratigraphy was evaluated according to seven criteria: sedimentary characteristics; paleontologic content; age; geotechnical properties; stacking patterns of facies; lateral facies variations; and stratigraphic position relative to other marker beds. Stratigraphically distinct key horizons of almost basin-wide significance were found at five correlatable levels (M1-M5 in Figs. 2, 3 and 4). Three of these (M1, M4, and M5) represent almost flat surfaces at the time of deposition. Precise chronologic constraints to markers M2-M5 derive from a total of 102 radiocarbon dates (Supplementary Table S1). For simplicity, stratigraphic markers will be subsequently denoted in chronologic order.

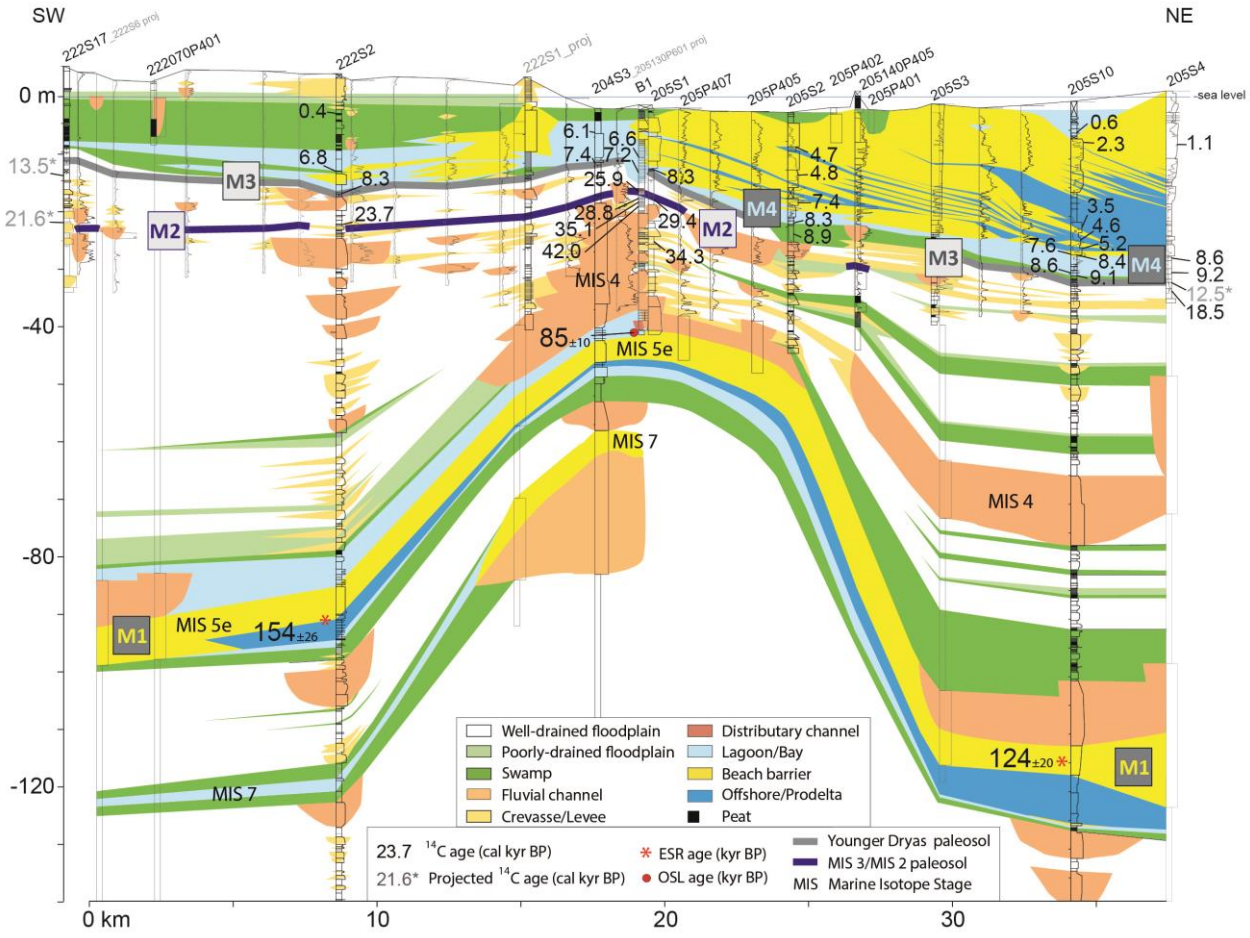

Fig. 3. Stratigraphic correlation panel showing deformation of marker horizons M1-M4 in the Longastrino area. Cores analyzed for paleontology are marked in red. For detailed stratigraphy of core B1, see Fig. 2.

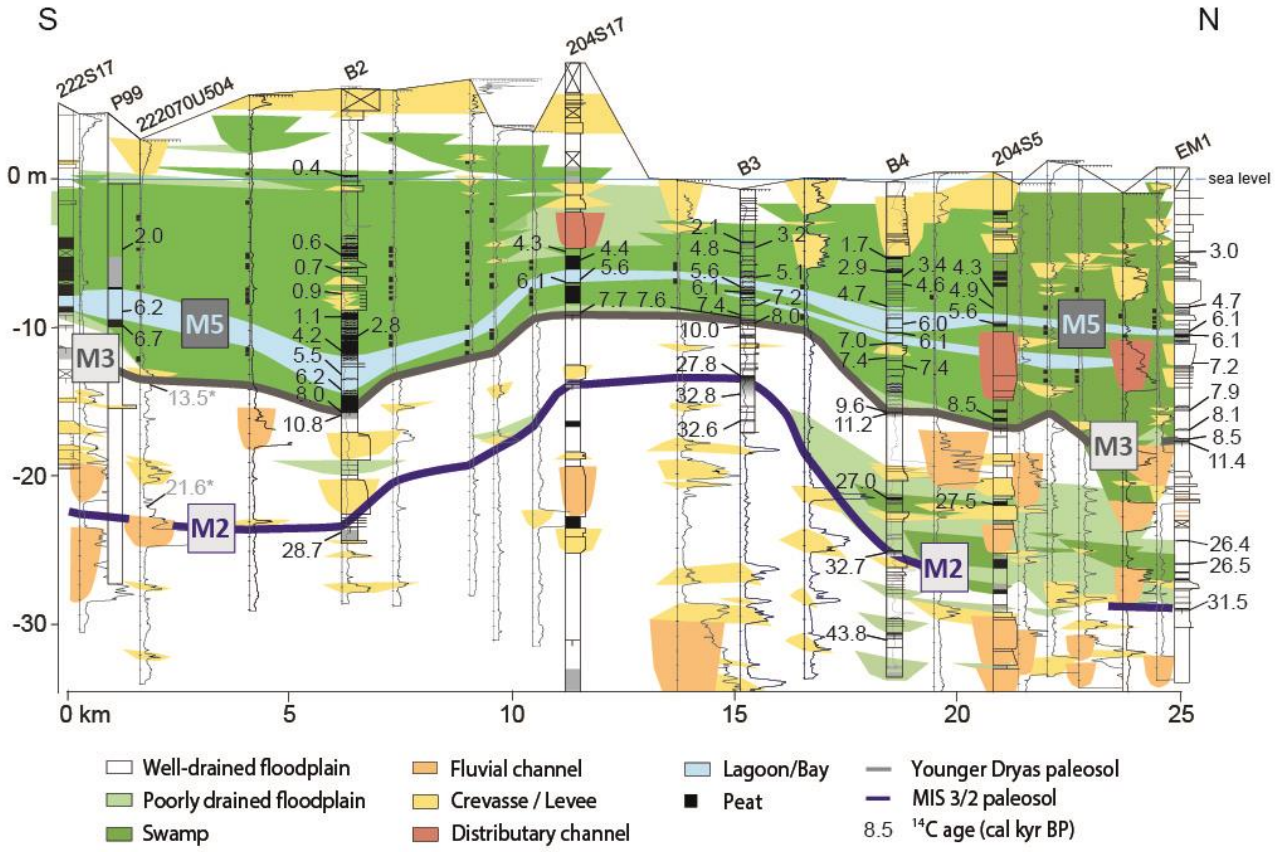

Fig. 4. Stratigraphic correlation panel showing deformation of marker horizons M2, M3, and M5 in the Argenta area. Cores analyzed for paleontology are marked in red. For detailed stratigraphy of cores B2, B3, and B4, see Fig. 2

Marker M1: Last Interglacial beach deposit (Marine Isotope Stage – MIS – 5e)

Last Interglacial (MIS 5e) beach-barrier deposits (marker M1) form a fossiliferous sand body of regional significance, 10-15 m thick, that extends continuously in S-N direction, parallel to the shoreline, and about 40-50 km along dip (Amorosi et al., 2004). This wedge-shaped sediment body formed in response to coastal progradation, when global mean sea-level reached a peak of 5-9 m above present-day sea level, during the MIS 5e highstand (O'Leary et al., 2013).

The Last Interglacial nearshore sand body is easily identified from core data, as it is sandwiched between non-marine deposits. It is typified by an abundance of mollusk shells (Fig. 5A) associated with characteristic shallow-marine foraminifera and ostracoda, such as *Ammonia beccarii*, *Elphidium* spp., and *Pontocythere turbida.* The common occurrence in the sandy deposit of poorly-preserved and size-selected specimens suggests hydraulic sorting by waves and longshore currents in a high-energy coastal paleoenvironment.

Although this sand body accumulated in a variety of coastal sub-environments that may span several meters in depth along the beach profile, marked differences in elevation make it an excellent

stratigraphic marker at the basin scale (Fig. 3). Chronologic constraints to MIS 5e arise primarily from: (i) two ESR absolute ages obtained from cores 222S2 and 205S10 (Ferranti et al., 2006 - Fig. 3); (ii) stratigraphic position (it is the first marine deposit encountered below the Holocene succession), and (iii) pollen spectra (Amorosi et al., 2004): the base of the Last Interglacial succession is typically marked by a major peak in pollen concentration, associated to an abrupt increase in mixed deciduous broad-leaved vegetation, dominated by *Quercus*, and a concomitant decrease in *Pinus* and shrubby–herbaceous communities. A similar signal has been reported from several European pollen series (Helmens, 2014).

In the rapidly subsiding Po Basin, the top of marker M1 commonly occurs at depths of 90-110 m (Fig. 3). In sharp contrast, Pleistocene sands containg a marine microfauna were penetrated in the Longastrino area at depths of just 40 m (cores 204S3 and 205S1 in Fig. 3). In core B1, an OSL date from a distributary-channel deposit above the marine sands yielded an age of 85±10 ky BP (Fig. 3), consistent with a MIS 5a to MIS 5c age attribution. Given that the MIS 5e nearshore sand body provides a reasonably accurate assessment of paleo-sea-level position with an uncertainty < 8 m (Ferranti et al., 2006), the Longastrino ridge in the core B1 area accommodates 40-60 m of vertical separation (Fig. 3) from anticline to syncline positions.

Markers M2 and M3: Late Pleistocene paleosols (29-24 and 13-11 cal kyr BP)

Two pedogenically modified horizons of Late Pleistocene age (M2 and M3 in Figs. 3 and 4) represent key stratigraphic markers across the late Quaternary succession of the Po Plain, because of their basin-wide occurrence and very high correlation potential (Amorosi et al., 2017b; Morelli et al., 2017). These weakly developed paleosols exhibit distinctive A-Bk, A-Bw or A-Bk-Bw profiles (Inceptisols) that make them easily recognizable within the thick non-marine Late Pleistocene succession (Fig. 5B, C). Soil profiles are typified by (i) upper dark grey/black ("A") horizons, with no reaction to hydrochloric acid, that reflect accumulation of organic matter and leaching of $CaCO_3$; (ii) lower, light grey, Ca-enriched ("Bk") horizons, with yellow-brownish mottles due to Fe and Mn oxides, that indicate fluctuating redox conditions with iron dissolution and redeposition (Fig. 5B, C). Markers M2 and M3 are also clearly identified by their geotechnical properties (well-indurated horizons with high pocket penetration values in Fig. 2).

Paleosols M2 and M3 have been chronologically anchored to temporally discrete paleoclimatic events that coincide with rapid shifts from relatively warm to colder phases (Amorosi et al., 2017b). In particular, M2 caps a set of closely-spaced, weakly developed paleosols (Fig. 5B) and spans approximately 29-24 ky BP. It is interpreted to reflect a phase of stepped channel entrenchment that

took place across the MIS 3/2 transition, culminating at the onset of the Last Glacial Maximum. Paleosol M3 was formed, instead, around the Pleistocene-Holocene boundary (13-11 cal ky BP) and correlates, in particular, to the short-lived Younger Dryas cold event. Correlation of markers M2 and M3 relies on radiocarbon-dated bulk-sediment samples from paleosols and on wood and peat from the overlying and underlying overbank facies.

Paleosols M2 and M3 exhibit large differences in vertical elevation across the study area, in the range of 10 m (M3) to 15 m (M2) (Figs. 3 and 4). In the Longastrino area, in particular, the offset of M2 and M3 insists on the underlying deformation of the coastal marker M1 (Fig. 3). The relatively short-lived exposure age of paleosols M2 and M3 resulting from ^{14}C ages (< 5,000 years – Figs. 3 and 4) allows their approximation to isochronous surfaces. While powerful (quasi-synchronous) chronostratigraphic indicators, paleosols M2 and M3 may reflect irregular paleo-reliefs, which represents a main limitation on their use to quantify strata deformation.

Markers M4 and M5: Holocene lagoon deposits (8.6-8.3 and 6.2-5.6 cal kyr BP)

Transgressive deposits of Early-Middle Holocene age include stacked peat layers and fossiliferous horizons with a high correlation potential, formed in inner-estuarine to delta-plain environments (Amorosi et al., 2017a; Bruno et al., 2017; 2019). Two well identifiable lagoon horizons (M4 in Fig. 3 and M5 in Fig. 4) were selected as Holocene marker beds. These key stratigraphic horizons are typified by a distinctive brackish meiofauna and appear to be tilted and/or folded in the Argenta-Longastrino area, with differences in elevation up to 10 m (Figs. 3 and 4).

Markers M4 and M5 show a marked lateral facies variability, characterized by distinct changes in lithofacies characteristics and fossil associations. Inner lagoon clays are dominated by the benthic foraminifera *Trochammina inflata*, whereas central lagoon clays exhibit a brackish oligotypic fauna (Fig. 5C) with an abundance of the ostracod *Cyprideis torosa* and benthic foraminifera *Ammonia tepida, Ammonia parkinsoniana*, and *Haynesina germanica*. This assemblage is a reliable indicator of permanently submerged, semi-enclosed brackish-water basins subject to salinity variations. In contrast, relatively open, brackish to marine conditions are recorded by thinly bedded, sharp-based alternations of fine sand and clay (Fig. 5D), with high species diversity, a dominance of *Ammonia tepida* and *Ammonia parkinsoniana* and the occurrence of lagoon to shallow-marine foraminifera (e.g. *Aubignyna perlucida, Porosononion granosum, Miliolinella* spp., and *Quinqueloculina seminula*).

Stratigraphic markers M4 and M5 provide robust signals of brackish sub-environments in a microtidal (< 1 m) setting. Therefore, they represent excellent indicators of the mean sea-level (with

an uncertainty of 2 m – Scarponi et al., 2013), Due to their limited thickness (< 2 m), they approximate almost perfect horizontal lines at the time of deposition. Marker beds M4 and M5 yielded consistent calibrated ages of 8.6-8.3 ky BP (M4) and 6.2-5.6 ky BP (M5), respectively, from basal peats, wood and shell samples.

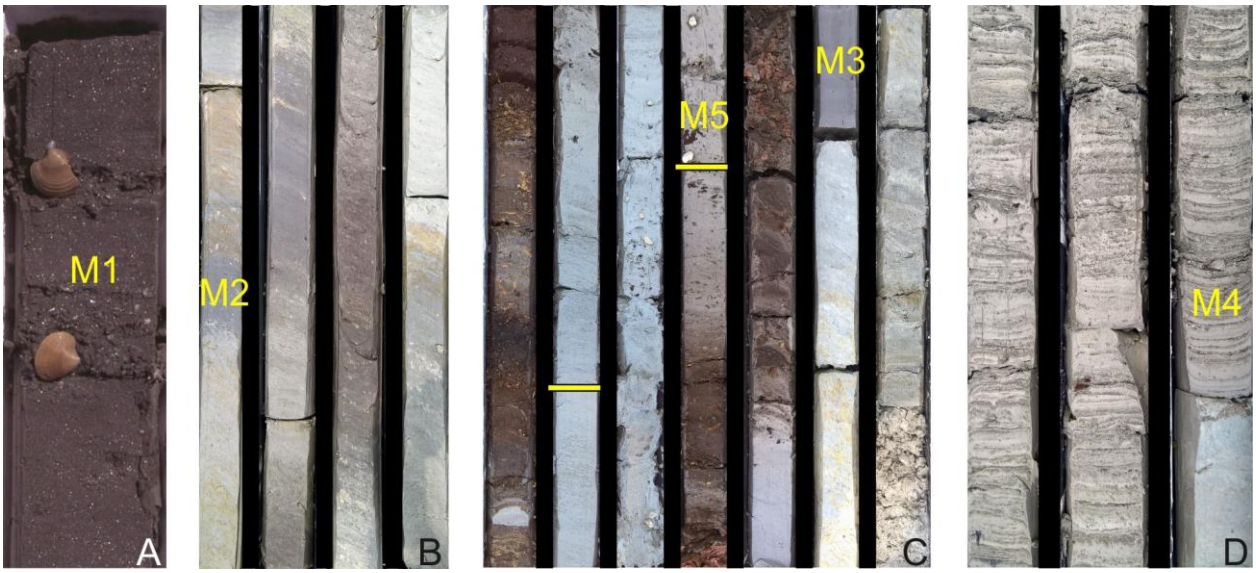

Fig. 5. Representative core photographs of key stratigraphic horizons M1-M5. A) Last Interglacial (MIS 5e) lower shoreface (beach-barrier) fine sands, with abundant mollusk shells (marker M1: core 223-S12, 117-118 m depth – from Amorosi et al., 2004); B) vertically stacked Late Pleistocene Inceptisols (marker M2: core B1, 15-19 m depth; C) Inceptisol marking the Pleistocene-Holocene boundary (marker M3), overlain by a thick swamp peat interval including *Cerastoderma glaucum*-rich lagoon grey clay (marker M5) (core B2, 17-24 core depth); D) bioturbated, fossiliferous clay-sand alternations (marker M4: core B1, 12-15 m depth) on top of Pleistocene floodplain clay deposits. Core bottom is lower right corner. Core width in the photographs is 10 cm. For core locations, see Fig. 1A.

6. Seismic Stratigraphy

Detailed reconstruction of deep stratal architecture in the study area was carried out through the interpretation of 95 2D seismic profiles from the Eni s.p.a. database, after calibration with 45 well logs available online at https://unmig.mise.gov.it/. Analysis and interpretation of seismic profiles focused on the identification of major unconformities and their correlative conformities (Vail et al., 1997).

The main tectonic structures in the subsurface of the Po Plain are well imaged by seismic lines with SSW-NNE orientation, i.e. perpendicular to the strike of major thrusts and anticlines (Fig. 6A). Three basin-scale unconformity-bounded units were identified and classified, based on their geometry and on seismic-reflector terminations: (i) a basal pre-tectonic unit showing parallel seismic reflectors, faulted and folded in the hangingwall; (ii) an intermediate, highly deformed and wedge-shaped syntectonic unit, with seismic reflectors converging towards the culmination of

thrust-related anticlines; and (iii) an upper unit with basin-wide occurrence, draping the whole succession and sealing the buried thrust fronts (Picotti and Pazzaglia, 2008 - Fig. 6A). Based on paleontological data (foraminifera and nannoplancton) available from well-log descriptions, the unconformities that separate these units were assigned to the Messinian and Calabrian, respectively.

According to the ENI stratigraphy (Ghielmi et al., 2013; Amadori et al., 2019), the post-tectonic unit includes two formations (Fig. 6): Carola Formation, of Calabrian age, and Ravenna Formation, of Middle Pleistocene-Holocene age. Within the Ravenna Formation, two unconformities identified on the basis of well log correlation and dated approximately to 0.87 My and 0.4 My (Regione Emilia-Romagna & ENI-AGIP, 1998), respectively, mark the lower boundaries of two minor unconformity-bounded stratigraphic units: Lower Po Synthem and Upper Po Synthem (Amorosi et al., 2008 – Fig. 6A), also referred to as "AEI" and "AES" (Regione Emilia-Romagna & ENI-AGIP, 1998) in the Geologic Map of Italy to 1:50,000 scale. The reader is referred to these studies for detailed description of such units.

Cross-sectional stratal geometries and seismic reflection terminations were used to isolate stratal discontinuities in the study area. Undeformed reflectors with planar onlap terminations onto the lower bounding unconformity are recurrent features in the post-tectonic Carola Formation, at comparatively southern locations (Fig. 6B). In contrast, SW to the structural culminations, onlapping reflectors from the upper Carola and Ravenna formations show distinctive inclined geometries that thin out towards the crest, suggesting they were tilted by the growth of the Longastrino structural high (Fig. 6C). Seismic resolution decreases dramatically atop the Ravenna formation, where the stratigraphic discontinuity at the base of the Lower Po synthem is gently deformed, whereas the base of the Upper Po Synthem seemingly looks as an undisturbed flat surface and can hardly be traced onto the structural high (Fig. 6A).

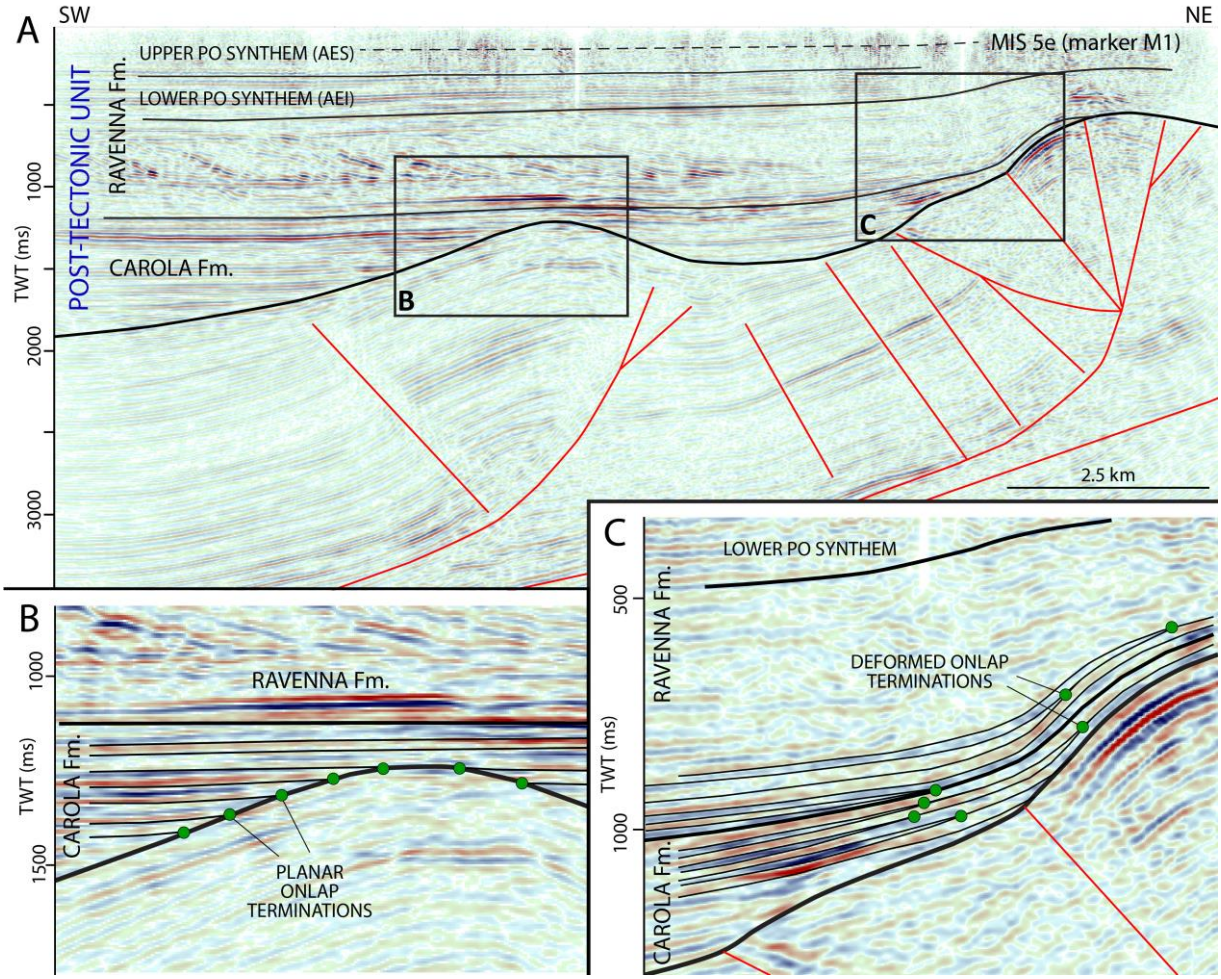

Fig. 6. Interpreted seismic profile in the Longastrino area, showing major tectonic structures and stratal geometries across the Po basin fill. A: seismic stratigraphy of the "post-tectonic unit". B: planar onlap terminations of the post-tectonic succession onto the highly deformed Miocene substrate. C: onlap terminations deformed into a gentle anticline and tilted by the growth of the active thrust front.

7. Can offset of buried stratigraphic markers reveal *LOCI* of active tectonic deformation?

Robust evidence of stratigraphic offsets of laterally extensive key horizons M1-M5 enables the reconstruction of a coherent, high-resolution record of Last Interglacial to Recent deformation focused in the Argenta-Longastrino area (Figs. 3 and 4). To test for possible links between near-surface deformation of stratigraphic markers M1-M5 and active tectonics in the area, the stratigraphic cross-sections of Figures 3 and 4 were plotted against the isobath map at the boundary between Lower and Upper Po Synthems (AEI/AES boundary in the Geological Map of Italy – Figs. 6 and 7). This stratigraphic discontinuity, which is not clearly imaged on seismic profiles (Fig. 6A), represents the youngest (~0.4 My) deformed horizon mapped in the literature in the Po Basin (Martelli et al., 2017).

The large overlap between deformation of recent stratigraphic markers (M1-M5), deformation of older stratigraphic markers (top Lower Po Synthem – Fig. 7), and earthquakes location (Fig. 7) is apparent and provides some support for the hypothesis that part of the observed deformation along the Argenta-Longastrino ridge could be the result of past eartquakes. Historic sources indicate that earthquakes took place in the Po Plain along the Ferrara-Romagna arc since the Roman Period (Stefani et al., 2018). The surface distribution of historical earthquakes points to clustered seismicity around the Mirandola, Ferrara, Argenta, and Longastrino ridges (Fig. 1A). Apart from the two major events in the epicentral area of the 2012 seismic sequence (close to Mirandola), historical and instrumental catalogs report 20 earthquakes with M_w>4.5 (Supplementary Table S2), but earthquakes greater than magnitude 5 are rare in the region (Fig. 1A). Historical data indicate that the nearest recent notable earthquakes occurred near Ferrara (M_w=5.44) and Argenta (M_w=5.43). These earthquakes date back to 1570 and 1624, respectively. The focal mechanisms of all instrumental events associated with the Ferrara arc show prevalent reverse and reverse-oblique kinematics, with P-axes nearly perpendicular to the average structural trend (Lavecchia et al., 2012).

The deformation of marker horizons M1-M5 in the Argenta-Longastrino region (Figs. 3 and 4) is remarkably coincident with the axis of the buried ramp anticline (Fig. 6A). The offsets inferred from the stratigraphic analysis might reflect complex interplay of slip along the buried thrust and associated ramp anticline uplift, as well as differential sediment compaction and loading. Since the anticlinal culmination pre-dates the studied succession, the recognized stratigraphic offset could have been enhanced by sediment compaction in the syncline successions, where highly compressible, swamp (peat-rich) deposits are abundant (Fig. 4).

Partitioning precisely the entire deformation budget into its tectonic (uplifting) and compaction components is problematic and largely beyond the scope of this paper (see Scrocca et al., 2007 and Bresciani and Perotti, 2014, for calculations of relative uplift rates from the adjacent Mirandola and other Quaternary buried anticlines). However, several lines of evidence from different fields (core stratigraphy, seismic stratigraphy, structural geology, seismology) suggest that offset of laterally continuous stratigraphic markers across the Argenta-Longastrino ridge could be, in part at least, the manifestation of active tectonic deformation. Major arguments for a tectonic enhancement of the observed deformation can be summarized, as follows:

(i) The areas of maximum deformation of Late Pleistocene-Holocene stratigraphic markers (Figs. 3 and 4) are strikingly coincident with the epicenters of historic and instrumental seismicity dating back to the last five centuries (Fig. 7).

(ii) The abrupt offset of marker horizons M1-M5 across the Argenta-Longastrino ridge (Figs. 3 and 4) shows strong correspondence with the location of major thrust fronts inferred indipendently from prior geophysical investigations (Figs. 1 and 7).

(iii) The Holocene facies distribution appears to have been strongly influenced by the underlying tectonic structures: in particular, (a) beach-barrier systems are abruptly replaced landwards by unusually thick lagoon deposits, just above the Longastrino ridge (Fig. 3). This suggests a morphologic (tectonic?) control on the Early Holocene landward shift of the shoreline and its subsequent seaward migration; (b) Late Pleistocene swamp deposits have remarkably lenticular geometries that thicken in the synclines and wedge out onto the structural highs (Fig. 4). This indicates that swamp environments occupied the lowest position in the landscape, as an effect of possibly growing, active structures.

(iv) Thrust-related folding of Middle Pleistocene-Holocene marker beds M1-M5 is consistent with the deformation of Lower Pleistocene seismic onlap terminations that elsewhere in the basin exhibit typical planar geometries (Fig. 6).

Further progress is required to constrain the spatial distribution of stratigraphic deformation. Future work should focus on developing an accurate 3D stratigraphic model for the Late Pleistocene-Holocene succession. There is a need, in particular, for comprehensive subsurface mapping of most prominent stratigraphic markers. The reconstructed stratigraphic model of the ramp anticline and its backstripping will serve as a basis for a dislocation model that could on one hand improve the structural definition of the active fault plane, and on the other hand provide a tectonic frame for detailed understanding of the relationships between stratigraphic architecture and co-seismic movements.

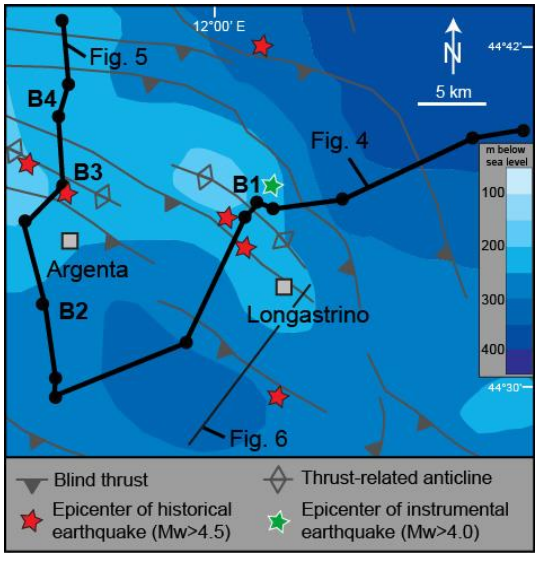

Fig. 7. Subsurface geology of the study area (from Martelli et al., 2017), with isobath map at the Lower/Upper Po Synthem boundary (= AEI/AES boundary, dated to ca. 400 ky BP), and the earthquake catalog of Fig. 1A. *Loci* of maximum deformation of marker horizons M1-M5, around cores B1 (Fig. 3) and B3 (Fig. 4) coincide with the structural culmination atop the Lower Po Synthem north of Argenta and Longastrino.

8. Summary and Outlook

Assessing the seismogenic potential of fault systems beneath alluvial and coastal plains is commonly hindered, especially in actively subsiding basins, by the lack of surface signatures and topographic relief. In such areas, where active tectonics has a poor geomorphic expression and thick Quaternary sedimentary covers preclude calculations of uplifting rates, only loosely constrained inferences on the surface propagation of tectonic deformation are generally available.

This paper has shown that high-resolution core-based stratigraphy used in conjunction with conventional seismic stratigraphy can represent an intriguing technique to assess a decipherable record of near-surface tectonic deformation. The notable deformation of the Last Interglacial nearshore sand body and of a series of prominent stratigraphic markers of Late Pleistocene-Holocene age across structural lineaments of the southern Po Plain correlates closely with seismic observations and historic/instrumental earthquake data. Detailed analysis of seismic-reflector terminations shows clear evidence of syn-tectonic deformation (onlap deformation, decreasing thickness and converging reflectors towards growing anticlines) close to targeted faults. In general, Quaternary deformation is clearly reproducing the general pattern of bedrock folds.

Stratigraphic markers of distinct ages and belonging to different sedimentary facies, were examined: (i) beach-barrier deposits (marker M1) of Last Interglacial age (about 125 ky BP); (ii) two Late Pleistocene paleosols (markers M2 and M3), assigned to the Marine Isotope Stage 3/2 transition (29-24 cal ky BP), and to the Younger Dryas cold spell (13-11 cal ky BP), respectively; and (iii) two Holocene lagoon horizons (M4 and M5), dated to 8.6-8.3 and 6.2-5.6 cal ky BP, respectively.

Beach-barrier and lagoon/outer estuary horizons are the most sensitive indicators of post-burial deformation, as they represent approximately horizontal surfaces at the time of deposition that can be delineated objectively over large portions of the basin. Brackish deposits, in particular, can be easily ascertained on the basis of refined paleontologic criteria and readily differentiated from adjacent freshwater (swamp/inner estuary) and coastal deposits.

In summary, this study documents that high-resolution, near-surface stratigraphy of Late Pleistocene to Holocene successions can have important implications for delineating areas of possible active tectonic deformation. The facies-controlled approach set out in this study is poorly represented in the literature, but might generate models widely applicable to flat, densely populated lowlands beyond the limits of geomorphologic and paleoseismic records.

Acknowledgments

This study was partially supported by the Basic Research Project of the Korean Institute of Geoscience and Mineral Resouces (KIGAM) funded by the Ministry of Science and ICT of Korea.

References

Aitken, M.J. (1985) Thermoluminescence Dating. Academic Press.

Amadori, C., Toscani, G., Di Giulio, A., Maesano, F.E., D'Ambrogi, C., Ghielmi, M. and Fantoni, R. (2019) From cylindrical to non-cylindrical foreland basin: Pliocene-Pleistocene evolution of the Po Plain-Northern Adriatic basin (Italy). *Bas. Res.*, 31, 991–1015.

Amorosi, A., Centineo, M.C., Colalongo, M.L., Pasini, G., Sarti, G. and Vaiani, S.C. (2003) Facies architecture and Latest Pleistocene–Holocene depositional history of the Po Delta (Comacchio area), Italy. *J. Geol.*, 111, 39–56.

Amorosi, A., Colalongo, M.L., Fiorini, F., Fusco, F., Pasini, G., Vaiani, S.C. and Sarti, G. (2004) Palaeogeographic and palaeoclimatic evolution of the Po Plain from 150-ky core records. *Global Planet. Change*, 40, 55–78.

Amorosi, A., Centineo, M.C., Colalongo, M.L. and Fiorini, F. (2005) Millennial-scale depositional cycles from the Holocene of the Po Plain, Italy. *Mar. Geol.*, 222–223, 7–18.

Amorosi, A., Pavesi, M., Ricci Lucchi, M., Sarti, G. and Piccin, A. (2008) Climatic signature of cyclic fluvial architecture from the Quaternary of the central Po plain, Italy. *Sed. Geol.*, 209, 58–68.

Amorosi, A., Bruno, L., Campo, B., Morelli, A., Rossi, V., Scarponi, D., Hong, W., Bohacs, K.M. and Drexler, T.M. (2017a) Global sea-level control on local parasequence architecture from the Holocene record of the Po Plain, Italy. *Mar. Petrol. Geol.*, 87, 99–111.

Amorosi, A., Bruno, L., Cleveland, D.M., Morelli, A. and Hong, W. (2017b) Paleosols and associated channel-belt sand bodies from a continuously subsiding late Quaternary system (Po Basin, Italy): New insights into continental sequence stratigraphy. *Geol. Soc. Am. Bull*., 129, 449–463.

Amorosi, A., Barbieri, G., Bruno, L., Campo, B., Drexler, T.M., Hong, W., Rossi, V., Sammartino, I., Scarponi, D., Vaiani, S.C. and Bohacs, K.M. (2019) Three-fold nature of coastal progradation during the Holocene eustatic highstand, Po Plain, Italy—close correspondence of stratal character with distribution patterns. *Sedimentology*, 66, 3029–3052.

Amorosi, A., Bruno, L., Campo, B., Costagli, B., Dinelli, E., Sammartino, I. and Vaiani, S.C. (2019) Tracing clinothem geometry and sediment pathways in the prograding Holocene Po Delta system through integrated core stratigraphy. *Bas. Res.*, in press.

Audemard, F.A. and Michetti, A.M. (2011) Geologic criteria for evaluating seismicity revisited: Forty years of paleoseismic investigations and the natural record of past earthquakes. In: Geologic criteria for evaluating seismicity revisited: Forty years of paleoseismic investigations and the natural record of past earthquakes (Eds FA Audemard, AM Michetti and JP McCalpin), *Geol. Soc. Am. Sp. Paper* 479, 1–22, Boulder, Colorado.

Azor, A., Keller, E.A. and Robert, S.Y. (2002) Geomorphic indicators of active fold growth: South Mountain–Oak Ridge anticline, Ventura basin, southern California. *Geol. Soc. Am. Bull.* 114, 745–753.

Barbieri, G. and Vaiani, S.C. (2018) Benthic foraminifera or Ostracoda? Comparing the accuracy of palaeoenvironmental indicators from a Pleistocene lagoon of the Romagna coastal plain (Italy). *J. Micropal*. 37, 203-230.

Barka, A., Akyüz, A., Altunel, H.S., Sunal, G., Çakir, Z., Dikbaş, A., Yeli, B., Armijo, R., Meyer, B., de Chabalier, J.B., Rockwel, T., Dolan, J.R., Hartleb, R., Dawson, T., Christoferson, S., Tucker, A., Fumal, T., Langridge, R., Stenner, H., Lettis, W., Bachhuber, J. and Page, W. (2002) The surface rupture and slip distribution of the 17 August 1999 Izmit earthquake (M 7.4), North Anatolian Fault. *Bull. Seismol. Soc. Am.* 92, 43–60.

Bonini, L., Toscani, G. and Seno, S. (2014) Three-dimensional segmentation and different rupture behavior during the 2012 Emilia seismic sequence (Northern Italy). *Tectonophysics*, 630, 33–42.

Bresciani, I. and Perotti, C. R. (2014) An active deformation structure in the Po Plain (N Italy): The Romanengo anticline, Tectonics, 33, 2059–2076.

Bronk Ramsey, C. (2009) Dealing with outliers and offsets in radiocarbon dating. Radiocarbon, *51*, 1023–1045.

Bruno, L., Campo, B., Di Martino, A., Hong, W. and Amorosi, A. (2019) Peat layer accumulation and post-burial deformation during the mid-late Holocene in the Po coastal plain (Northern Italy). Bas. Res. 31, 621–639.

Campo, B., Amorosi, A. and Vaiani, S.C. (2017) Sequence stratigraphy and late Quaternary paleoenvironmental evolution of the Northern Adriatic coastal plain (Italy). *Palaeogeogr. Palaeoclimatol. Palaeoecol.*, 466, 265–278.

Caputo, R., Pellegrinelli, A., Bignami, C., Bondesan, A., Mantovani, A., Stramondo, S. and Russo, P. (2015) High-precision levelling, DInSAR and geomorphological effects in the Emilia 2012 epicentral area. *Geomorphology* 235, 106–117.

Carannante, S., Argnani, A., Massa, M., D'Alema, E., Lovati, S., Moretti, M., Cattaneo, M. and Augliera, P. (2015) The May 20 (Mw 6.1) and 29 (Mw 6.0), 2012, Emilia (Po Plain, northern Italy) earthquakes: New seismotectonic implications from subsurface geology and high-quality hypocenter location. *Tectonophysics* 655, 107–123.

Carminati, E., Martinelli, G. and Severi, P. (2003) Influence of glacial cycles and tectonics on natural subsidence in the Po Plain (northern Italy): Insights from ^{14}C ages. G^3 4, doi: 10.1029/2002GC000481

Debenay, J.P., Guillou, J.J., Redois, F. and Geslin, E. (2000) Distribution trends of foraminiferal assemblages in paralic environments: a base for using foraminifera as bioindicators. In: E*nvironmental Micropaleontology: the Application of Microfossils to Environmental Geology*, (Ed. R.E Martin), Kluwer Academic/Plenum Publishers, New York, 39–67.
DISS Working Group (2018) Database of individual seismogenic sources (DISS), version 3.2.0: A compilation of potential sources for earthquakes larger than M 5.5 in Italy and surrounding areas. Istituto Nazionale di Geofisica e Vulcanologia. https://doi.org/10.6092/INGV.IT-DISS3.2.0. Retrieved from http://diss.rm.ingv.it/diss/

Dura, T., Hemphill-Haley, E., Saway, Y. and Horton, B.P. (2016) The application of diatoms to reconstruct the history of subduction zone earthquakes and tsunamis. *Earth Sci. Rev.* 152, 181–197.

Durcan, J.A., King, G.E. and Duller, G.A.T. (2015) DRAC: Dose rate and age calculator for trapped charge dating. *Quat. Geochron.*, 28, 54–61.

Fantoni, R. and Franciosi, R. (2010), Tectono-sedimentary setting of the Po Plain and Adriatic foreland, *Rend. Fis. Acc. Lincei* 21, 1, S197–S209.

Ferranti, L., Antonioli, F., Mauz, B., Amorosi, A., Dai Pra, G., Mastronuzzi, G., Monaco, C., Orrù, P., Pappalardo, M., Radtke, U., Renda, P., Romano, P., Sansò, P. and Verrubbi, V. (2006) Markers of the last interglacial sea-level high stand along the coast of Italy: Tectonic implications. *Quat. Int.* 145-146, 30–54.

Garzanti, E., Vezzoli, G. and Andò, S. (2011) Paleogeographic and paleodrainage changes during Pleistocene glaciations (Po Plain, Northern Italy). *Earth-Sci. Rev.*, 105, 25–48.

Geological Map of Italy at 1:50,000 scale (Geological Survey of Italy and CARG Project). http://www.isprambiente.gov.it/Media/carg/emilia.html

Ghielmi, M., Minervini, M., Nini, C., Rogledi, S., Rossi, M. and Vignolo, A. (2010) Sedimentary and tectonic evolution in the eastern Po Plain and northern Adriatic Sea area from Messinian to Middle Pleistocene (Italy). *Rend. Fis. Acc. Lincei*, 21, 131–166.

Ghielmi, M., Minervini, M., Nini, C., Rogledi, S. and Rossi, M. (2013) Late Miocene–Middle Pleistocene sequences in the Po Plain–Northern Adriatic Sea (Italy): The stratigraphic record of modification phases affecting a complex foreland basin. *Mar. Petrol. Geol.* 42, 50–81.

Govoni, A., Marchetti, A., De Gori, P., Di Bona, M., Lucente, F.P., Improta, L., Chiarabba, C., Nardi, A., Margheriti, L., Piana Agostinetti, N., Di Giovambattista, R., Latorre, D., Anselmi, M., Ciaccio, M.G, Moretti, M., Castellano, C. and Piccinini, D. (2014) The 2012 Emilia seismic sequence (Northern Italy): Imaging the thrust fault system by accurate aftershock location. *Tectonophysics*, 622(21), 44–55.

Gunderson, K. L., Anastasio, D. J., Pazzaglia, F. J. and Kodama, K. P. (2018) Intrinsically variable blind thrust faulting. *Tectonics*, 37, 1454–1471.

Guerin, G., Mercier, N. and Adamiec, G. (2011) Dose-rate conversion factors. *Ancient TL*, 29, 5-8.

Helmens, K.F. (2014) The Last Interglacial-Glacial cycle (MIS 5-2) re-examined based on long proxy records from central and northern Europe. *Quat. Sci. Rev.* 86, 115–143.

ISIDe Working Group (2015) Italian Seismological Instrumental and parametric Data-base. Istituto Nazionale di Geofisica e Vulcanologia. http://cnt.rm.ingv.it/en/iside.

Keller, E. A. and Pinter, N. (2002) *Active Tectonics: Earthquakes, Uplift, and Landscape*, 2nd edition. Prentice Hall, New Jersey.

Lavecchia, G., de Nardis, R., Cirillo, D., Brozzetti, F. and Boncio, P. (2012) The May-June 2012 Ferrara Arc earthquakes (northern Italy): structural control of the spatial evolution of the seismic sequence and of the surface pattern of coseismic fractures. *Annals of Geophysics,* 55, 533–540.

Livani, M., Scrocca, D., Arecco, P. and Doglioni, C. (2018) Structural and stratigraphic control on salient and recess development along a thrust belt front: The Northern Apennines (Po Plain, Italy). *Journal of Geophysical Research: Solid Earth*, 123(5), 4360–4387.

Maesano, F.E., D'Ambrogi, C., Burrato, P. and Toscani, G. (2015) Slip-rates of blind thrusts in slow deforming areas: Examples from the Po Plain (Italy). *Tectonophysics*, 643, 8–25.

Malinverno, A. and Ryan, W.B.F. (1986) Extension in the Tyrrhenian Sea and shortening in the Apennines as result of arc migration driven by sinking of the litosphere. *Tectonics*, 5, 227–245.

Martelli, L., Bonini, M., Calabrese, L., Corti, G., Ercolessi, G., Molinari, F.C., Piccardi, L., Pondrelli, S., Sani, F. and Severi, P. (2017) The new seismotectonic map of the Emilia-Romagna Region and surrounding areas. GNGTS 2017, Trieste.

Matsu'ura, T. and Sugaya, K. (2017). Late Quaternary crustal shortening rates across thrust systems beneath the Ou Ranges in the NE Japan arc inferred from fluvial terrace deformation. *J. Asian Earth Sci.*, 140,13–30.

Morelli A., Bruno L., Cleveland D.M., Drexler T.M. and Amorosi A. (2017) Reconstructing Last Glacial Maximum and Younger Dryas paleolandscapes through subsurface paleosol stratigraphy: An example from the Po coastal plain, Italy. *Geomorphology* 295, 790–800.

Murray, J.W. (2006) *Ecology and applications of benthic foraminifera*. Cambridge University Press, Cambridge.

Muttoni, G., Carcano, C., Garzanti, E., Ghielmi, M., Piccin, A., Pini, R., Rogledi, S. and Sciunnach, D. (2003) Onset of major Pleistocene glaciations in the Alps. *Geology*, 31, 989–992.

O'Leary M.J., Hearty, P.J., Thompson, W.G., Raymo, M.E., Mitrovica, J.X. and Webster, J.M. (2013) Ice-sheet collapse following a prolonged period of stable sea level during the last interglacial. *Nat. Geo*., 6, 796–800.

Picotti, V., Capozzi, R., Bertozzi, G., Mosca, F., Sitta, A. and Tornaghi M. (2007) The Miocene petroleum system of the Northern Apennines in the central Po Plain (Italy). In: *Thrust belts and foreland basins. From fold Kinematics to Hydrocarbon Systems* (Eds. O. Lacombe, J. Lavé, F. Roure, and J. Vergés), Springer Verlag, 117-131.

Picotti, V. and Pazzaglia, F.J. (2008) A new active tectonic model for the construction of the Northern Apennines mountain front near Bologna (Italy). *J. Geophys. Res.*, 113, B08412.

Pieri, M. and Groppi, G. (1981) Subsurface geological structure of the Po Plain, Italy. In: *Progetto Finalizzato Geodinamica* (Eds. M. Pieri and G. Groppi) 414th edn, pp. 1–23. C.N.R, Roma.

Prentice, C.S., Mann, P., Crone, A.J., Gold, R.D., Hudnut, K.W., Briggs, R.W., Koehler, R.D. and Jean, P. (2010) Seismic hazard of the Enriquillog-Plantain fault in Haiti inferred from palaeoseismology. *Nat. Geo.* 3, 789–793.

Prescott, J. R. and Hutton, J. T. (1994) Cosmic ray contributions to dose rates for luminescence and ESR dating: large depths and long-term time variations. *Radiation Measurements*, 23, 497–500.

Preti, M. (1999) The Holocene transgression and the land-sea interaction south of the Po delta. *Giorn. Geol.* 61, 143–159.

Regione Emilia-Romagna and ENI-AGIP (1998). Riserve idriche sotterranee della Regione Emilia-Romagna. S.EL.CA., Florence.

Reimer, P.J., Bard, E., Bayliss, A., Beck, J.W., Blackwell, P.G., Bronk Ramsey, C., Buck, C.E, Cheng, H., Edwards, R.L., Friedrich, M., Grootes, P.M., Guilderson, T.P., Haflidason, H., Hajdas, I., Hatté, C., Heaton, T.J., Hoffmann, D.L., Hogg, A.G., Hughen, K.A., Kaiser, K.F., Kromer, B., Manning, S.W., Niu, M., Reimer, R.W., Richards, D.A., Scott, E.A., Southon, J.R., Staff, R.A., Turney, C.S.M. and Van Der Plicht, J. (2013) IntCal13 and Marine13 radiocarbon age calibration curves, 0-50,000 years cal BP. Radiocarbon, *55*, 1869–1887.

Ricci Lucchi F. (1986) Oligocene to Recent foreland basins of northern Apennines. In: Foreland Basins (Eds P Allen and P. Homewood), *IAS Special Publication*, 8, 105-139.
Rossi, V. and Vaiani, S.C. (2008) Benthic foraminiferal evidence of sediment supply changes and fluvial drainage reorganization in Holocene deposits of the Po Delta. *Mar. Micropaleontol.*, 69, 106–118.

Rovida, A., Locati, M., Camassi, R., Lolli, B. and Gasperini, P. (2019) Italian Parametric Earthquake Catalogue (CPTI15), version 2.0. Istituto Nazionale di Geofisica e Vulcanologia (INGV). https://doi.org/10.13127/CPTI/CPTI15.2

Royden, L., Patacca, E. and Scandone, P. (1987) Segmentation and configuration of subducted lithosphere in Italy: An important control on thrust-belt and foredeep-basin evolution. *Geology*, 15, 714–717.

Scarponi, D., Kaufman, D., Amorosi, A. and Kowalewski, M. (2013) Sequence stratigraphy and the resolution of the fossil record. *Geology*, 41, 239–242.

Sinha, R., Tandon, S.K., Gibling, M.R., Bhattacharjee, P.S. and Dasgupta A.S. (2005) Late Quaternary geology and alluvial stratigraphy of the Ganga basin. *Himalayan Geol.*, 26, 223–240.

Stefani, M., Minarelli, L., Fontana, A. and Hajdas, I. (2018) Regional deformation of late Quaternary fluvial sediments in the Apennines foreland basin (Emilia, Italy). *Int. J. Earth Sci.* 107, 2433–2447.

Toscani, G., Burrato, P., Di Bucci, D., Seno, S. and Valensise, G. (2009) Plio-Quaternary tectonic evolution of the northern Apennines thrust fronts (Bologna–Ferrara section, Italy): Seismotectonic implications. *Italian Journal of Geosciences*, 128, 605–613.

Supplementary Material

Supplementary Table S1. List of radiocarbon dated samples of Figures 3 and 4. KGM: samples dated at KIGAM Laboratory, South Korea.

Core	Sample depth (m)	Sample code	C14 age	Cal year BP (2σ range)	Cal year BP (mean value)	Material	References	Figure	
B1	9.2	KGM-TWd180564a	6060±30	6720-6500	6610±110	Wood	This paper	2 and 3	
	11.8	KGM-TWd180566a	6580±30	7320-7170	7240±70	Wood	This paper	2 and 3	
	15.1	KGM-TSa180029a	21690±80	26110-25780	25950±160	Organic clay	This paper	2 and 3	
	16.2	KGM-TSa180031a	24820±110	29170-28560	28850±300	Organic clay	This paper	2 and 3	
	16.95	KGM-TSa180032a	31270±160	35550-34760	35150±400	Organic clay	This paper	2 and 3	
	17.7	KGM-TSa180033a	37590±260	42390-41570	41980±400	Organic clay	This paper	2 and 3	
B2	5.8	KGM-TWd180568b	320±20	460-300	380±80	Peat	This paper	2 and 4	
	11.15	KGM-TWd180570a	650±30	610-550	610±30	Wood	This paper	2 and 4	
	12.35	KGM-TWd180571a	730±20	700-660	680±20	Wood	This paper	2 and 4	
	13.8	KGM-TWd180572a	960±40	960-780	860±90	Wood	This paper	2 and 4	
	15.3	KGM-TWd180574a	1190±20	1180-1060	1120±60	Peat	This paper	2 and 4	
	16.6	KGM-TWd180575a	2730±30	2880-2760	2820±60	Wood	This paper	2 and 4	
	17.6	KGM-TWd180576a	3820±30	4341-4140	4220±100	Peat	This paper	2 and 4	
	19.2	KGM-TCa180070a	5030±30	5590-5460	5530±60	Shell	This paper	2 and 4	
	20.25	KGM-TWd180577a	5390±30	6290-6170	6210±60	Wood	This paper	2 and 4	
	21.6	KGM-TWd180578a	7150±30	8020-7930	7970±20	Peat	This paper	2 and 4	
	22.05	KGM-TSa180035a	9500±40	10870-10650	10840±110	Bulk sediment	This paper	2 and 4	
	29.8	KGM-TSa180036a	246300±90	28900-28410	28660±240	Bulk sediment	This paper	2 and 4	
B3	3.55	KGM-TWd190145	2120±20	2160-2000	2090±80	Peat	This paper	2 and 4	
	3.95	KGM- TWd190146	3020±30	3340-3140	3210±100	Peat	This paper	2 and 4	
	4.35	KGM- TWd190147	4250±40	4880-4790	4830±40	Wood	This paper	2 and 4	
	5.95	KGM- TWd190148	4500±30	5300-5040	5170±130	Wood	This paper	2 and 4	
	6.6	KGM- TWd190149	4910±30	5720-5590	5630±60	Wood	This paper	2 and 4	
	6.95	KGM- TWd190150	5330±30	6210-5990	6110±110	Peat	This paper	2 and 4	
	7.9	KGM- TWd190151	6280±30	7210-7160	7210±20	Plant fragment	This paper	2 and 4	
	8.5	KGM- TWd190152	6480±30	7440-7310	7380±60	Peat	This paper	2 and 4	
	8.67	KGM- TWd190153	6780±30	7680-7580	7630±50	Peat	This paper	2 and 4	
	9.85	KGM- TWd190154	7130±40	8020-7920	7960±50	Peaty clay	This paper	2 and 4	
	9.2	KGM-TSa190025	8870±50	10180-9760	10000±210	Bulk sediment	This paper	2 and 4	
	12.6	KGM- TSa190026	23750±140	28130-27580	27820±270	Bulk sediment	This paper	2 and 4	
	13.8	KGM- TSa190027	28700±270	33550-31860	32790±840	Organic Clay	This paper	2 and 4	
	15.6	KGM- TSa190028	28590±200	33300-31840	32630±730	Organic Clay	This paper	2 and 4	
B4	5.15	KGM- TWd190155	1780±20	1810-1610	1700±100	Peat	This paper	2 and 4	
	6.05	KGM- TWd190156	2770±30	2950-2780	2860±80	Peat	This paper	2 and 4	
	6.36	KGM- TWd190157	3230±30	3520-3380	3450±70	Wood	This paper	2 and 4	
	6.9	KGM- TWd190158	4070±30	4650-4430	4560±110	Wood	This paper	2 and 4	
	8.4	KGM- TWd190159	4180±30	4770-4610	4720±80	Wood	This paper	2 and 4	
	9.58	KGM- TWd190161	5240±30	6030-5920	5980±50	Peat	This paper	2 and 4	
	10.1	KGM- TWd190162	5290±30	6190-5990	6080±100	Peat	This paper	2 and 4	
	10.9	KGM- TWd190163	6120±30	7160-6910	7000±120	Peat	This paper	2 and 4	
	11.85	KGM- TWd190164	6440±30	7430-7290	7370±70	Wood	This paper	2 and 4	
	12.4	KGM- TWd190165	6470±30	7440-7320	7380±60	Wood	This paper	2 and 4	
	15.5	KGM- TWd190166	8710±40	9890-9820	9650±30	Wood	This paper	2 and 4	
	15.6	KGM- TSa190029	9780±60	11320-11080	11200±120	Organic Clay	This paper	2 and 4	
	21.3	KGM- TWd190167	22710±90	27350-26690	27080±330	Peat	This paper	2 and 4	
	24.96	KGM- TSa190030a	28660±210	33420-31920	32740±750	Organic Clay	This paper	2 and 4	
	30.85	KGM- TSa190031	40130±450	44620-42980	43760±820	Organic Clay	This paper	2 and 4	
EM1	5.75	KGM-OWd150177	2680±40	3080-2860	2970±110	Peat	Amorosi et al., 2017	4	
	9.50	KGM-OWd150178	4190±40	4770-4605	4690±80	Plant fragment	Amorosi et al., 2017	4	
	11.30	KGM-OWd150179	5630±40	6280-6020	6150±130	Shell	Amorosi et al., 2017	4	
	11.40	KGM-OWd150180	5340±40	6215-5935	6105±110	Wood	Amorosi et al., 2017	4	
	13.30	KGM-OWd150181	6340±50	7335-7165	7250±80	Plant fragment	Amorosi et al., 2017	4	
	16.50	KGM-OWd160062	7040±50	7970-7750	7870±110	Peat	Amorosi et al., 2017	4	
	17.85	KGM-OWd150182	7340±50	8225-8020	8125±100	Wood	Amorosi et al., 2017	4	
	18.40	KGM-OWd160063	7730±50	8600-8410	8510±90	Peat	Amorosi et al., 2017	4	
	18.70	KGM-OSn150001	9950±60	11625-11235	11430±190	Organic clay	Amorosi et al., 2017	4	
	25.3	KGM-TSa180006	22190±100	26740-26090	26400±320	Wood	This paper	4	
	26.90	KGM-OWd150183	22200±120	26840-	26450±390	Wood	Amorosi et al., 2017	4	
	30.1	KGM-TSa180007	27810±150	31940-31210	31520±360	Peaty clay	This paper	4	
P 99	9.5	CAMS-P99_9.5	2000±60	-	1940	Peat	Preti, 1999	4	
	13.5	CAMS-P99_13.5	5600±50	-	6170	Shell	Preti, 1999	4	
	14.5	CAMS-P99_14.5	5870±60	-	6720	Peat	Preti, 1999	4	
204 S3	4.25	KGM-TWd180291	5520±40	6175-5935	6050±120	Plant Fragm.	Amorosi et al., 2019	3	
	9.65	KGM-OCa170047	6760±40	7490-7310	7400±90	Shell Fragm.	This paper	3	
204 S5	8.50	KGM-OWd170533-1	3910±30	4425-4245	4345±90	Plant fragment	Bruno et al., 2019	4	
	9.30	KGM-OWd170534-1	4390±30	5045-4865	4955±90	Plant fragment	Bruno et al., 2019	4	
	10.30	KGM-OWd170535-1	5140±30	5690-5570	5620±60	Plant fragment	Bruno et al., 2019	4	
	16.95	ETH-204S5_16.95	7735±70	8640-8390	8520±120	Wood	Amorosi et al., 2005	4	
	22.70	ETH-204S5_22.7	23320±210	27850-27220	27545±310	Peat	CARG Project, Sheet 204	4	
204 S17	12.8	KGM-OWd170537-1	3850±30	4410-4150	4270±130	Plant fragment	This paper	4	
	13.40	KGM-OWd170538-1	3930±30	4440-4240	4370±100	Plant fragment	This paper	4	
	14.75	KGM-OWd170539-1	5170±30	5720-5590	5630±70	Plant fragment	This paper	4	
	14.95	KGM-OWd170600-1	5530±30	6210-5990	6100±110	Plant fragment	This paper	4	
	17	KGM-OWd170601-1	6840±30	7740-7600	7670±70	Plant fragment	This paper	4	
205 S1	9.80	ETH-205 S1_9.80	7535±70	8450-8185	8335±130	Shell	Amorosi et al., 2003	3	
	14.80	ENEA-205 S1_14.80	25300±180	29860-28870	29365±490	Organic Clay	Amorosi et al., 2003	3	
	24.50	ENEA-205 S1_24.50	30150±520	35260-33350	34260±950	Organic Clay	Amorosi et al., 2003	3	
205 S2	6.05	KGM-OCa160037	4610±40	4805-4515	4660±140	Shell	Amorosi et al., 2019	3	
	10.95	KGM-OCa170048	4480±40	4875-4640	4795±120	Shell	Amorosi et al., 2019	3	
	16.00	KGM-OCa160038	7000±50	7480-7255	7370±70	Shell	This paper	3	
	19.30	KGM-OWd170604	7780±40	8430-8220	8350±100	Plant Fragm.	This paper	3	
	21.15	KGM-OWd170605	7970±40	9000-8650	8840±180	Plant Fragm.	This paper	3	
205 S4	9.30	KGM-OCa170055	1680±40	1220-970	1100±120	Shell Fragm.	Amorosi et al., 2019	3	
	28.80	KGM-OWd170606	8070±50	8870-8480	8650±190	Plant Fragm.	This paper	3	
	31.60	UCIAMS-47525	8485±30	9385-9120	9230±130	Shell	Scarponi et al., 2013	3	
	34.40	ENEA-205 S4_34.40	15280±380	19455-17700	18545±870	Organic Clay	Amorosi et al., 2003	3	
205 S10	5.50	KGM-OWd170607	970±30	720-560	660±80	Plant Fragm.	Amorosi et al., 2019	3	
	7.30	KGM-OCa170051	2540±40	2440-2170	2320±130	Shell	Amorosi et al., 2019	3	
	21.75	KGM-OCa170052	3750±40	3640-3380	3510±40	Shell Fragm.	Amorosi et al., 2019	3	
	24.5	UCIAMS-51673	4590±20	4780-4515	4635±130	Shell	Scarponi et al., 2013	3	
	25.1	UCIAMS-51672	4960±15	5255-4985	5120±130	Shell	Scarponi et al., 2013	3	
	26.70	KGM-OCa170053	7310±50	7780-7530	7640±120	Shell	This paper	3	
	26.85	KGM-OWd170608	7820±40	8460-8310	8390±70	Plant Fragm.	This paper	3	
	29.80	KGM-OWd170610	8010±50	8700-8420	8560±140	Plant Fragm.	This paper	3	
	30.45	KGM-OWd170611	8360±50	9250-8980	9080±130	Plant Fragm.	This paper	3	
205 S14	31.70	Beta Analytic-205 S14_31.70	10480±40	12570-12375	12430±100	Organic Clay	Amorosi et al., 2003	3	proj. in 205 S4
222 S2	7.0	Beta Analytic-222 S2_7.0	340±60	-	400±40	Peat	CARG Project, Sheet 222	3	
	17.0	Beta Analytic-222 S2_17.0	6000±60	-	6850±40	Peat	CARG Project, Sheet 222	3	
	20.9	Beta Analytic-222 S2_20.9	7420±60	-	8270±40	Organic Clay	CARG Project, Sheet 222	3	
	26.2	Beta Analytic-222 S2_26.2	19770±150	-	23660±490	Peat	CARG Project, Sheet 222	3	
222 S6	18.8	Beta Analytic-222 S2_18.8	11560±60	-	13445±190	Organic Clay	CARG Project, Sheet 222	3 and 4	proj. in 222 S17 and 222070U504
	26.8	Beta Analytic-222 S2_26.8	18000±150	-	21590±500	Peat	CARG Project, Sheet 222	3 and 4	proj. in 222 S17 and 222070U504

Supplementary Table S2. List of historical and instrumental earthquakes reported in Figure 1.

Year	Epicentral Area	Latitude N	Longitude E	Magnitude (Mw)	Historical/ Instrumental	Reference
1234	Ferrara	44,835	11,620	5,10	Historical	CPTI15
1285	Ferrara	44,835	11,620	5,10	Historical	CPTI15
1339	Ferrara	44,835	11,620	4,63	Historical	CPTI15
1365	Bologna	44,494	11,343	5,33	Historical	CPTI15
1409	Ferrara	44,835	11,620	4,63	Historical	CPTI15
1410	Ferrara	44,835	11,620	4,86	Historical	CPTI15
1411	Ferrara	44,835	11,620	5,10	Historical	CPTI15
1425	Ferrarese	44,835	11,620	4,63	Historical	CPTI15
1433	Bologna	44,494	11,343	4,63	Historical	CPTI15
1504	Bolognese	44,494	11,343	5,02	Historical	CPTI15
1505	Bolognese	44,507	11,230	5,62	Historical	CPTI15
1505	Bolognese	44,494	11,343	4,76	Historical	CPTI15
1570	Ferrarese	44,824	11,632	5,44	Historical	CPTI15
1574	Finale Emilia	44,833	11,294	4,63	Historical	CPTI15
1620	Ravennate	44,517	12,017	4,86	Historical	CPTI15
1624	Argenta	44,642	11,848	5,43	Historical	CPTI15
1639	Finale Emilia	44,833	11,294	5,33	Historical	CPTI15
1688	Romagna	44,390	11,942	5,84	Historical	CPTI15
1743	Ferrara	44,835	11,620	4,86	Historical	CPTI15
1779	Bolognese	44,443	11,479	5,22	Historical	CPTI15
1779	Bolognese	44,424	11,529	4,70	Historical	CPTI15
1780	Bolognese	44,567	11,310	5,06	Historical	CPTI15
1787	Ferrara	44,835	11,620	4,86	Historical	CPTI15
1796	Emilia orientale	44,614	11,670	5,45	Historical	CPTI15
1796	Emilia orientale	44,614	11,670	5,45	Historical	CPTI15
1801	Bolognese	44,466	11,421	4,90	Historical	CPTI15
1834	Bolognese	44,479	11,320	4,71	Historical	CPTI15
1878	Bolognese	44,424	11,543	4,84	Historical	CPTI15
1895	Comacchio	44,721	12,017	4,65	Historical	CPTI15
1898	Romagna settentrionale	44,657	11,821	4,59	Historical	CPTI15
1898	Romagna settentrionale	44,657	11,821	4,59	Historical	CPTI15
1909	Emilia Romagna orientale	44,579	11,688	5,36	Historical	CPTI15
1929	Bolognese	44,445	11,387	5,05	Historical	CPTI15
1929	Bolognese	44,539	11,478	4,82	Instrumental	CPTI15
1929	Bolognese	44,496	11,202	5,13	Historical	CPTI15
1931	Ferrarese	44,821	11,764	4,74	Historical	CPTI15
1931	Modenese	44,541	11,022	4,59	Historical	CPTI15
1956	Argenta	44,621	11,982	4,96	Historical	CPTI15
1963	Romagna	44,416	11,977	5,23	Instrumental	CPTI15
1967	Emilia Romagna orientale	44,604	11,997	5,05	Instrumental	CPTI15
1970	Adriatico settentrionale	44,600	12,500	4,57	Instrumental	CPTI15
2012	Pianura emiliana	44,895	11,263	6,09	Instrumental	ISIDE; CPTI15
2012	Pianura emiliana	44,905	11,165	4,95	Instrumental	ISIDE; CPTI15
2012	Pianura emiliana	44,873	11,270	5,17	Instrumental	ISIDE; CPTI15
2012	Pianura emiliana	44,859	11,152	5,04	Instrumental	ISIDE; CPTI15
2012	Pianura emiliana	44,813	11,440	5,16	Instrumental	ISIDE; CPTI15
2012	Pianura emiliana	44,879	11,253	4,56	Instrumental	ISIDE; CPTI15
2012	Pianura emiliana	44,841	11,065	5,90	Instrumental	ISIDE; CPTI15
2012	Pianura emiliana	44,883	11,041	4,64	Instrumental	ISIDE; CPTI15
2012	Pianura emiliana	44,873	11,120	4,95	Instrumental	ISIDE; CPTI15

4.2 Paper 2

Deformed stratigraphic markers from the late Quaternary succession of the Po Plain and their relation to buried tectonic structures

Bianca Costagli, Luigi Bruno, Alessandro Amorosi.

Geomorphology

Submitted to Geomorphology

Deformed stratigraphic markers from the late Quaternary succession of the Po Plain and their relation to buried tectonic structures

Bianca Costagli[1], Luigi Bruno[2], Alessandro Amorosi[1].

[1]*Department of Biological, Geological and Environmental Sciences, University of Bologna, Via Zamboni 67, 40126, Bologna, Italy.*

[2]*Department of Chemical and Geological Sciences, University of Modena and Reggio Emilia, Via Campi 103, 41125 Modena, Italy*

Abstract

Deformation patterns of three shallow stratigraphic markers of Late Pleistocene to Holocene age and their relation to deep blind tectonic structures was examined on a sub-seismic scale over a 1500 km^2 wide area of the SE Po Plain. Two Late Pleistocene paleosols, formed at the onset of the Last Glacial Maximum and during the Younger Dryas cold event, respectively, and a mid-Holocene, thin lagoon horizon were mapped, based primarily on facies analysis of 64 cores and stratigraphic interpretation of 442 piezocone tests framed into a chronologically constrained stratigraphic model with 140 radiocarbon dates. The three stratigraphic markers record remarkable and consistent deformation in an area supposed to be unaffected by recent tectonic activity, with maximum values above the blind thrusts. Spatial changes in stratigraphic architecture and folding of key marker horizons also coincide with the spatial distribution of historical and instrumental earthquakes in the area. Stratigraphic deformation was likely impacted by the combination of tectonic activity and differential sediment compaction along the buried structures.

Keywords: Stratigraphic marker, Deformation; Paleosol; Quaternary; Po Plain.

1. Introduction

The Po Plain, one of the largest alluvial plains in Europe, has long been considered a low seismic-risk area until May 2012, when an earthquake sequence, with two mainshocks (M_w=6.1 and M_w=5.9 - Anzidei et al., 2012; Carannante et al., 2015; Govoni et al., 2014), followed by several aftershocks (up to M_w 5.1) hit the area, resulting in loss of human life, injury, and severe damage to buildings and infrastructures. The earthquake sequence was generated by the most external thrusts of the Northern Apennines that are now buried below the alluvial plain (Pieri and Groppi, 1981). Instrumental (INGV Instrumental Bulletin, http://bollettinosimico.rm.ingv.it) and historical (Rovida et al., 2011) seismicity data testify to significant past seismic events in the area. However, poor or no associated geomorphological evidence of recent tectonic activity in the Po Plain has been reported in the literature, with very few exceptions (Burrato et al, 2003).

High-resolution stratigraphic studies beneath modern alluvial and coastal plains based on sediment core correlations have led to detailed reconstructions of Late Pleistocene-Holocene stratigraphic successions. Distinct types of stratigraphic markers have been traced in the subsurface over tens of kilometers: fluvial channel-belt sand bodies (Lavé and Avouac, 2000; Cohen et al., 2002; Stefani and Vincenzi 2005; Picotti and Pazzaglia, 2008; Wilson et al., 2009; Stefani et al., 2018), weakly developed paleosols (Amorosi et al., 2014; 2015; 2017a; Tsatskin et al.,2015) and marine flooding surfaces with their lateral equivalents (Törnqvist et al., 2008; Piovan et al., 2012; Chamberlain et al., 2018). Due to their remarkable lateral extent, peat horizons of mid-late Holocene age intercalated with overbank fine sediments have also been used for stratigraphic correlations (Campo et al., 2017; Bruno et al., 2019).

In the Po Plain, sparse geological cross-sections across the major tectonic structures have highlighted the local deformation of Late Pleistocene to Holocene marker beds above the culminations of the buried thrust-related anticlines (Amorosi et al., 2017a; in press; Stefani et al., 2018; Bruno et al., 2019; in press). However, these studies addressed the link between structural development and sedimentary architecture in 2D only, without considering 3D variations, nor providing a 3D representation of the geometry of buried stratigraphic markers. In this study, stratigraphic correlations of selected Late Pleistocene and Holocene marker beds allowed for the first time 3D detailed examination of stratigraphic deformation over a large portion of the Po Basin (1500 km^2), between Ferrara and Ravenna (Fig. 1a). Our specific aim is to assess the link between observed stratigraphic deformation and the location of buried tectonic structures through subsurface mapping.

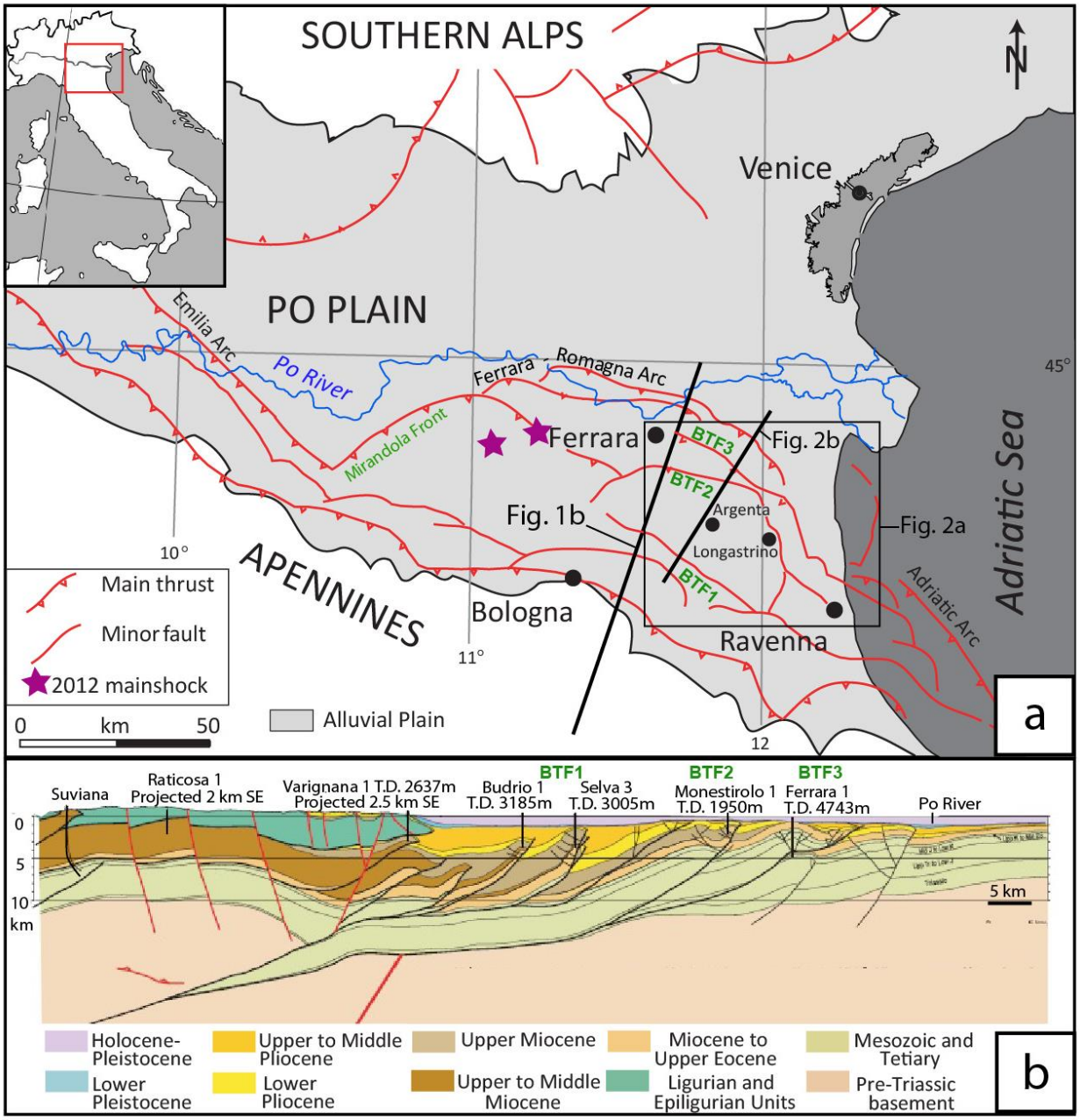

Fig. 1. (a) The Po Plain, with location of the Apennine and Alpine blind thrusts (red lines). The section traces of Figs. 1b and 2b are also shown. The study area (Figs. 2 and 5) is bordered by a black box. (b) Fold-and-thrust belt buried structures beneath the Po Plain (modified after Picotti and Pazzaglia., 2008; see Fig. 1a for location). The red faults represent active features, normal faults at the surface and compressional structures in the middle crust (modified from Picotti and Pazzaglia, 2008). BTF: buried thrust front

2. Geological setting

2.1 Structural setting

The Po Plain, bounded by the Apennines to the south and by the Alps to the north, is the surface expression of the Po Basin, a sedimentary basin developed atop a system of blind thrusts (Pieri and Groppi, 1981) that represent the most external structures of the Alpine and Apennine chains (Fig.

1b). The buried thrust front of the northern Apennines is composed of north-verging thrusts arranged in four asymmetric arcs: from west to east, Monferrato Arc, Emilia Arc, Ferrara-Romagna Arc, and Adriatic Arc (Fig. 1a - Pieri and Groppi, 1981). The Ferrara-Romagna Arc is in turn subdivided into three main buried fold-thrust systems (BTF 1-3 in Fig. 1): (i) BTF1 is located in the Budrio area (Fig. 1b); its SE prolongation, south of Ravenna, is the Cotignola thrust system. (ii) BTF2 corresponds to the Longastrino thrust front; its prolongation to the NW is the Mirandola thrust system, which was active during the 2012 earthquakes. (iii) BTF3 (Ferrara-Casaglia thrust) is the most external buried thrust front. Thrusts SE of Ferrara have been active since the Early Pliocene (Toscani et al., 2009; Burrato et al., 2003; Boccaletti et al., 2011).

The study area is centered above BTF2 (Fig. 2a): this buried thrust front consists of a series of closely-spaced, imbricated and NE-verging thrusts, locally associated with back-thrusts (Fig. 2b). Two major unconformities, dated to 5.5 and 1.5 Myr, mark approximately the base of the Pliocene and of the Quaternary, respectively (Fig. 2b – Ghielmi et al., 2013). The 1.5 Myr unconformity depicts a major fold, with a wavelength of ~30 km resulting from faults propagation and imbrication. Lower-rank folds, with wavelengths of ~3-5 km, associated with single-fault propagation, are highlighted, instead, by the 5.5 Myr unconformity (Fig. 2b). The thickness of the post-1.5 Myr succession ranges between 300 m (at the culmination of the main anticline) and 2,000 m (in the syncline depocentres – Fig. 2b).

The main phase of tectonic activity of these structures has been dated to the Late Miocene-Early Pliocene (Picotti et al., 2009), based on seismic data. Younger strata appear, instead, to be poorly affected (or unaffected) by stratigraphic deformation, and Late Pliocene-Holocene tectonic activity has been considered negligible.

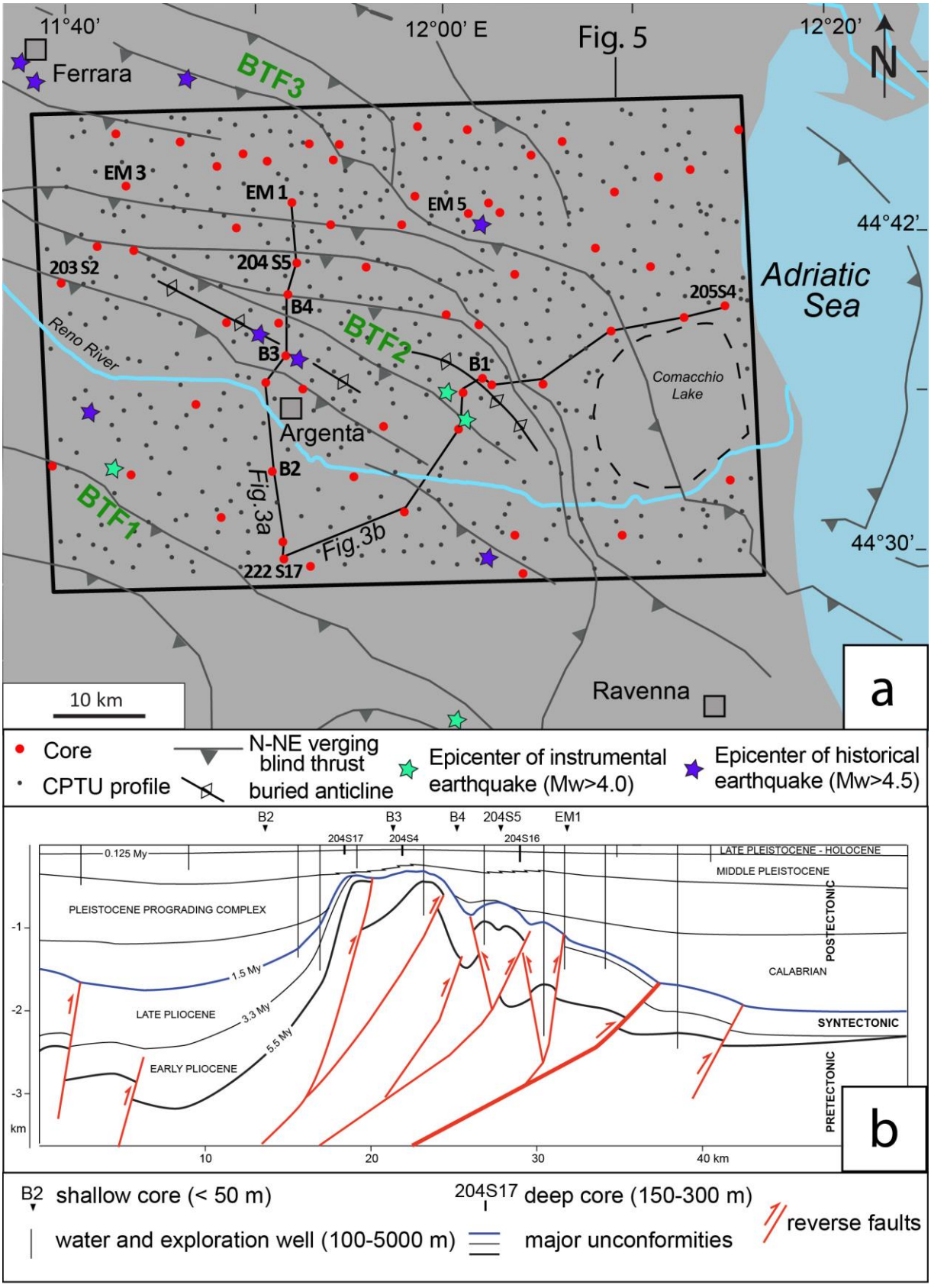

Fig. 2. (a) Study area, with location of the stratigraphic data discussed in the text. Section traces of Fig. 3 are also shown. BTF: buried thrust front. (b) Interpreted seismic profile across the buried thrust fronts (from Bruno et al., in press).

2.2 Stratigraphic framework

The Late Pliocene-Holocene basin fill exceeds 7,000 meters in the depocentres and is less than 500 m-thick above the thrust-related anticlines (Pieri and Groppi, 1981; Castellarin et al., 1985). The topmost portion of the basin fill, Middle Pleistocene-Holocene in age, consists of alternating alluvial and coastal deposits that reflect prominent 100 kyr (Milankovitch)-scale cyclicity (Amorosi et al., 2004; 2008).

Late Pleistocene (> 11.5 cal kyr BP) deposits in the Po coastal plain are dominated by a thick succession of well-drained overbank fines (floodplain silts and clays) that commonly includes lens-shaped, fluvial-channel sand bodies (Fig. 3a, b). Directly overlying Late Pleistocene alluvial facies is the 15-30 m-thick, Holocene transgressive-regressive succession. This stratigraphic interval has the greatest lateral variability in sedimentary architecture and displays an increasing marine influence toward the east (Fig. 3b): in a relatively proximal setting, the Holocene succession is dominated by lagoon and swamp (estuarine and delta plain) deposits that distally grade into a coastal wedge made up of beach barrier, offshore and prodelta facies. In a sequence-stratigraphic perspective, Holocene deposits reflect well-constrained balance between accommodation and sediment supply (Bruno et al., 2017a) and include an early Holocene transgressive systems tract (TST) and an overlying, middle-late Holocene highstand systems tract (HST) (Amorosi et al., 2017b; 2019; Bruno et al., 2017b).

The Holocene succession has been subdivided into eight lower-rank cycles (parasequences), reflecting millennial-scale cyclicity (Amorosi et al., 2017b). Three major flooding surfaces and their landward equivalents have been recognized within the TST and dated to about 11.5, 9.2 and 7.7 kyr BP, respectively. These surfaces mark the base of three transgressive parasequences that developed in response to the eustatic rise (Bruno et al., 2017b). On the other hand, HST parasequences have been interpreted to reflect predominantly autogenic control due to river avulsion and delta lobe abandonment (Amorosi et al., 2017b).

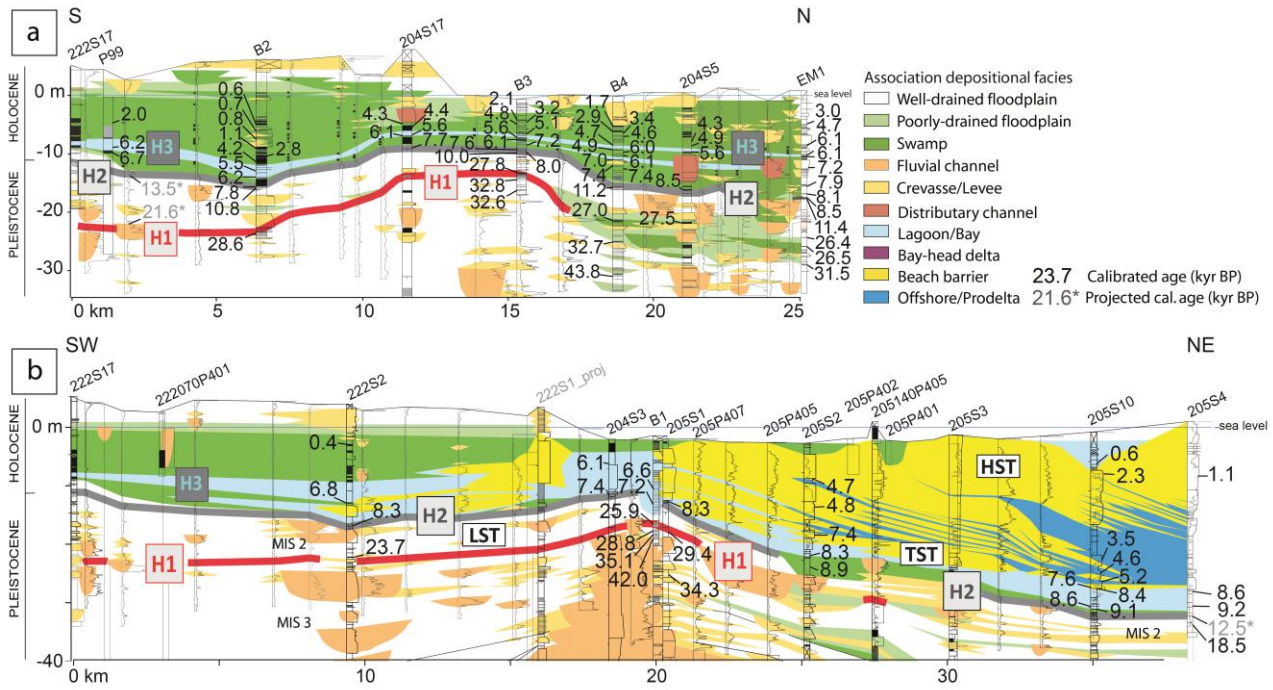

Fig. 3. Stratigraphic cross-sections across the study area (from Amorosi et al., in press), showing facies architecture of the Late Pleistocene-Holocene succession and deformation of prominent stratigraphic markers H1-H3 (see Fig. 2a, for location).

3. Materials and Methods

In this work, we examined a 1500 km^2 wide area in the SE Po Plain, between Ferrara and Ravenna (Fig. 2a). Sixty-four core logs (20-204 depth) and 442 piezocone penetration tests (CPTUs) served as a basis for the identification and mapping of key stratigraphic markers. Four sediment cores (B1-B4 in Fig. 3), 17-35 m long, were recovered between May and October 2018 and utilized for detailed facies characterization. Piezocone tests were interpreted based on Amorosi et al. (2017a) and Bruno et al. (2019), following stratigraphic calibration with nearby cores. The chronostratigraphic framework was ensured by 140 radiocarbon dates that were employed to improve log-to-log correlations: 125 radiocarbon dates were taken from the literature (Preti 1999; Amorosi et al., 2005; 2008; 2017a, b; 2019; Scarponi et al., 2013; Campo et al., 2017; Bruno et al., 2019), whereas 15 are from the Emilia-Romagna Geological Survey database, available at the following link http://ambiente.regione.emilia-romagna.it/it/geologia/cartografia/webgis-banchedati.

This contribution is not intended to provide a detailed sedimentological analysis of the study area, but rather to highlight the geometry of selected stratigraphic markers (see below). For the detailed characterization of facies assemblages, the reader is referred to Amorosi et al. (2017b).

In order to reconstruct 3D maps of stratigraphic markers, a grid of cross-sections was generated and analyzed through the software package Petrel 2014. Isobath maps of distinct key horizons were constructed using the convergent interpolation algorithm, which takes into account a set of randomly distributed scattered points and computes an output grid showing a high-quality model representation of the input data. This type of algorithm adapts to a sparse or dense data distribution through converging iterations at finer grid resolution. Finally, the surfaces were manually modified, especially where data resolution was insufficient to generate a reliable interpretation.

4. Key stratigraphic markers

Three laterally extensive key horizons (H1-H3 in Figs. 3), reported for the first time in previous studies (Amorosi et al., 2017a; in press; Bruno et al., 2019), were chosen as key surfaces for stratigraphic correlation. These stratigraphic markers, of almost basin-wide significance, were first identified in core (Fig. 4) and then tracked laterally with the aid of radiocarbon dating, on the basis of core characteristics and diagnostic stratigraphic position. Markers H1 and H2 are pedogenically modified horizons of Late Pleistocene age (Amorosi et al., 2017a; Morelli et al., 2017). H1, in particular, has been dated to 30-24 cal kyr BP, whereas H2 has been assigned to 12.9-11.7 cal kyr BP. Marker H3 is a stratigraphic horizon of mid-Holocene age (6.2-5.6 cal kyr BP), made up of swamp peat (layer T1 in Bruno et al., 2019) grading seawards into a brackish horizon.

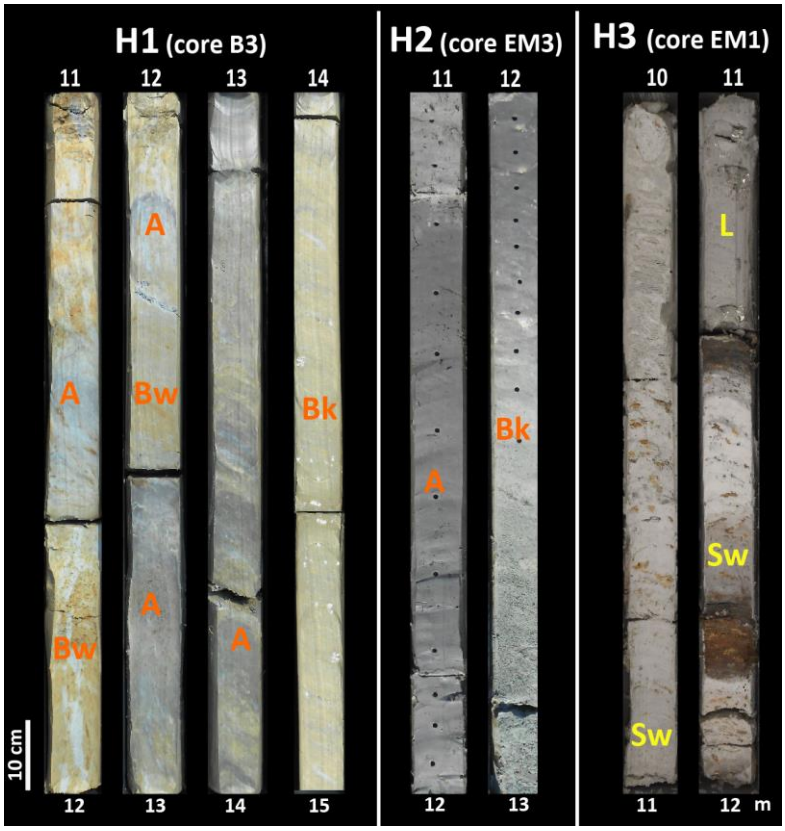

Fig. 4. Representative core photographs of key stratigraphic markers H1-H3. (a) Thick pedogenized interval with a compound soil profile (core B2 - see Fig. 2a, for location). (b) Weakly developed paleosol, with typical A-Bk profile (core EM3 - see Fig. 2a, for location). (c) 30-cm thick lagoon horizon (L) sandwiched between peat-rich swamp deposits (core EM1 - see Fig. 2a, for location).

4.1 Key horizon H1 (30-24 cal ky BP)

Key horizon H1, marked in red in Fig. 3, is observed atop a laterally continuous package, a few meters thick, of vertically stacked, weakly-developed paleosols that are separated by thin overbank deposits (Fig. 4a). Individual paleosols, 0.5-1.5 m thick, are typified by (i) upper dark grey-brownish "A" horizons, with no reaction to hydrochloric acid, that reflect the accumulation of organic matter and leaching of $CaCO_3$; (ii) lower light grey, Ca-enriched ("Bk") horizons, with yellow-brownish mottles due to Fe and Mn oxides that reflect fluctuating redox conditions with iron dissolution and redeposition; (iii) "Bw" horizons, generally ranging from greyish brown to yellowish brown. In CPTU tests, H1 is characterized by a distinctive down-profile increase in cone tip resistance and lateral friction (both are suggestive of overconsolidation) and by an abrupt decrease in pore pressure (Amorosi et al., 2017a). In core descriptions, this paleosol is generally marked by high (>3.5 kg/cm^2) pocket penetration values. This key surface has a high correlation potential.

H1 is anchored to a paleoclimatic event that coincides with the rapid shift from a warm to colder phase. In particular, it has been assigned to the Marine Isotope Stage 3/2 transition, i.e. the onset of

the Last Glacial Maximum (Amorosi et al., 2017a). Its compound soil profile (Kraus, 1999) and the local occurrence of intercalated overbank deposits suggest that soil-forming processes around the MIS 3-2 transition were repeatedly interrupted by alluviation in a continuously accommodating system, and that soils had relatively short time intervals in which to form (Flaig et al., 2013), implying continuous generation of accommodation.

4.2 Key horizon H2 (12.9-11.7 cal ky BP)

Paleosol H2, marked in gray in Fig. 3, has a very high correlation potential and invariably separates well-drained alluvial Pleistocene deposits from overlying, poorly drained floodplain to organic-rich, freshwater swamp facies of Holocene age (Fig. 3) that reflect increased accommodation rates (Bruno et al, 2017a). This stratigraphic marker displays relatively flat to slightly undulating geometry and has specific sequence-stratigraphic significance, as it separates the lowstand systems tract (LST) from TST, thus coinciding with the transgressive surface (Fig. 3 - Amorosi et al., 2016). This paleosol is about 1.0-1.5 m thick and shows a characteristic single profile (Fig. 4b). Like for H1, H2 exhibits a typical A-Bk profile (Fig. 4b) and has diagnostic CPTU signature, marking the boundary between unconsolidated or poorly consolidated deposits of Holocene age and underlying, stiff Pleistocene alluvial facies. The origin of this paleosol has been inferred to reflect a short-lived phase of fluvial incision related to the onset of the Younger Dryas cold event (Amorosi et al., 2017a).

4.3 Key horizon H3 (6.2-5.6 cal kyr BP)

Peat layers from the mid-late Holocene succession of the Po coastal plain display a high correlation potential (Bruno et al., 2019). In this study, we took as key horizon H3 a laterally extensive peat layer identified by Bruno et al. (2019), which grades distally into a brackish clay horizon, less than 1 m thick (L in Fig. 4c), with relatively little variation in grain size (light blue color in Fig. 3). H3 consist of soft, grey silt and clay with an abundance of shell fragments, rare vegetal remains and a lack of iron and manganese oxides and carbonate concretions (Fig. 4c). It is typically sandwiched between thick swamp clay intervals (Sw in Fig.4c), rich in wood fragments. This fossiliferous horizon can be readily identified in core by the diagnostic presence of brackish mollusks and ostracods. This marker is a reliable indicator of post-burial deformation, as it formed in a low-gradient coastal plain environment (Giacomelli et al., 2018; Bruno et al., 2019), and thus can be assumed as horizontal at the time of its deposition. The disadvantage of this type of marker is its relatively limited areal extent: it is replaced by coeval nearshore sands at distal locations and by alluvial deposits in a proximal position (Fig. 3).

5. Subsurface mapping

Three stratigraphically distinct key horizons (H1-H3) were identified over a wide area of the Po Plain, between Ferrara and Ravenna; these marker beds were correlated over tens of kilometers (Fig. 5). Three isobaths maps were generated connecting all points having the same elevation above sea level (Fig. 5). A summary description of the three maps is provided below.

5.1 H1 map (Fig. 5a)

The morphology of marker H1, reconstructed through the correlation of 307 stratigraphic data in a dense network of cross-sections, is represented through 3 m-spaced contour lines ranging between 0 and -40 m above sea level (asl). The elevation of H1 decreases towards NE. In the northern part of the study area, paleosol H1 is replaced by the genetically related fluvial channel-belt sand body of the Po River (Amorosi et al., 2017a). Maximum elevations are observed in the SW corner of the study area, above BTF1. An intensely deformed area, corresponding to the culmination of the Longastrino anticline (BTF2), is observed north of Argenta, in coincidence of cores B3 and B1. On the other hand, H1 was found to be 10 m lower in syncline areas.

5.2 H2 map (Fig. 5b)

The morphology of the Younger Dryas paleo-landscape is represented through 3 m-spaced contour lines ranging between 0 and -35 m asl. The geometry of H2, which was reconstructed through the analysis of 436 data, shares many similarities with that of H1: (i) an overall progressive deepening, from SW to NE; (ii) maximum elevation in coincidence with the north-verging BTF1; (iii) significant deformation just above above the Longastrino thrust front (BTF2), as shown by cores B3 and B1, with development of an anticline structure.

5.3 H3 map (Fig. 5c)

The geometry of H3, which is a freshwater peat layer west of Argenta and a brackish horizon to the east, was reconstructed through the analysis of 286 stratigraphic data and is represented through 2 m-spaced contour lines ranging between -5 and -14 m asl. Coastal sands and shallow-marine deposits replace the thin lagoon horizon in a relatively distal (eastern) setting (see Fig. 3), whereas the coeval peat deposits grade into alluvial plain deposits at more proximal (western) locations. Like for H1 and H2, the maximum elevation of this stratigraphic marker is encountered above the

thrust-related anticline of BTF2, between cores B3 and B1, whereas it is 5 m lower in the adjacent synclines.

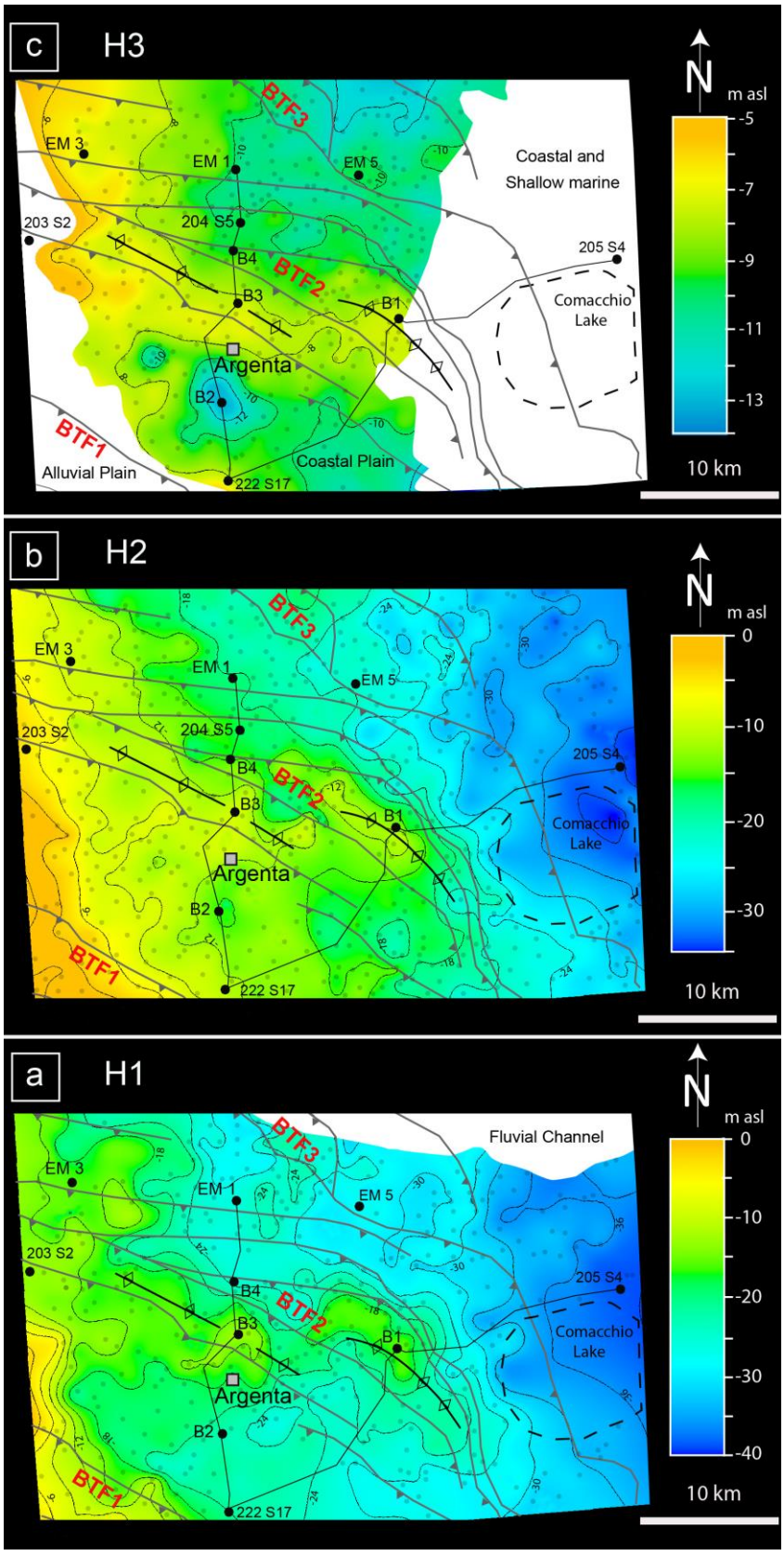

Fig. 5. Three-dimensional geometry of marker beds H1-H3 in the study area and their relation to the buried thrust fronts (BTFs).

6. Linking stratigraphic deformation and structural mechanisms

Subsurface mapping greatly aids visualization of the morphology of deformed markers H1, H2, and H3. The three marker beds exhibit a similar geometry irrespective of their stratigraphic position, and delineate a simple style of deformation. with a consistent dipping trend toward the E/NE and two deformation zones, characterized by two anticline structures (Fig. 5). If projected into a broader context, the most intensely deformed areas presented here clearly follow the regional structural trend: in particular, they coincide with the location of the buried thrust-related faults, especially BTF1, BTF2 and, to a lesser extent, BFT3 (Figs. 2 and 5).

Pedogenically modified horizons H1 and H2, which are associated with the Late Pleistocene alluvial succession, exhibit a high correlation potential across the Po Plain, and for this reason represent key markers for high-resolution stratigraphic analysis (Amorosi et al., 2017a; Morelli et al., 2017; Bruno et al., 2019). However, the main limitation on their use is that the primary morphology of these surfaces is poorly known. As a result, post-burial deformation of paleosols H1 and H2 is barely quantifiable.

In contrast, the Holocene fossiliferous horizon H3 can be used as a reliable indicator of post-burial deformation, as it accumulated under low sedimentation rates in a low-gradient lower-delta-plain environment (Törnqvist et al., 2008). For this marker bed, we can reasonably assume a nearly horizontal geometry at the time of deposition, with a gradient towards the coeval shoreline comparable to the modern one (~0.0025% in the last 40 km, from the primary bifurcation of the Po River). As a consequence, the displacement of this surface above the buried anticlines can be inferred to reflect post-burial deformation.

The morphology of key surfaces H1-H3 also highlights a good match with historical and instrumental seismicity (Fig. 3). Particularly, the area of Argenta, close to core B3, was hit by two devastating earthquakes in 1624 (Mw=5.86) and in 1898 (Mw=4.59). The 1624 earthquake sequence, described in several historical notes (Guidoboni et al., 2018), started on the 19th of March and led to the destruction of about 200 buildings in the town of Argenta, which was re-built on the opposite bank of Reno River. Co-seismic effects included liquefaction, ground collapse, hydrogeological anomalies and seiches (Livio et al., 2014). Two earthquakes of Mw 4.96 and 5.05 hit the area of Longastrino, around core B1 (Fig. 3) in 1956 and 1967, respectively (INGV, https://emidius.mi.ingv.it/CPTI15-DBMI15/index_en.htm). Fault-plane solution of instrumental earthquakes indicates NW oriented compression (Seismotectonic Map of Regione Emilia Romagna, 2016), in agreement with GPS data that indicate shortening across the Po Basin, at rates of 1/3 mm/yr (Devoti et al., 2011).

All these data concur with the hypothesis of tectonic activity of closely-spaced thrusts of BTF2 as a major triggering factor of deformation for H1-H3. However, the possible contribution of differential sediment compaction to deformation cannot be ruled out, as changes in thickness from anticline to sincline areas in the Po Basin fill are in the range of several hundreds of metres (Fig. 2b). Additionally, highly compressive poorly-drained, swamp and prodelta facies associations are increasingly abundant towards syncline areas (Fig. 2), enhancing the effects of differential compaction. The ongoing deformation of H1-H3 is continuously compensated by the accumulation of thicker sediment packages in syncline depocentres. Here, the addition of great amounts of sediment enhances compaction of the underlying units.

High elevations of H1 and H2, suggestive of possible stratigraphic deformation, were also observed at the southern and northern margins of the study area (Fig. 5). The possible relation between stratigraphic deformation and tectonic activity of BT1 (and possibly BT3) is plausible. However, a reliable interpretation of the paleo-topographic anomalies presented in this study can only be achieved through additional data, outside the study area. In particular, refinement of regional models of structural evolution and the quantification of the relative role of active tectonics vs differential sediment compaction require additional structural and geotechnical data and a full picture, on a basin scale, of the 3D stratigraphic complexity, which are beyond the scope of this paper.

7. Conclusions

High-resolution stratigraphic correlation and subsurface mapping of Late Pleistocene to Holocene deposits from a large portion of the Po Basin on a sub-seismic scale highlight a marked relation between the morphology of three stratigraphic markers and the location of the buried thrust fronts. Based on a well-constrained sedimentological framework supplemented by 172 radiocarbon dates, two weakly developed Late Pleistocene paleosols, dated to the Marine Isotope Stage 3/2 transition (30-24 cal ky BP) and to the Younger Dryas cold event, (12.9-11.7 cal ky BPa), respectively, and a swamp-to-lagoon marker horizon dated to 6.2-5.6 cal ky BP were recognized in 64 cores and 442 CPTU test. These key horizons were tracked over an area of ~1500 km^2.

The 3D geometry of Late Pleistocene-Holocene stratigraphic markers, which in general dip in E/NE direction, appears to be highly sensitive to the deep structures and clearly delineates intensely deformed zones above the buried Longastrino thrust front and other buried tectonic structures. The fold axis of the shallow marker beds follows the regional (NW-SE oriented) trend of the buried thrust fronts. Recent tectonic activity along the buried Longastrino thrust front, combined with

differential sediment compaction, is likely to have influenced stratigraphic deformation in the Ferrara-Ravenna area, as documented by the striking coincidence between patterns of stratigraphic deformation, thrust zone localization and the geographic position of the historical and instrumental earthquakes that hit the Longastrino-Argenta area over the last centuries.

References

Amorosi, A., Colalongo, M.L., Fiorini, F., Fusco, F., Pasini, G., Vaiani, S.C., Sarti, G., 2004. Palaeogeographic and palaeo climatic evolution of the Po Plain from 150-ky core records. Glob. Planet. Chang. 40, 55-78. https://doi.org/10.1016/S0921-8181(03)00098-5.

Amorosi, A., Centineo, M.C., Colalongo, M.L., Fiorini, F., 2005. Millennial-scale depositional cycles from the Holocene of the Po Plain, Italy. Mar. Geol. 222-223, 7-18. https://doi.org/10.1016/j.margeo.2005.06.041.

Amorosi, A., Pavesi, M., Ricci Lucchi, M., Sarti, G., Piccin, A., 2008. Climatic signature of cyclic fluvial architecture from the Quaternary of the central Po plain, Italy. Sediment. Geol. 209, 58-68. https://doi/10.1016/j.sedgeo.2008.06.010.

Amorosi, A., Bruno, L., Rossi, V., Severi, P., Hajdas, I., 2014. Paleosol architecture of a late Quaternary basin–margin sequence and its implications for high-resolution, non-marine sequence stratigraphy. Glob. Planet. Chang. 112, 12-25. https://doi.org/10.1016/j.gloplacha.2013.10.007.

Amorosi, A., Bruno, L., Campo, B., Morelli, A., 2015. The value of pocket penetration tests for the high-resolution palaeosol stratigraphy of late Quaternary deposits: Geol. J. 50, 670-682. https://doi.org/ 10.1002/gj.2585.

Amorosi, A., Maselli, V., Trincardi, F., 2016. Onshore to offshore anatomy of a late Quater-nary source-to-sink system (Po Plain-Adriatic Sea, Italy): Earth Sci. Rev. 153:212–237.http://doi.org/10.1016/j.earscirev.2015.10.010.

Amorosi, A., Bruno, L., Cleveland, D.M., Morelli, A., and Hong, W., 2017a. Paleosols and associated channel-belt sand bodies from a continuously subsiding late Quaternary system (Po Basin, Italy): New insights into continental sequence stratigraphy. Geol. Soc. Am, Bull. 129 (3-4), 449-463. https://doi.org/10.1130/B31575.1.

Amorosi, A., Bruno, L., Campo, B., Morelli, A., Rossi, V., Scarponi, D., Drexler, T. M., 2017b. Global sea-level control on local parasequence architecture from the Holocene record of the Po Plain, Italy. Mar. Pet. Geol 87, 99–111. https://doi.org/10.1016/j.marpetgeo.2017.01.020

Amorosi, A., Bruno, L., Campo, B., Costagli, B., Dinelli, E., Hong, W., Sammartino, I., Vaiani, S.C., 2019a. Tracing clinothem geometry and sediment pathways in the prograding Holocene Po Delta system through integrated core stratigraphy: Basin Res. https://doi.org/10.1111/bre.12360.

Amorosi, A., Bruno, L., Campo, B., Costagli, B., Hong, W., Picotti, V., Vaiani, S.C., in press. Offset of buried stratigraphic markers reveals loci of active tectonic deformation. Sci. Rep. SREP-19-37407-T.

Anzidei, M., Maramai, A., Montone, P., 2012. The Emilia (Northern Italy) seismic sequence of May–June, 2012: Preliminary data and results. Ann. Geophys. 55(4), 515–842. https://www.annalsofgeophysics.eu/index.php/annals/issue/view/483.

Boccaletti, M., Corti, G., and Martelli, L., 2011. Recent and active tectonics of the external zone of the Northern Apennines (Italy). Int. J. Earth Sci. 100 (6), 1331-1348. https://doi.org/10.1007/s00531-010-0545-y.

Bruno, L., Amorosi, A., Severi, P., Costagli, B., 2017a. Late Quaternary aggradation rates and stratigraphic architecture of the southern Po Plain, Italy. Basin Res. 29 (2), 234–348. http://doi.org/10.1111/bre.12174.

Bruno, L., Bohacs, K. M., Campo, B., Drexler, T. M., Rossi, V., Sammartino, I., Amorosi, A., 2017b. Early Holocene transgressive paleogeography in the Po coastal plain (Northern Italy). Sedimentology 64 (7), 1792–1816. http://doi.org/10.1111/sed.12374.

Bruno, L., Campo, B., Di Martino, A., Hong, W., Amorosi, A., 2019. Peat layer accumulation and post-burial deformation during the mid-late Holocene in the Po coastal plain (Northern Italy). Basin Res. http://doi.org/10.1111/bre.12339.

Bruno, L., Campo, B., Costagli, B., Stouthamer, E., Teatini, P., Zoccarato, C., Amorosi, A., in press. Factors controlling natural subsidence in the Po Plain**.** Proceedings of the TISOLS Conference, Delft April 2020

Burrato, P., Ciucci, F., and Valensise, G., 2003. An inventory of river anomalies in the Po Plain, Northern Italy: Evidence for active blind thrust faulting: Ann. Geophys. 46, 865–882.

Campo, B., Amorosi, A., Bruno, L., 2017. Contrasting alluvial architecture of Late Pleistocene and Holocene deposits along a 120-km transect from the central Po Plain (northern Italy). Sediment. Geol. 341, 265-275. http://doi.org/10.1016/j.sedgeo.2016.04.013.

Carannante, S., Argnani, A., Massa, M., D'Alema, E., Lovati, S., Moretti, M., Augliera, P., 2015. The May 20 (MW 6.1) and 29 (MW 6.0), 2012, Emilia (Po Plain, northern Italy) earthquakes: New seismotectonic implications from subsurface geology and highquality hypocenter location. Tectonophysics 655, 107–123. https://doi.org/10.1016/j.tecto.2015.05.015.

Castellarin, A., Eva, C., Giglia, G., Vai, G.B., Rabbi, E., Pini, G.A., Crestana, G., 1985. Analisi strutturale del Fronte Appenninico Padano. Giorn. Geol. 47, 47-75.

Cohen, K. M., Stouthamer, E., and Berendsen, H. J. A., 2002. Fluvial deposits as a record for Late Quaternary neotectonic activity in the Rhine-Meuse delta, the Netherlands. Netherlands Journal of Geosciences-Geologie en Mijnbouw 81(3–4), 389–405. https://doi. org/10.1017/S0016774600022678.

Chamberlain, E.L., Törnqvist, T. E., Shen, Z., Mauz, B., Wallinga, J., 2018. Anatomy of Mississippi Delta growth and its implications for coastal restoration. Sci. Adv. 4(4). https://doi.org/ 10.1126/sciadv.aar4740.

Devoti, R., Esposito, A., Pietrantonio, G, Pisani, A.R., Riguzzi, F., 2011. Evidence of large scale deformation patterns from GPS data in the Italian subduction boundary. Earth Planet. Sci. Lett. 311(3,4), 230-241. https://doi.org/10.1016/j.epsl.2011.09.034

Flaig, P.P., McCarthy, P.J., and Fiorillo, A.R., 2013, Anatomy, evolution, and paleoenvironmental interpretation of an ancient Arctic coastal plain: Integrated paleopedology and palynology from the Upper Cretaceous (Maastrichtian) Prince Creek Formation, North Slope, Alaska, USA, in: Driese, S.C., Nordt, L.C., and Mc-Carthy, P.J. (Eds.), New Frontiers in Paleopedology and Terrestrial Paleoclimatology: Paleosols and Soil Surface Analog Systems. SEPM Special Publication 104, 179–230. https://doi.org/10 .2110/sepmsp .104 .14.

Ghielmi, M., Minervini, M., Nini, C., Rogledi, S., Rossi, M., 2013. Late Miocene–Middle Pleistocene sequences in the Po Plain – Northern Adriatic Sea (Italy): The stratigraphic record of modification phases affecting a complex foreland basin. Mar. Pet. Gol. 42, 50-81. https://doi.org/10.1016/j.marpetgeo.2012.11.007.

Giacomelli S., Rossi, V., Amorosi, A., Bruno, L., Campo, B., Ciampalini, A., Civa, A., Hong, W., Sgavetti, M., de Souza Fiho, C.R., 2018. A mid-late Holocene tidlly-influenced drainage system revealed by integrated remote sensing, sedimentological and stratigraphic data. Geomorphology 318, 421-436. https://doi.org/10.1016/j.geomorph.2018.07.004.

Govoni, A., Marchetti, A., De Gori, P., Di Bona, M., Lucente, F.P., Improta, L., Chiarabba, C., Nardi, A., Margheriti, L., Piana Agostinetti, N., Di Giovambattista, R., Latorre, D., Anselmi, M., Ciaccio M.G., Moretti, M., Castellano, C., Piccinini, D., 2014. The 2012 Emilia seismic sequence (Northern Italy): Imaging the thrust fault system by accurate aftershock location. Tectonophysics 622, 44-55. https://doi.org/10.1016/j.tecto.2014.02.013.

Guidoboni,E., Ferrari, G., Mariotti, D., Comastri, A., Tarabusi, G., Sgattoni, G., Valensise, G., (2018). CFTI5Med, Catalogo dei Forti Terremoti in Italia (461 a.C.-1997) e nell'area Mediterranea (760 a.C.-1500). Istit. Naz. Geofis. Vulcanol. (INGV). http://storing.ingv.it/cfti/cfti5/.

http://bollettinosimico.rm.ingv.it.

https://emidius.mi.ingv.it/CPTI15-DBMI15/index_en.htm.

http://mappegis.regione.emilia-romagna.it/gstatico/documenti/sismotett_2016/Carta_Sismotettonica.pdf.

ISIDe Working Group INGV, 2015: Italian Seismological Instrumental and parametric Database. http://cnt.rm.ingv.it/en/iside.

Kraus, M.J., 1999. Paleosols in clastic sedimentary rocks: their geologic applications. Earth-Sci. Rev. 47, 41–70. http://dx.doi.org/10.1016/S0012-8252(99)00026-4.

Lavé, J., Avouac, P., 2000. Active folding of fluvial terraces across the Siwaliks Hills, Himalayas of central Nepal. J. Geophys. Res. Solid Earth 105, 5735-5770. https://doi.org/10.1029/1999JB900292.

Livio, F.A., Berlusconi, A., Zerboni, A., Trombino, L., Sileo, G., Michetti, A.M., Rodnight, H., Spötl, C., 2014. Progressive offset and surface deformation along a seismogenic blind thrust in the Po Plain foredeep (Southern Alps, Northern Italy). J. Geophys. Res. Solid Earth 119, 7701–7721, doi:10.1002/2014JB011112.

Morelli, A., Bruno, L., Cleveland, D.M., Drexler, T.M., Amorosi, A., 2017. Reconstructing Last Glacial Maximum and Younger Dryas paleolandscapes through subsurface paleosol stratigraphy: An example from the Po coastal plain, Italy. Geomorphology 295, 790–800. http://dx.doi.org/10.1016/j.geomorph.2017.08.013. .

Picotti, V., Pazzaglia, F.J., 2008. A new active tectonic model for the construction of the Northern Apennines mountain front near Bologna (Italy). J. Geophys. Res. Solid Earth 113, http://dx.doi.org/10.1029/2007JB005307.

Picotti, V., Ponza, A., Pazzaglia, F.J., 2009. Topographic expression of active faults in the foothills of the Northern Apennines. Tectonophysics 474(1-2), 285-294. https://doi.org/10.1016/j.tecto.2009.01.009.

Pieri, M., Groppi, G., 1981. Subsurface geological structure of the Po Plain, Italy. Progetto Finalizzato Geodinamica, 414. CNR Pubblication, p. 23.

Piovan, S., Mozzi P., and Zecchin, M., 2012. The interplay between adjacent Adige and Po alluvial systems and deltas in the late Holocene (Northern Italy). Géomorphologie 18(4), 427-440. https://journals.openedition.org/geomorphologie/10034.

Preti, M., 1999. The Holocene transgression and the land-sea interaction south of the Po delta. Giorn. Geol. 61, 143–159.

Rovida, A., Camassi, R., Gasperini, P., Stucchi, M., 2011. Version of the Parametric Catalogue of Italian Earthquakes, Milano, Bologna. Retrieved from http://emidius.mi.ingv.it/CPTI/.

Scarponi, D., Kaufman, D., Amorosi, A. Kowalewski, M., 2013. Sequence stratigraphy and the resolution of the fossil record. Geology 41(2), 239-242. https://doi.org/10.1130/G33849.1.

Stefani, M., Vincenzi, S., 2005. The interplay of eustasy, climate and human activity in the late Quaternary depositional evolution and sedimentary architecture of the Po Delta system. Mar.Geol. 222–223, 19–48. https://doi.org/10.1016/j.margeo.2005.06.029.

Stefani, M., Minarelli, L., Fontana, A., Hajdas, I., 2018. Regional deformation of late Quaternary fluvial sediments in the Apennines foreland basin (Emilia, Italy). Int. J. Earth Sci. 107(7), 2433-2447. https://doi.org/10.1007/s00531-018-1606-x.

Törnqvist, T. E., Wallace, D. J., Storms, J. E., Wallinga, J., van Dam, R., L., Blaauw, M., Snijders, E. M., 2008. Mississippi Delta subsidence primarily caused by compaction of Holocene strata. Nature Geosci. 1, 173–176. https://doi.org/10.1038/ngeo129.

Toscani, G., Burratp, P., Di Bucci, D., Seno, S., Valensise, G., 2009. Plio-Quaternary tectonic evolution of the Northern Apennines thrust fronts (Bologna-Ferrara section, Italy): seismotectonic implications. Ital. J. Geosci. 128 (2), 605-613. https://doi.org/10.3301/IJG.2009.128.2.605.

Tsatskin, A., Sandler, A., and Avnaim-Katav, S., 2015. Quaternary subsurface paleosols in Haifa Bay, Israel: A new perspective on stratigraphic correlations in coastal settings. Palaeogeogr., Palaeoclimatol., Palaeoecol. 426, 285-296. https://doi.org/10.1016/j.paleo.2015.03.018.

Wilson, L.F., Pazzaglia, F.J., Anastasio, D.J., 2009. A fluvial record of active fault-propagation folding, Salsomaggiore anticline, northern Apennines, Italy. J. Geophys. Res. Solid Earth 114. https://doi.org/10.1029/2008JB005984.

4.3 Paper 3

Factors controlling natural subsidence in the Po Plain

Luigi Bruno, Bruno Campo, **Bianca Costagli,** Esther Stouthamer, Pietro Teatini, Claudia Zoccarato, Alessandro Amorosi.

Proceedings of the TISOLS Conference, Delft April 2020.

Submitted in September 2019

Factors controlling natural subsidence in the Po Plain

Luigi Bruno[1], Bruno Campo[2], Bianca Costagli[2], Esther Stouthamer[3], Pietro Teatini[4], Claudia Zoccarato[4], Alessandro Amorosi[2]

[1] *Department of Chemical and Geological Sciences, University of Modena and Reggio Emilia, Modena, 41125, Italy*

[2] *Department of Biological, Geological and Environmental Sciences, University of Bologna, Bologna, 40126, Italy*

[3] *Department of Physical Geography, Utrecht University, Utrecht, The Netherlands*

[4] *Department of Civil, Environmental and Architectural Engineering, University of Padova, Padova, 35131, Italy*

Correspondence to: Luigi Bruno (luigibruno@unimore.it)

Abstract

Understanding the causes and mechanisms of land subsidence is crucial, especially in densely populated coastal plains. In this work, we calculated subsidence rates (SR) in the Po coastal plain, averaged over the last 5.6 and 120 ky, providing information about land movements on intermediate (10^3-10^5 y) time scales. The calculation of SR relied upon core-based correlation of two lagoon horizons over tens of km. Subsidence in the last 120 ky appears to be controlled mainly by the location of buried tectonic structures, which in turn controlled sedimentation rates and location of highly compressible depositional facies. Numerical modelling shows that subsidence in the last 5.6 ky is mainly due to compaction of the Late Pleistocene and Holocene deposits (uppermost 30 m).

1. Introduction

The effects of land subsidence could be devastating on heavily settled, low-gradient, coastal plains, in a scenario of 0.9 m of relative sea-level rise by 2100 (Rohling *et al.*, 2013). Increasingly high costs are expected to protect coastal cities and touristic hotspots and to keep drained reclaimed lands (Syvitski et al., 2009; Erkens et al., 2016).

In the Po coastal plain, extending more than 100 km south of the Venice lagoon, decadal to centennial land movements in the order of several cm y^{-1} (Teatini et al., 2011; Cenni et al., 2013), were strongly driven by human activities (mostly water and gas withdrawal, Teatini et al., 2006). To separate anthropogenic from natural subsidence, understanding the role of subsidence through time before human intervention is required. Long-term (10^6 y) natural subsidence has been calculated based on deep seismic analysis (Carminati and Di Donato, 1999). On the contrary, spatial distribution of SR on intermediate (10^3-10^5 y) time scales is poorly known.

In this work, we measured SR in the last 120 ky along a 40 km-long transect in the Po coastal plain. We used as reference marker beds two lagoon horizons identified in sediment cores, from the Last and Present Interglacials. To discuss the relations between subsidence and structural setting, we reconstructed stratal architecture down to 3 km through seismic analysis. We focused on the stratigraphic significance of marker beds and on their use for SR calculation. The contribution of sediment compaction to land subsidence was assessed through geotechnical analysis and decompaction modelling.

2. Geological Setting

The Po Plain is a ~40.000 km^2-wide alluvial plain bounded by the Alps to the north and by the Apennines to the south. Frontal thrusts of both chains are sealed beneath the Po Plain (Amadori et al., 2019). The Apennine thrusts are north-verging and exhibit arcuate shapes. Thrusts SE of Ferrara (Fig. 1) were active since the Early Pliocene. The Po Basin fill shows a shallowing-upward trend from deep-marine turbidites to coastal and continental units (Ghielmi et al., 2013). The rhythmical alternation of Middle-Late Pleistocene coastal and alluvial deposits reflects glacio-eustatic fluctuations at the Milankovitch scale (Amorosi et al., 2004). Two transgressive-regressive coastal wedges in the uppermost 130 m were assigned to the Last (MIS 5e) and to the Present (MIS 1) Interglacials based on pollen data, ^{14}C dates and electron-spin-resonance age determinations (Ferranti et al., 2006). Landwards, the maximum marine ingression is marked by a thin brackish-

lagoon horizon, sandwiched between inner estuary (below) and upper delta plain freshwater deposits. Laterally extensive brackish water bodies settled in the Po coastal Plain around 7-5 cal ky BP, after sea-level stabilization (Vacchi et al., 2016), in areas sheltered by fluvial sedimentary input (Amorosi et al., 2017).

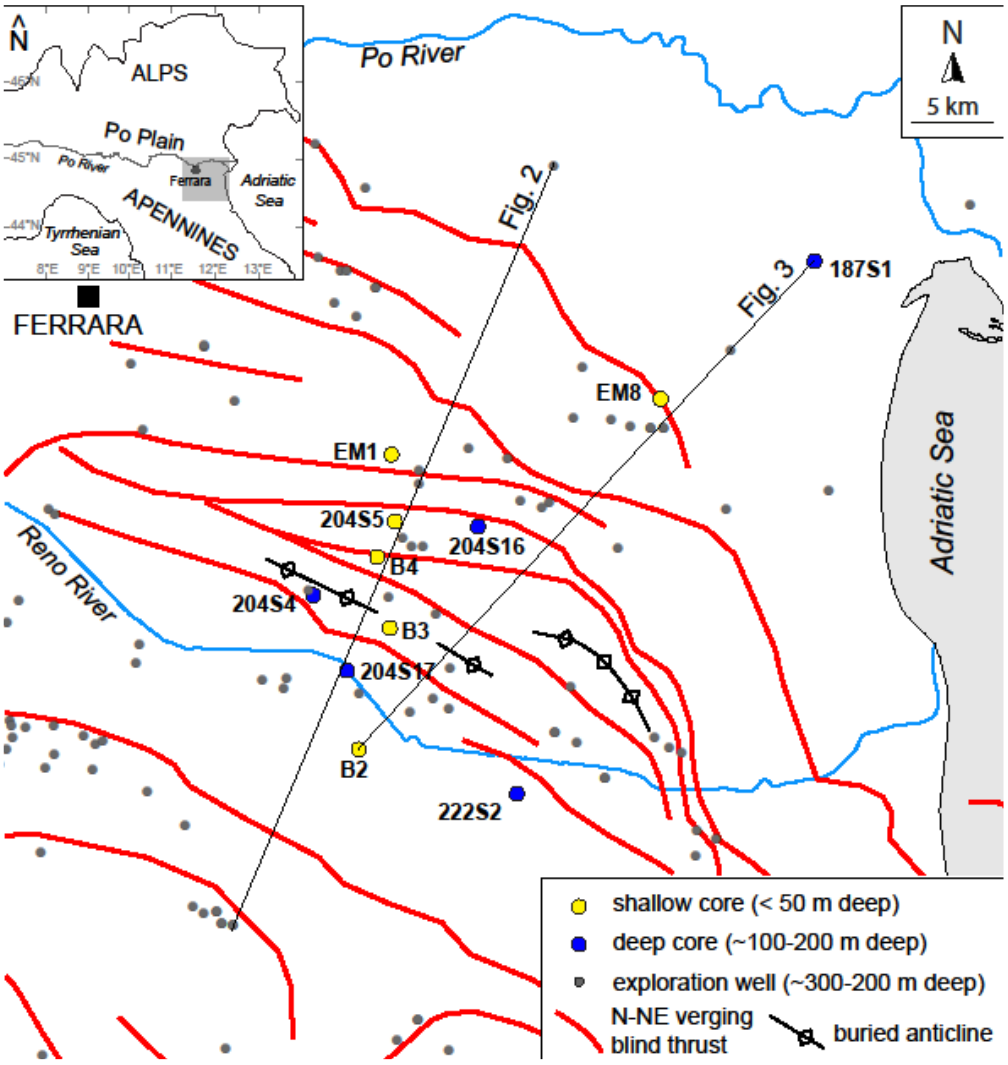

Figure 1. study area with location of cores, exploration wells and cross sections of Figs. 2 and 3. The projection of north-verging buried thrusts is depicted.

3. Methods

3.1 Stratigraphy

Calculation of Late Pleistocene and Holocene SR relies on the elevation (meters above modern sea level – m amsl) of two stratigraphic markers. The lower one is a lagoon horizon marking the top of the MIS 5e coastal wedge. The upper one is a thin lagoon horizon, dated to

5.6±0.5 cal ky BP, encountered at depths < 20 m. Chronological constraints for core correlation are provided by 76 ^{14}C ages (see supplementary material).

In order to assess the impact of buried faults and folds on lateral changes in SR, correlations were carried out perpendicular to these structures. A similarly oriented seismic profile was interpreted and time-depth converted through calibration with exploration-well logs (depth of 300-5000 m). Seismic interpretation relied on the identification and tracking of the main discontinuities (i.e. reverse faults) and unconformities.

3.2 Subsidence rates calculation

The calculation of SR for a selected time interval (Δt) between the time of deposition (t_d) and the Present (t_0=0) was based on Eq. 1.

$$SR(\Delta t) = \frac{Z_{td} - Z_{t0}}{\Delta t}, \qquad (1)$$

where Z_{td} is the elevation of the stratigraphic marker at the time of deposition and Z_{t0} is the present elevation. An error of 0.15 m associated to Z_{t0} due to core stretchening/shortening was included in the calculation (Hijma et al., 2015). Sedimentological data (Amorosi et al., 2017) indicate that the 5.6 ky BP lagoon horizon accumulated in a lower delta plain environment (~ 0 m above coeval sea level). Estimation of sea level at 5.6 cal ky BP was based on the prediction curve of Vacchi et al. (2016). As sediment deposition presumably took place in a water body < 1 m deep, an error of ±0.5 m was taken into account in SR calculation.

The MIS 5e lagoon horizon likely accumulated in water depths < 2 m (associated error of ±1 m; Amorosi et al., 2004). An additional error of ±1 m was added to compensate possible inaccuracy in correlation due to low chronologic resolution. The lagoon horizon was generically assigned to the MIS 5e highstand (120-116 cal ky BP, Rovere et al., 2016), 7±2 m above modern sea level.

Subsidence rates between 120-116 and 5.6-0 cal ky BP were compared with SR averaged over the last 1.5 My. The 1.5 My unconformity (Amadori et al., 2019) is marked in exploration-well logs by the first occurrence of *Hyalinea Baltica* (Carminati and Di Donato, 1999).

3.3 Sediment compaction

In order to assess the contribution of sediment compaction to natural subsidence, a finite-element 1D decompaction model (Gambolati et al. 1998; Zoccarato and Teatini, 2017) was applied to core B4 (see supplementary material). The mechanical characterization of the main lithofacies

associations was based on oedometer tests, bulk-density and loss on ignition tests (van Asselen, 2009).

3. Results and discussion

4.1 Deep stratal architecture

The subsurface of the study area, down to 3 km depth, consists of imbricated thrusts, locally associated with backthrusts (Fig. 2). Two major unconformities, dated to 5.5 and 1.5 My (Ghielmi et al., 2013), respectively, allow identification of three tectono-stratigraphic units (Fig. 2): (i) an intensely deformed and faulted pre-tectonic unit; (ii) a syn-tectonic wedge, made up of marine turbidites (Ghielmi et al., 2013); and (iii) a nearly undeformed, post-tectonic unit, sealing the main structures.

The 1.5 My unconformity depicts a major fold, with a wavelength of ~30 km resulting from faults propagation and imbrication. Lower-rank folds (wavelength of ~3-5 km) are associated with single-fault propagation. The thickness of the post-tectonic unit ranges between 300 m at the culmination of the main anticline and 2000 in the backlimb and forelimb depocentres. Post-1.5 My turbidites accumulated in synclinal areas (Ghielmi et al., 2013), whereas truncation of Pliocene strata is observed above the anticline. Deformation of Pleistocene strata was observed close to the anticline culmination, suggesting local post-1.5 My tectonic activity.

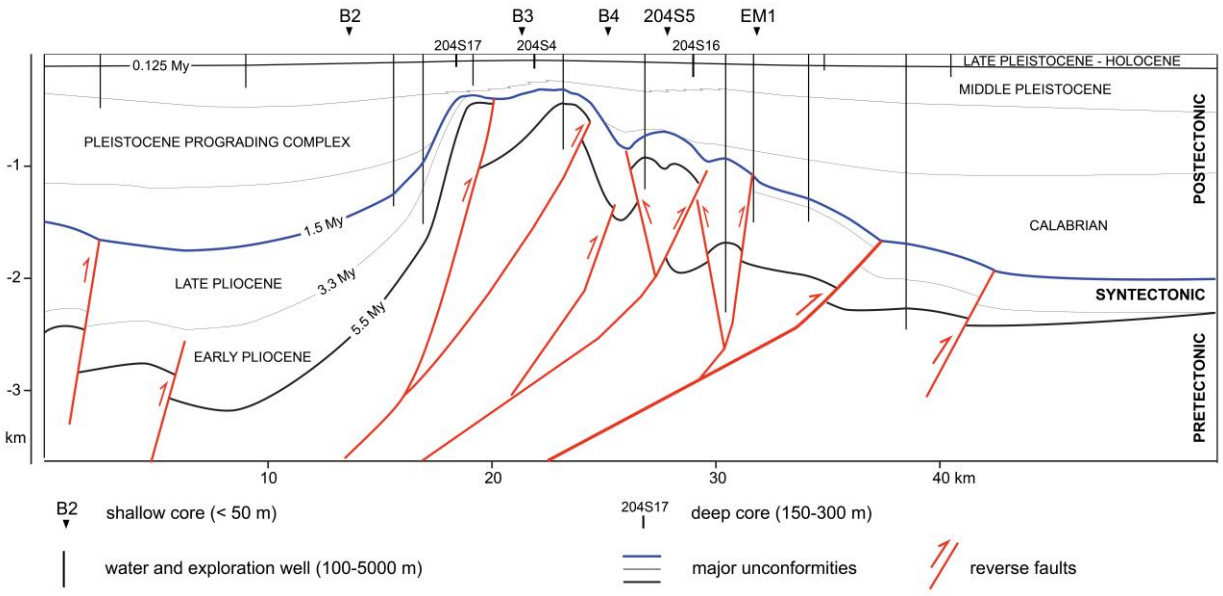

Figure 2. interpreted seismic profile (see Fig. 1 for location) perpendicular to the main buried tectonic structures.

4.2 Shallow stratigraphy

The stratigraphy of the uppermost 140 m is depicted in the correlation panel of Fig. 3 (see supplementary material for facies description). The MIS 5e sediment wedge, at 60-100 m depth, consists of coastal sands, replaced by lagoon deposits at inland locations (core 204S4). A thin (0.5-3 m) lagoon horizon drapes the coastal sands and is overlain by a shallowing upward succession of coastal plain and alluvial deposits, 35-65 m thick, deposited between ~ 110 and 10 ky BP. Delta plain estuarine and swamp deposits, pinch out toward the anticline culmination. Fluvial-channel deposits are abundant around MIS 4 and MIS 2, whereas closely spaced paleosols mark MIS 3 floodplain deposits. A prominent paleosol marks the Late Pleistocene-Holocene boundary and is overlain by estuarine deposits (Bruno et al., 2017). A thin lagoon horizon, mostly sandwiched between freshwater deposits and dated to ~ 5.6 cal ky BP, is clearly recognizable along the whole cross-section.

4.3 Factors controlling subsidence rates

Subsidence rates in the Po coastal plain appear to be strongly influenced by the buried tectonic structures. Particularly, SR averaged over the last 5.6 ($SR_{5.6}$), 120 (SR_{120}), and 1500 (SR_{1500}) ky decrease towards the anticline culmination (Fig. 3). In syncline areas, subsidence may have been enhanced by high sedimentation rates and by the preferential accumulation of highly compressible prodelta, delta plain and swamp muds (Fig. 3).

Subsidence rates in the last 5.6 ky are in the range of 0.8-2.0 mm y^{-1}, about twice the values measured for the last 120 ky (0.4-0.8 mm y^{-1}). Superimposed to the structurally controlled trend, Holocene stratigraphic architecture influenced lateral changes in $SR_{5.6}$. For example, $SR_{5.6}$ are higher in EM1, where the 5.6 ky BP horizon overlies soft estuarine muds, and lower in EM8, where the same marker bed lies onto the less compressible, 7 m-thick coastal sand body. The 5.6 ky lagoon horizon, encountered at ~-9 m amsl in core B4, was placed at -3.5 m after decompaction, ~1 m below sea-level predictions (Vacchi et al., 2016). Therefore, subsidence at this location is almost entirely accommodated by the compaction of the uppermost 30 m-thick sediment package. Particularly, the Late Pleistocene succession did not act as an ‘incompressible substratum’ but compacted of ~23% (see supplementary material), likely due to soft swamp peaty clays.

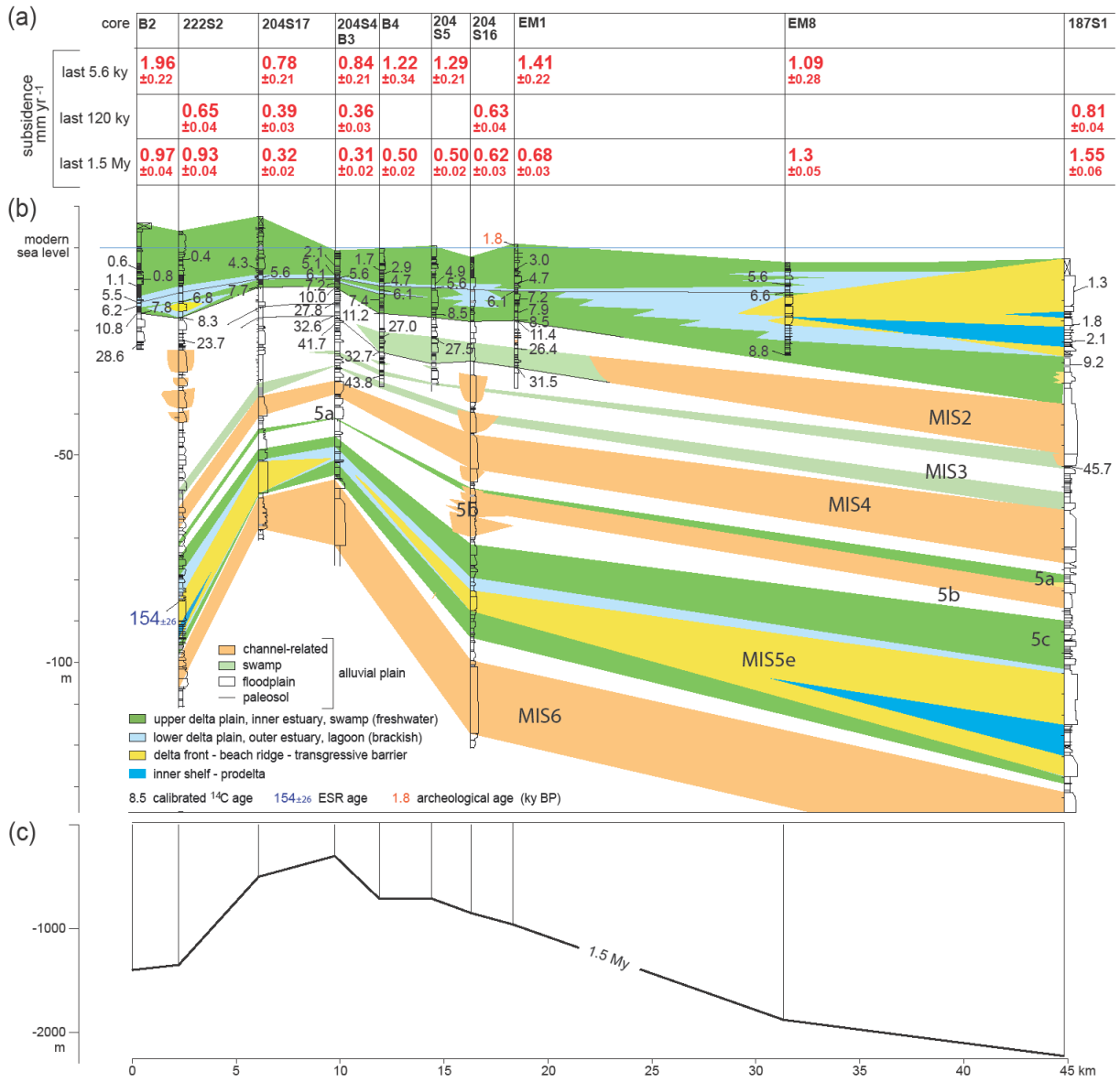

Figure 3. (a) subsidence rates averaged over the last 5.6, 120 and 1500 ky; (b) core correlation of Late Pleistocene-Holocene deposits (see Fig. 1 for core location); (c) elevation of the 1.5 My BP unconformity.

4.4 Conclusion

Subsidence rates for the last 5.6 and 120 ky were assessed in the Po coastal plain within a chronologically constrained stratigraphic framework. Two laterally extensive lagoon horizons were used as reference marker beds.

Subsidence rates in the last 120 ky appear to be mainly controlled by the location of buried Apennines thrust-related folds, which in turn influenced sedimentation rates and distribution of highly compressible depositional facies. Compaction of Late Pleistocene and Holocene sediments strongly impacted SR in the last 5.6 ky.

Data availability

Exploration-well logs used in this work are available at https://www.videpi.com. Oedometer tests were downloaded from the database of the Geological Seismic and Soil Survey of Regione Emilia Romagna.

Author contribution

This work relies on a stratigraphic study carried out by L. Bruno, B. Campo and B. Costagli and coordinated by A. Amorosi. Laboratory analyses were carried out by B. Costagli under the supervision of E. Stouthamer. Decompaction modelling was carried out by C. Zoccarato and P. Teatini. L. Bruno prepared manuscript and figures, with the contribution of all co-authors,

Competing interest

The authors declare that they have no conflict of interest.

Financial support

This research has been supported by the RFO grant to A. Amorosi. This paper is also a contribution to the International Geoscience Programme (IGCP) Project 663 “Impact, Mechanism, Monitoring of Land Subsidence in Coastal Cities”.

References

Amadori, C., Toscani, G., Maesano, F.E., D’Ambrogi, C., Ghielmi, M. and Fantoni, R.: From cylindrical to non-cylindrical foreland basin: Pliocene-Pleistocene evolution of the Po Plain-Northern Adriatic basin (Italy), Basin Research, doi:10.1111/bre.12369, 2019.

Amorosi, A., Colalongo, M.L., Fiorini, F., Fusco, F., Pasini, G., Vaiani, S.C. and Sarti, G.: Palaeogeographic and palaeoclimatic evolution of the Po Plain from 150-ky core records, Global and Planetary Change 40, 55-78, doi: 10.1016/S0921-8181(03)00098-5, 2004.

Amorosi, A., Bruno, L., Campo, B., Morelli, A., Rossi, V., Scarponi, D., Bohacs, K.M and Drexler, T.M.**:** Global sea-level control on local parasequence architecture from the Holocene record of the Po Plain, Italy, Marine and Petroleum Geology, 87, 99–111, doi: 10.1016/j.marpetgeo.2017.01.020, 2017.

Bruno, L., Bohacs, K. M., Campo, B., Drexler, T. M., Rossi, V., Sammartino, I. and Amorosi, A.: Early Holocene transgressive paleogeography in the Po coastal plain (Northern Italy), Sedimentology, 64(7), 1792–1816, doi: 10.1111/sed.12374, 2017.

Carminati, E. and di Donato, G.: Separating natural and anthropogenic vertical movements in fast subsiding areas: The Po Plain (N.Italy) case, Geophysical Research Letters, 26, 2291-2294, doi.org/10.1029/1999GL900518, 1999.

Cenni, N., Viti, M., Baldi, P., Mantovani, E., Bacchetti, M. and Vannucchi, A.: Present vertical movements in Central and Northern Italy from GPS data: Possible role of natural and anthropogenic causes, Journal of Geodynamics, 71, 74–85., doi:10.1016/j.jog.2013.07.004, 2013.

Erkens, G., Van der Meulen, M. & Middelkoop, H.: Double trouble: subsidence and CO2 respiration due to 1000 years of cultivation of the Dutch coastal peatlands. Hydrogeological Journal, 24, 551–568, doi:10.1007/s10040-016-1380-4, 2016

Ferranti, L., Antonioli, F., Mauz, B., Amorosi, A., Dai Pra, G., Mastronuzzi, G., Monaco, C., Orru, P., Pappalardo, M., Radtke, U., Renda, P., Romano, P., Sanso, P. and Verrubbi, V.: Markers of the last interglacial sea-level high stand along the coast of Italy: Tectonic implications. Quat. Int., 145-146, 30–54, doi: 10.1016/j.quaint.2005.07.009, 2006.

Gambolati, G., Giunta, G., Teatini, P., 1998. Numerical modeling of natural land subsidence over sedimentary basins undergoing large compaction. In: Gambolati, G. (Ed.), CENAS - Coastiline Evolution of the Upper Adriatic Sea due to Sea Level Rise and Natural and Anthropogenic Land Subsidence. Klwer Acedemic Publ., pp. 77–102.

Ghielmi, M., Minervini, M., Nini, C., Rogedi, S. and Rossi, M.: Late Miocene–Middle Pleistocene sequences in the Po Plain–Northern Adriatic Sea (Italy): The stratigraphic record of modification phases affecting a complex foreland basin, Mar. Petrol. Geol. 42**,** 50–81, doi: 10.1016/j.marpetgeo.2012.11.007, 2013.

Hijma, M., Engelhart, S.E., Tornqvist, T.E., Horton, B.P., Hu, P. and Hill, D.: A protocol for a Geological Sea-level Database. In: Shennan, I., Long, A. and Horton, B.P. (Eds.), Handbook of Sea Level Research, Wiley, 536–553, doi:10.1002/9781118452547.ch34 2015.

Pieri, M. and Groppi, G.: Subsurface geological structure of the Po Plain, Italy. Progetto Finalizzato Geodinamica, CNR Publication 414, 23, 1981.

Rohling, E.J., Haigh, I.D., Foster, G.L., Roberts, A.P. and Grant, K.M.: A geological perspective on potential future sea-level rise. Sci. Rep., 3, 3461, doi:10.1038/srep03461, 2013

Rovere, A., Raymo, M.E., Vacchi, M., Lorscheid, T., Stocchi, P., Gómez-Pujol, L., Harris, D.L., Casella, E., O'LearyM.J. and Hearty, P.J.: The analysis of Last Interglacial (MIS 5e) relative

sea-level indicators: Reconstructing sea-level in a warmer world, Earth.Science Reviews 159, 404-427, doi: 10.1016/j.earscirev.2016.06.006, 2016.

Syvitski, J.P.M., Kettner, A.J., Overeem, I., Hutton, E.W.H., Hannon, M.T., Brakenridge, G.R., Day, J., Vörösmarty, C., Saito, Y., Giosan, L. and Nicholls, R.J.: Sinking deltas due to human activities, Nature Geoscience, 2, 681-686, doi:10.1038/NGEO629, 2009.

Teatini, P., Gambolati, G., Ferronato, M. and Gonella, M.: Groundwater pumping and land subsidence in the Emilia-Romagna coastland, Italy: Modeling the past occurrence and the future trend, Water Resources Research, 42, doi:10.1029/2005WR004242, 2006.

Teatini, P., Tosi, L. and Strozzi, T.: Quantitative evidence that compaction of Holocene sediments drives the present land subsidence of the Po Delta, Italy, Journal of Geophysical research 116, doi:10.1029/2010JB008122, 2011.

Vacchi, M., Marriner, N., Morhange, C., Spada, G., Fontana, A. and Rovere, A.: Multiproxy assessment of Holocene relative sealevel changes in the western Mediterranenan: Sea-level variability and improvements in the definition of the isostatic signal, Earth-Science Reviews, 155, 172–197, doi: 10.1016/j.earscirev.2016.02.002, 2016.

van Asselen, S., Stouthamer, E. and van Asch, T.W.J.: Effects of peat compaction on delta evolution: a review on processes, responses, measuring and modeling. Earth-Sci. Rev., 92 (1–2), 35–51. doi:10.1016/j.earscirev.2008.11.001, 2009.

Zoccarato, C. and Teatini, P., 2017: Numerical simulations of Holocene salt-marsh dynamics under the hypothesis of large soil deformations. Adv. in Water Res., 110, 107–119, doi:10.1016/j.advwatres.2017.10.006, 2017.

Supplementary Material

Radiocarbon dates

Chronological constrain for core correlation is provided by 28 published ^{14}C ages (Sheets 204 and 222 of the Geological Map of Italy to scale 1:50000; Amorosi et al., 2005; Amorosi et al., 2017; Bruno et al., 2017) and from 48 ^{14}C dates carried out at the at the KIGAM Laboratory (Korea Institute of Geoscience and Mineral Resources, Daejeon, Republic of Korea). Conventional ^{14}C ages (Tab. 1) were calibrated using OxCal 4.2 (Bronk Ramsey & Lee, 2013) with the IntCal 13 and Marine13 curves (Reimer et al., 2013).

Core	Sample depth (m)	Sample code	C14 age	Cal year BP (mean value)	Material	References	Figure
B2	5.8	KGM-TWd180568b	320±20	380±40	Peat	This paper	4
	11.15	KGM-TWd180570a	650±30	610±40	Wood	This paper	3,4
	12.35	KGM-TWd180571a	730±20	680±10	Wood	This paper	4
	13.8	KGM-TWd180572a	960±40	860±50	Wood	This paper	3,4
	15-3	KGM-TWd180574a	1190±20	1120±40	Peat	This paper	3,4
	16.6	KGM-TWd180575a	2730±30	2820±30	Wood	This paper	3
	17.6	KGM-TWd180576a	3820±30	4220±60	Peat	This paper	3
	19.2	KGM-TCa180070a	5030±30	5530±40	Shell	This paper	3,4
	20.25	KGM-TWd180577a	5390±30	6210±60	Wood	This paper	3,4
	21.6	KGM-TWd180578a	7150±30	7970±20	Peat	This paper	3,4
	22.05	KGM-TSa180035a	9500±40	10840±130	Bulk sediment	This paper	3,4
	29.8	KGM-TSa180036a	246300±90	28660±120	Bulk sediment	This paper	3,4
B3	3.55	KGM-TWd190145	2120±20	2090±40	Peat	This paper	3,4
	3.95	KGM- TWd190146	3020±30	3210±60	Peat	This paper	4
	4.35	KGM- TWd190147	4250±40	4830±70	Wood	This paper	4
	5.95	KGM- TWd190148	4500±30	5170±80	Wood	This paper	3,4
	6.6	KGM- TWd190149	4910±30	5630±30	Wood	This paper	3,4
	6.95	KGM- TWd190150	5330±30	6110±60	Peat	This paper	3,4
	7.9	KGM- TWd190151	6280±30	7210±30	Plant fragment	This paper	3,4
	8.5	KGM- TWd190152	6480±30	7380±40	Peat	This paper	4
	8.67	KGM- TWd190153	6780±30	7630±20	Peat	This paper	4
	9.08	KGM- TWd190154	7130±40	7960±40	Peaty clay	This paper	4
	9.2	KGM-TSa190025	8870±50	10000±120	Bulk sediment	This paper	3,4
	12.6	KGM- TSa190026	23750±140	27820±130	Bulk sediment	This paper	3,4
	15.6	KGM- TSa190028	28590±200	32630±370	Organic Clay	This paper	3,4
B4	5.15	KGM- TWd190155	1780±20	1700±50	Peat	This paper	3,4
	6.05	KGM- TWd190156	2770±30	2860±40	Peat	This paper	3,4
	6.36	KGM- TWd190157	3230±30	3450±40	Wood	This paper	4
	6.9	KGM- TWd190158	4070±30	4560±90	Wood	This paper	4

	8.4	KGM- TWd190159	4180±30	4720±60	Wood	This paper	3,4
	9.58	KGM- TWd190161	5240±30	5980±70	Peat	This paper	4
	10.1	KGM- TWd190162	5290±30	6080±60	Peat	This paper	3,4
	10.9	KGM- TWd190163	6120±30	7000±70	Peat	This paper	4
	11.85	KGM- TWd190164	6440±30	7370±40	Wood	This paper	4
	12.4	KGM- TWd190165	6470±30	7380±30	Wood	This paper	3,4
	15.5	KGM- TWd190166	8710±40	9650±80	Wood	This paper	Supp. Mat.
	15.6	KGM- TSa190029	9780±60	11200±70	Organic Clay	This paper	3,4
	21.3	KGM- TWd190167	22710±90	27080±170	Peat	This paper	3,4
	24.96	KGM- TSa190030a	28660±210	32740±380	Organic Clay	This paper	3,4
	30.85	KGM- TSa190031	40130±450	43760±420	Organic Clay	This paper	3,4
EM 1	5.75	KGM-OWd150177	2680±40	2970±110	Peat	Amorosi et al., 2017	3,4
	9.50	KGM-OWd150178	4190±40	4690±85	Plant fragment	Amorosi et al., 2017	3,4
	11.30	KGM-OWd150179	5630±40	6150±130	Shell	Amorosi et al., 2017	4
	11.40	KGM-OWd150180	5340±40	6105±110	Wood	Amorosi et al., 2017	3,4
	13.30	KGM-OWd150181	6340±50	7250±85	Plant fragment	Amorosi et al., 2017	3,4
	16.50	KGM-OWd160062	7040±50	7870±50	Peat	Amorosi et al., 2017	3,4
	17.85	KGM-OWd150182	7340±50	8125±105	Wood	Amorosi et al., 2017	4
	18.40	KGM-OWd160063	7730±50	8510±50	Peat	Amorosi et al., 2017	3,4
	18.70	KGM-OSn150001	9950±60	11430±195	Organic clay	Amorosi et al., 2017	3,4
	25.3	KGM-TSa180006	22190±100	26400±160	Wood	This paper	3,4
	26.90	KGM-OWd150183	22200±120	26450±390	Wood	Amorosi et al., 2017	4
	30.1	KGM-TSa180007	27810±150	31520±190	Peaty clay	This paper	3,4
EM 8	5.45	OWd160064	4890±50	5630±50	Wood	Bruno et al., 2017	3
	7.3	OWd160065	5800±40	6600±50	Wood	Bruno et al., 2017	3
	22.4	OWd160066	7950±40	8820±100	Wood	Bruno et al., 2017	3
187 S1	7.95	KGM-TCa180071	1860±30	1270±40	Shell	Amorosi et al., 2019	3
	15.90	KGM-TCa180072	2340±30	1800±50	Shell	Amorosi et al., 2019	3
	19.75	KGM-TWd180579	2570±20	2070±60	Wood	Amorosi et	3

						al., 2019	
	25.85	Beta Analytic-187 S1_25.85	8250±60	9230±100	Plant fragment	CARG Project, Sheet 187	3
	50.05	Beta Analytic-187 S1_50.05	41750±1000	45700±1900	Peat	CARG Project, Sheet 187	3
204 S4	21	ENEA-204 S4_26.8	35500±3000	41730±6620	Organic clay	CARG Project, Sheet 204	3
204 S5	8.50	KGM-OWd170593-1	3910±30	4345±50	Plant fragment	Bruno et al., 2019	4
	9.30	KGM-OWd170594-1	4390±30	4955±60	Plant fragment	Bruno et al., 2019	3
	10.30	KGM-OWd170595-1	5140±30	5620±30	Plant fragment	Bruno et al., 2019	3
	16.95	ETH-204S5_16.95	7735±70	8520±70	Wood	Amorosi et al., 2005	3
	22.70	ETH-204S5_22.7	23320±210	27545±155	Peat	CARG Project, Sheet 204	4
204 S17	12,8	KGM-OWd170597-1	3850±30	4270±70	Plant fragment	This paper	3,4
	13.40	KGM-OWd170598-1	3930±30	4370±60	Plant fragment	This paper	4
	14.75	KGM-OWd170599-1	5170±30	5630±30	Plant fragment	This paper	3,4
	14.95	KGM-OWd170600-1	5530±30	6100±60	Plant fragment	This paper	4
	17	KGM-OWd170601-1	6840±30	7670±30	Plant fragment	This paper	3,4
222 S2	7.0	Beta Analytic-222 S2_7.0	340±60	400±40	Peat	CARG Project, Sheet 222	3
	17.0	Beta Analytic-222 S2_17.0	6000±60	6850±40	Peat	CARG Project, Sheet 222	3
	20.9	Beta Analytic-222 S2_20.9	7420±60	8270±40	Organic Clay	CARG Project, Sheet 222	3
	26.2	Beta Analytic-222 S2_26.2	19770±150	23660±490	Peat	CARG Project, Sheet 222	3

Decompaction model

Decompacted thickness H_0 of a soil column presently comprised between depth z_1 and z_2 can be computed as (Gambolati et al., 1998):

$$H_0 = (1 + e_0) \int_{z_1}^{z_2} \frac{dz}{1 + e(z)}$$

where e_0 initial void index and $e(z)$ is the void index at depth z. The behavior of $e(z)$ in virgin loading conditions is given by

$$e(z) = e_0 - C_c \log \sigma_z$$

with C_c the compression index and σ_z the intergranular effective stress.

Application of decompaction model to core B4

The above described decompaction model was applied to core B4 (Fig. 1) where six depositional facies association were identified. The reader is referred to Amorosi et al. (2005 2017a, b), Bruno et al. (2017) and Giacomelli et al. (2018) for detailed description. A brief description is provided in Tab. 2, together with geothecnical parameters e_0 and C_c.

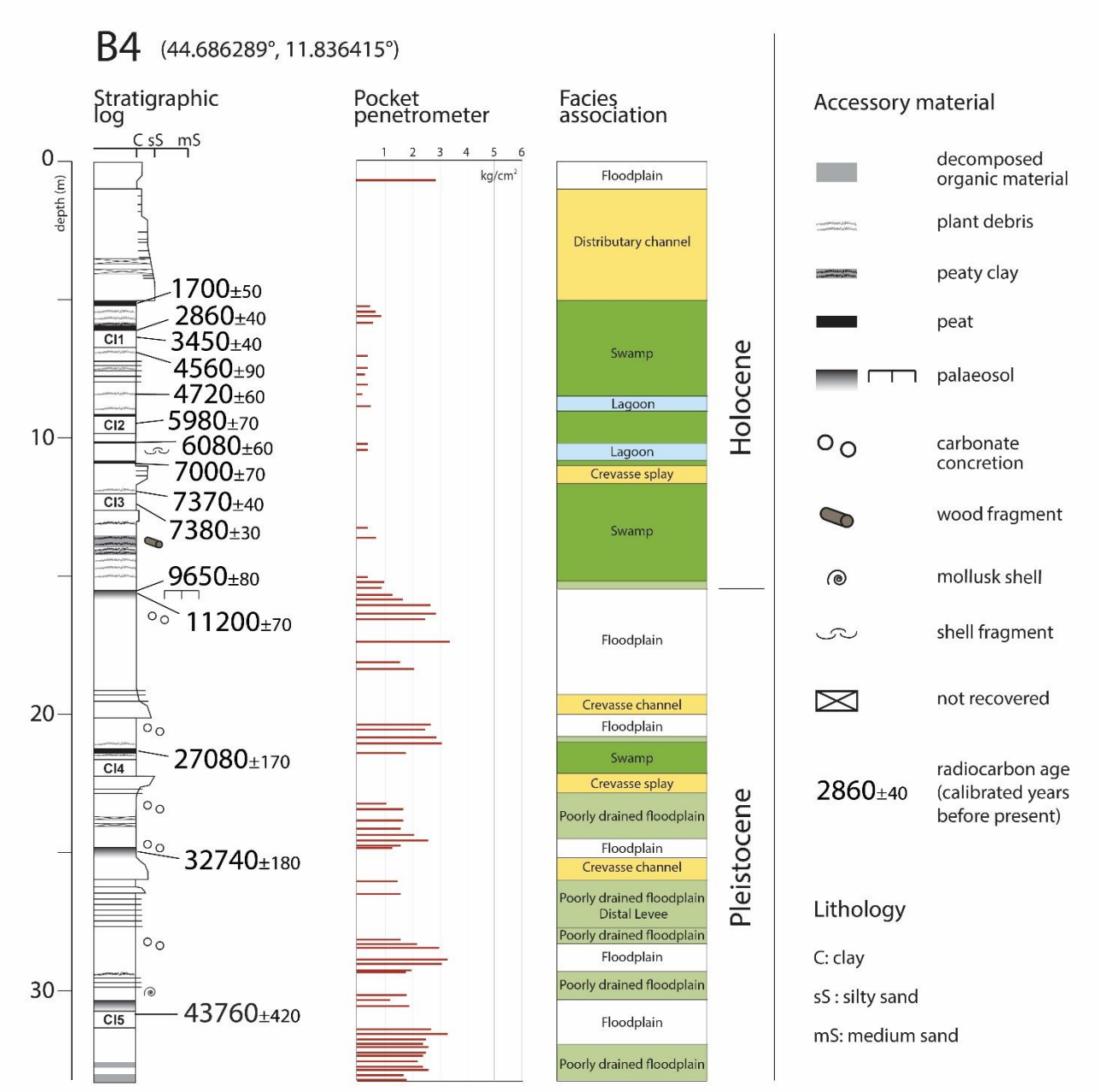

Fig. 1. Stratigraphic log of core B4

Geothecnical characterization of facies associations was based on; (i) loss on ignition and bulk density determination carried out on 6 undisturbed samples from core B4 (ii) 22 oedometer tests carried out on nearby cores from the database of the Geological Seismic and Soil Survey of Regione Emilia Romagna.

Depositional system	facies association	lithology	Accessory material, sedimentary structures	PP	e0	cc
Lowed delta plain – outer estuary	Lagoon	silty clay	Brackish fossils	< 1.2	1.56	0.15
Upper delta plain – inner estuary	Swamp	peat	Wood, plant debris	-	2.29	0.86
		clay	Freshwater to low brackish fossils, plant debris	< 1.2	1.56	0.15
	Poorly drained floodplain	silty clay	Parallel lamination	1.2 – 1.8	0.99	0.23
Alluvial Plain	Floodplain	clayey silt	carbonate concretions, Fe and Mn oxides	> 1.8	0.84	0.12
	Crevasse and levee	silty sand	Parallel and cross lamination	-	0.42	0.17

Tab. 2. Geomechanical parameters e_0 and C_c used to decompact the units of core B4. PP = pocket penetrometer.

A simplified stratigraphy was used for decompaction of core B4 (Tab. 3). The deformation of each unit is computed as $(H_0 - H)/H_0$, with H the actual thickness of the unit. The higher compaction is associated with the peat horizons.

Facies association	H (m)	H0 (m)	Deformation (%)
Crevasse and levee	4.15	5.14	19.26
Swamp peat	0.10	0.19	47.09
Swamp clay and lagoon	4.23	4.76	11.13
Swamp peat	0.10	0.21	51.92
Lagoon	1.32	1.50	12.00
Crevasse and levee	0.95	1.26	24.60
Swamp clay	2.25	2.57	12.45
Poorly drained floodplain	1.40	1.87	25.13
Floodplain	5.30	6.22	14.79
Swamp peat	0.55	1.56	64.74
Poorly drained floodplain	3.50	4.93	29.01
Floodplain	6.00	7.16	16.20

Tab. 3. Result of the decompaction model for each unit of core B4. Boulder line marks the Pleistocene/Holocene boundary

References

Amorosi, A., Centineo, M.C., Colalongo, M.L. and Fiorini, F.: Millennial-scale depositional cycles from the Holocene of the Po Plain, Italy, Marine Geology, 222-223, 7-18, doi:10.1016/j.margeo.2005.06.041, 2005.

Amorosi, A., Bruno, L., Campo, B., Morelli, A., Rossi, V., Scarponi, D., Bohacs, K.M and Drexler, T. M.**:** Global sea-level control on local parasequence architecture from the Holocene record of the Po Plain, Italy, Marine and Petroleum Geology, 87, 99–111, doi.org/10.1016/j.marpetgeo.2017.03.03, 2017a.

Amorosi, A., Bruno, L., Cleveland, D.M., Morelli, A. and Hong, W.**:** Paleosols and associated channel-belt sand bodies from a continuously subsiding late Quaternary system (Po Basin, Italy): New insights into continental sequence stratigraphy. Geological Society of America Bulletin, 129(3), 1-15, doi: 10.1130/B31575.1, 2017b.

Amorosi A., Bruno L., Campo B., Costagli B., Dinelli E., Hong W., Sammartino I. and Vaiani S.C.: Tracing clinothem geometry and sediment pathways in the prograding Holocene Po Delta system through integrated core stratigraphy, Basin Research, doi.org/10.1111/bre.12360, 2019.

Bronk Ramsey, C. and Lee, S.: Recent and planned developments of the program OxCal, Radiocarbon, 55(2–3), 720–730, doi:10.2458/azu_js_rc.55.16215, 2013.

Bruno, L., Bohacs, K. M., Campo, B., Drexler, T. M., Rossi, V., Sammartino, I. and Amorosi, A.: Early Holocene transgressive paleogeography in the Po coastal plain (Northern Italy), Sedimentology, 64(7), 1792–1816, doi:10.1111/sed.12374, 2017.

Gambolati, G., Giunta, G. and Teatini, P.: Numerical modeling of natural land subsidence over sedimentary basins undergoing large compaction. In: Gambolati, G. (Ed.), CENAS - Coastiline Evolution of the Upper Adriatic Sea due to Sea Level Rise and Natural and Anthropogenic Land Subsidence. Klwer Acedemic Publ., 28 (4), 77–102, 1998.

Giacomelli S., Rossi, V., Amorosi, A., Bruno, L., Campo, B., Ciampalini, A., Civa, A., Hong, W., Sgavetti, M. and de Souza Fiho, C.R.: A mid-late Holocene tidlly-influenced drainage system revealed by integrated remote sensing, sedimentological and stratigraphic data, Geomorphology 318, 421-436, doi:10.1016/j.geomorph.2018.07.004, 2018.

Reimer, P. J., Bard, E., Bayliss, A., Beck, J. W., Blackwell, P. G., Ramsey, C. B. and van der Plicht, J.: IntCal13 and Marine13 radiocarbon age calibration curves, 0–50,000 years cal BP, Radiocarbon, 55, 1869–1887, doi.org/10.2458/azu_js_rc.55.16947, 2013.

4.4 Paper 4

Tracing clinothem geometry and sediment pathways in the prograding Holocene Po Delta system through integrated core stratigraphy

Alessandro Amorosi, Luigi Bruno, Bruno Campo, **Bianca Costagli,** Enrico Dinelli, Wan Hong, Irene Sammartino, Stefano Claudio Vaiani.

Basin Research (2019)

In press

Tracing clinothem geometry and sediment pathways in the prograding Holocene Po Delta system through integrated core stratigraphy

Alessandro Amorosi[1], Luigi Bruno[2], Bruno Campo[1], Bianca Costagli[1], Enrico Dinelli[1], Wan Hong[3], Irene Sammartino[4] and Stefano Claudio Vaiani[1]

[1]*Department of Biological, Geological and Environmental Sciences, University of Bologna, Italy*

[2]*Department of Chemical and Geological Sciences, University of Modena and Reggio Emilia, Italy*

[3]*KIGAM Korea Institute of Geoscience and Mineral Resources, Daejeon Metropolitan City, Korea*

[4]*Geologic Consultant, Bologna, Italy*

Abstract

Though clinothem geometry represents a key control on fluid flow in reservoir modeling, tracing clinothem boundaries accurately is commonly limited by the lack of sufficiently precise outcrop or subsurface data. This study shows that in basin systems with strongly heterogeneous compositional signatures, the combination of bulk-sediment geochemistry and benthic foraminiferal distribution can help identify clinothem architecture and generate realistic models of 3D deltaic upbuilding and evolution.

Middle-late Holocene deposits in the Po Delta area form an aggradational to progradational parasequence set that reveals the complex interaction of W-E Po Delta progradation, S-directed longshore currents (from Alpine rivers) and Apennines rivers supply. Unique catchment lithologies (ophiolite rocks and dolostones) were used to delineate basin-wide geochemical markers of sediment provenance (Cr and Mg) and to assess distinctive detrital signatures. The geochemical characterization of cored intervals across different components of the sediment routing system enabled a direct linkage between clinothem growth, transport pathways and provenance mixing to be established. On the other hand, abrupt microfaunal variations at clinothem boundaries were observed to reflect the paleoenvironmental response to sharp changes in sediment flux and fluvial influence.

This study documents the ability of an integrated geochemical and paleoecological approach to delineate three distinct sources (Po, Alps, Apennines) that contributed to coastal progradation and to

outline the otherwise lithologically cryptic geometries of clinothems that using conventional sedimentological methods it would be virtually impossible to restore.

1. Introduction

Prograding coastal and deltaic depositional systems are commonly examined across their downdip components, which afford the observation of clinoforms, stratal terminations and stacking patterns. In contrast, scarce attention is paid to parallel-to-depositional-strike delta architecture (Olariu et al., 2010). Clinothems are key sedimentary elements of prograding systems that are typically bounded by hiatal surfaces. Clinothem boundaries mark abrupt shifts in depositional systems configuration and sediment dispersal pathways that might impact significantly hydrocarbon reservoirs. Changes in outbuilding directions within sets of clinothems, in particular, are likely to generate heterogeneities that represent potential barriers to fluid flow (Enge et al., 2010).

In subsurface studies, at the resolution of data commonly available, the geometry of individual clinothems can hardly be assessed on a sub-seismic scale. This is increasingly evident in mudstone-dominated systems (Bohacs et al., 2014; Lazar et al., 2015; Birgenheier et al., 2017; Pellegrini et al., 2017; 2018), where the presence of subtle heterogeneities within seemingly homogeneous sediment bodies cannot be deciphered based on physical sedimentary structures alone.

Sequence-stratigraphic models assume that nearshore strata have relatively consistent and laterally persistent stacking at the systems tract scale (Madof et al., 2016). However, a significant 3D variability of the stratigraphic architecture commonly develops in response to variations in accommodation and sedimentation across a sedimentary basin (Olariu and Steel, 2009). In along-strike direction, the autogenic shift of distributary channels or delta lobes may affect the pattern of sediment distribution. Furthermore, rates of accommodation and sedimentation may change significantly at any particular location within a basin, resulting in slightly diachronous sedimentary units (Catuneanu, 2019).

The middle-late Holocene highstand succession of the Po Plain, in northern Italy, is a 30 m-thick, mud-prone depositional system that records a complex pattern of coastal progradation and delta outbuilding. The stepped progradation of the coastal plain includes a set of five millennial-scale parasequences that have been well portrayed by depositional dip-oriented (SW-NE) cross-sections (Amorosi et al., 2017). Dynamics of Po Delta progradation have been outlined in detail by Correggiari et al. (2005a). Since the Bronze Age, the Po Delta occupied a broad stretch of the Adriatic coastal system, with cuspate and arcuate (wave-dominated) shorelines. After 2,000 cal ky

BP, river sediment discharge changed and the evolution of the Po Delta took place under anthropogenic influence (Maselli and Trincardi, 2013).

Clinothem stacking patterns along strike have been portrayed accurately from the adjacent Adriatic Sea through high-resolution seismic stratigraphy. Individual prodelta lobes overlap laterally and can be traced along-strike as identifiable seismic-stratigraphic units over relatively short (10-20 km) distances (Correggiari et al., 2005b). Along the mud-dominated Adriatic coastline, inner-shelf mud belts are typically elongated downdrift of the Po River mouth, reflecting prevailing sediment dispersal to the south (Cattaneo et al., 2003). Based on seismic-stratigraphic studies, Trincardi et al. (2004) and Correggiari et al. (2005b) documented that individual Po prodelta lobes emanating from the southward oriented delta outlets are more easily preserved compared to those advancing episodically to the NE. When a newly prograding lobe is located updrift (north), the abandoned lobe is sheltered by the new one. In contrast, when the retreating lobe is updrift of the new lobe location, it is partly cannibalized and transported downdrift to the new active lobe (Correggiari et al., 2005b).

The aim of this study, which is focused on the high-resolution sequence stratigraphy of the entire prograding, middle-late Holocene Po Delta system, is to examine the potential of an integrated geochemical and paleoecological approach to decipher clinothem boundaries based on sediment core characteristics within lithologically homogeneous successions. Specific objective is to document the along-strike variability of sediment composition and foraminiferal distribution as a function of the interplay of fluvial dynamics and longshore currents reflected in delta evolution. This variability may have profound impact on the elemental geometry of individual clinothems, the stacking relations among clinothems, and ultimately on reservoir heterogeneity.

2. Holocene stratigraphy

The Po River Basin is a foreland basin system bounded by two mountain chains: the Alps to the north and the Apennines to the south (Fig. 1A). The Po River watershed is generated by the catchments of tens of tributaries extending from the Western Alps to the Adriatic Sea. The Po River is the longest river in Italy, and flows from west to east for 652 km.

Holocene deposits in the Po coastal plain form a typical transgressive-regressive sedimentary wedge made up of coastal to shallow-marine facies assemblages that overlie Pleistocene alluvial deposits and extend both updip and downdip into the fully continental and fully marine settings. Transgressive facies architecture reflects a dominant role of eustasy on sequence development (Amorosi et al., 2017). Highstand deposits, instead, denote a dominantly autogenic delta

architecture. These latter are genetically related to the rapidly deposited mud wedge that accumulated on the shelf for 600 km along the Adriatic coast of Italy (Trincardi et al., 1996; Cattaneo et al., 2003; Amorosi et al., 2016).

Major architectural components of the Holocene succession are sediment packages developed on millennial timescales and framed by flooding surfaces, i.e. surfaces of chronostratigraphic significance (parasequences 1-8 in Amorosi et al., 2017). In along-strike direction, beneath the modern shoreline, the Holocene transgressive-regressive cycle translates into a muddy (offshore/prodelta) unit that is sandwiched between laterally continuous, transgressive barrier sands below and highstand beach-ridge/delta front units above (Campo et al., 2017 - Fig. 1B).

The switch from continental to early Holocene estuarine depositional systems (Bruno et al., 2017) is documented by the retrogradational stacking of thin parasequences 1-3 that denote complex, backstepping relationships punctuated by higher-frequency (centennial-scale) flooding surfaces (Amorosi et al., 2017; Bruno et al., 2017). Above a condensed offshore succession, five middle-late Holocene parasequences (4-8 in Fig. 1B) stack and shingle to form a thick, aggradational to progradational highstand systems tract (HST) that preserves evidence for deltaic and coastal progradation, with thick prodelta clay packages overlain by sand-prone, delta front facies. Within the HST, fossil assemblages depict an upward trend from wave-influenced (lower HST) to river-dominated (upper HST) coastal systems (Amorosi et al., 2017).

Highstand clinothems form shallowing-upward packages that are typically represented by thickening-upward trends in sand layers and by general coarsening-upward patterns (parasequences in Fig. 1B). Heterolithic facies typically develop between prodelta clays and extensive sheet sands made up of delta front deposits (Bhattacharya and Giosan, 2003). In 1D, clinothem boundaries can locally be recognized by the sharp decrease in the sand/mud ratio atop older delta lobes, reflecting delta lobe abandonment. Laterally, the onset of new delta lobes may occur at mud-on-mud contacts, generally above a stratigraphically condensed horizon. In marginal settings, clinothem boundaries commonly occur within homogeneous sandy lithosomes, where such boundaries cannot be easily detected (Fig. 1B). In these instances, assessing clinothem boundaries and the potential geometry of delta lobes from core data, relies exclusively on the interpolation of radiometric data (Amorosi et al., 2017). This approach, however, is not necessarily a viable option, as radiocarbon dating of strongly heterogeneous material (wood, peat, mollusk shells, benthic foraminifers) and possible reworking may affect high-resolution stratigraphic correlation.

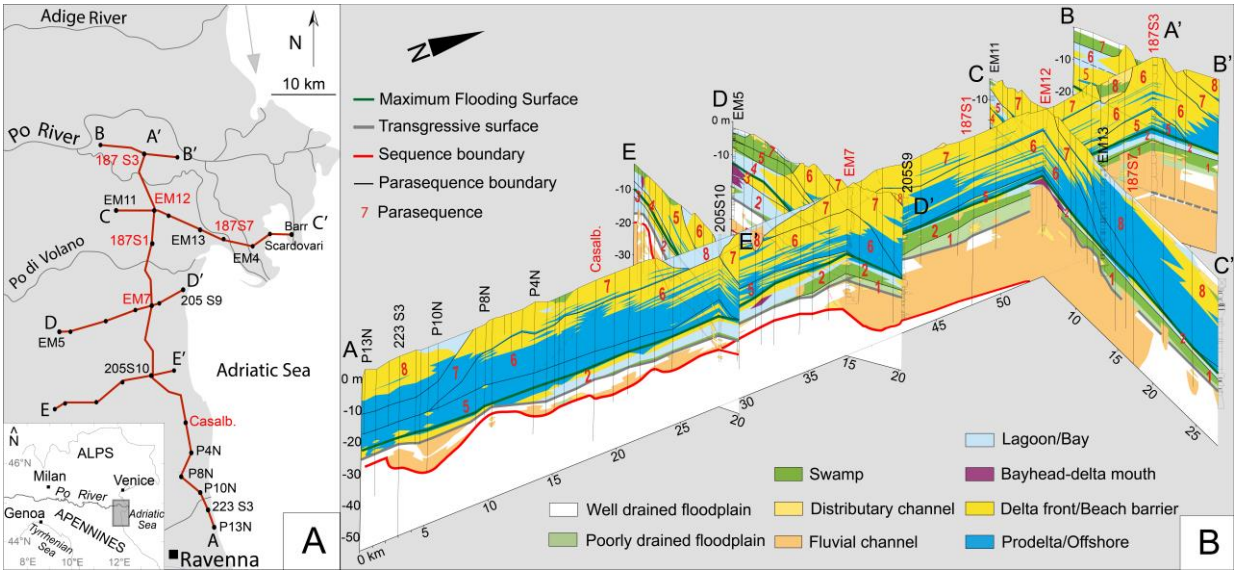

Fig. 1. A: Regional setting and location of the study area. B: Strike-oriented fence diagram, showing the three-dimensional stratigraphic architecture of the Holocene succession of the Po Basin, and its subdivision into parasequences (based on Amorosi et al., 2017). Cores of Figures 3 and 4 are marked in red. The grey arrow indicates the main direction of current circulation in the Adriatic Sea.

3. Methods

A total of 166 core samples were analyzed for bulk-sediment geochemistry. Samples were collected at depths < 30 m from 12 cores (Fig. 1B): P13N, P14N, P10N, P8N, P4N, CB, and 205S10 (Greggio et al., 2018), core 187S1 (Amorosi et al., 2007), Barr (Core1 in Amorosi et al., 2008), EM7, EM12, and 187S3 (this study). The dataset includes 51 additional modern river sediment samples that were used as reference samples for the geochemical characterization of source areas (Fig. 2). With the aim of making geochemical data from modern river sediments comparable with the variety of lithofacies assemblages identified in cores, sampling covered a broad grain-size spectrum, from coarse sand to clay. Recent to sub-recent sediments were collected from subaqueous channel beds, exposed bars, and overbank fine-grained deposits of Po, Apennines, and Alps rivers.

Samples were analyzed at Bologna University laboratories for 10 major element oxides, the loss on ignition (LOI) and 21 trace elements. LOI, evaluated after overnight heating at 950°C (LOI_{950}), represents a measure of volatile substances (weight %, wt%), including pore water, inorganic carbon and organic matter. The estimated precision and accuracy for trace-element determinations was 5%, except for elements with low concentrations (< 10 ppm), for which the accuracy was lower (10%).

A review of micropaleontological data from cores 187S1, 205S9, 205S10, 223S3 and Barr (e.g. Campo et al., 2017; Barbieri et al., 2017), with a special emphasis on benthic foraminiferal assemblages from core 187S7, was carried out to refine facies interpretation and, specifically, to characterize parasequence boundaries within muddy intervals.

The chronological framework relies upon 46 radiocarbon dates provided in the supplementary material (Table 1). Thirty-three radiocarbon dates are from previously published papers, whereas 13 new samples were analyzed at KIGAM Laboratory (Daejeon, Republic of Korea). Conventional ^{14}C ages were calibrated using OxCal 4.2 (Bronk Ramsey, 2009) with the IntCal 13 and Marine13 curves (Reimer *et al.*, 2013).

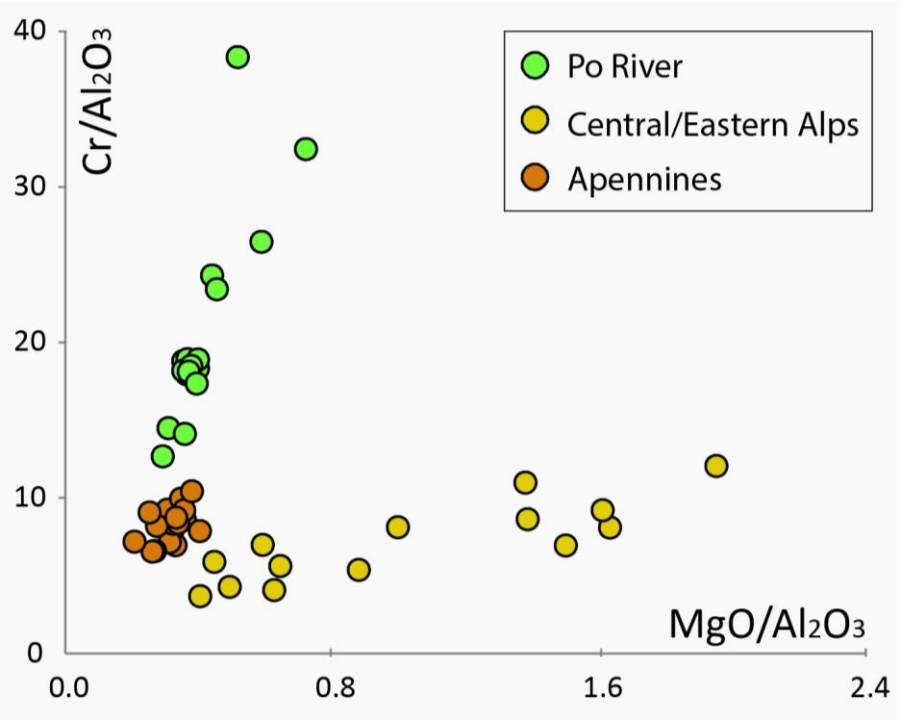

Fig. 2. Scatterplots of MgO/Al_2O_3 versus Cr/Al_2O_3, showing contrasting sediment composition of modern Po River, and selected Alpine and Apennine rivers.

4. Geochemical tracers of sediment provenance

Owing to its situation in a complex tectonic setting, the Po Basin is supplied by a variety of sediment sources that display strongly heterogeneous compositional signatures. The Po River catchment comprises crystalline rocks, in the Western Alps, sedimentary rocks of variable composition in the Central Alps and highly erodible fine-grained units in the Northern Apennines. Bedload sand from the modern Po Delta appears to derive about one-third from Penninic units of the Western Alps, whereas the rest is supplied in sub-equal proportion from External Massifs

(Monte bianco, Argentera), Austroalpine units, Lepontine Dome, Southern Alps, and Northern Apennines (Garzanti et al., 2012).

Mafic and ultramafic rocks crop out extensively in the western Alps and at the northwestern tip of the Apennines, and represent exclusive catchment lithologies that were adopted to delineate basin-wide markers of sediment provenance. These ophiolite successions consist primarily of peridotite, gabbro, basalt and ophiolitic breccia, and deliver large volumes of Cr-rich (and Ni-rich) detritus to the alluvial and coastal systems (Amorosi et al., 2002; Curzi et al., 2006; Amorosi and Sammartino, 2018; Greggio et al., 2018).

Thick dolostone and limestone successions are largely exposed in the Eastern (and Central) Alps, where they make a substantial portion of Triassic platforms and build-ups. Therefore, major elements, such as Mg and Ca (and their oxides MgO and CaO), can be used to discriminate these source areas. Calibration with mineralogical data (Marchesini et al., 2000) has shown that Mg enrichments in modern coastal deposits reflect erosion and transport of detrital dolomite from the North Adriatic river catchments, which acted as sources of particular detritus to the Po coastal plain (Amorosi et al., 2002; 2007; Curzi et al., 2006; Amorosi and Sammartino, 2018; Greggio et al., 2018).

As sediment composition also reflect hydraulic sorting (Garzanti et al., 2009) and absolute Cr, Ni, Mg and Ca concentrations can be affected by changes in grain size, normalization of geochemical data using one element as grain size proxy is necessary to compensate for mineralogical and granular variability of metal concentrations. Al_2O_3, which is routinely used as an efficient normalization factor, proved very effective in reducing the grain size effect and to differentiate sediment sources with distinct parent-rock compositions (Fig. 2).

Plots of modern river samples from three different catchments (Po River, Apennines, Central/Eastern Alps) display poor overlap in composition, and distinctive geochemical signatures can be observed across all grain-size grades (Fig. 2). The geochemical composition of modern stream sediments, thus, delineates primary end-members and strongly constrains provenance inferences from Holocene deposits (Fig. 2). River sediment from the Po River invariably exhibits high Cr/Al_2O_3 levels (> 12) and is associated with relatively low MgO/Al_2O_3 values. On the other hand, samples from modern Alpine rivers plot considerably off this general trend, revealing a distinctive geochemical facies with significantly higher MgO/Al_2O_3 values (> 0.35) that can be readily differentiated from modern Po River samples. Modern Apennine river sediment is, instead, typified by comparatively lower Cr/Al_2O_3 (< 12) and MgO/Al_2O_3 (< 0.4) values.

Compositional features of fluvial end-members were adopted to trace detrital signatures of Holocene cored samples across along-strike segments of the sediment dispersal system (Fig. 3).

Chemostratigraphic correlations, in particular, were employed to trace provenance shifts across lithologically uniform prodelta muds. As an example, a cut-off value of the MgO/Al_2O_3 ratio targeted around 0.35 (Fig. 2) represents an effective tool for the discrimination on vertical profiles between the Po River sediment source and dolostone-derived detritus from the Central/Eastern Alpine rivers (Fig. 3): relatively high MgO/Al_2O_3 values denote sediment supplied, in part at least, by Alpine sources and are interpreted to reflect a mixed signature of chiefly Po-derived sediment, with a considerable supply from Eastern Alps sources. The abrupt upward decrease in the MgO/Al_2O_3 ratio (Fig. 3), which is paralleled by a remarkable increase in Cr/Al_2O_3 values, has stratigraphic significance and is inferred to reflect primarily the shift in sediment provenance from a wave-influenced coastal environment, where S-directed longshore dispersal was an important transport mechanism, to a fluvial-dominated, deltaic system, fed almost uniquely by the Po River.

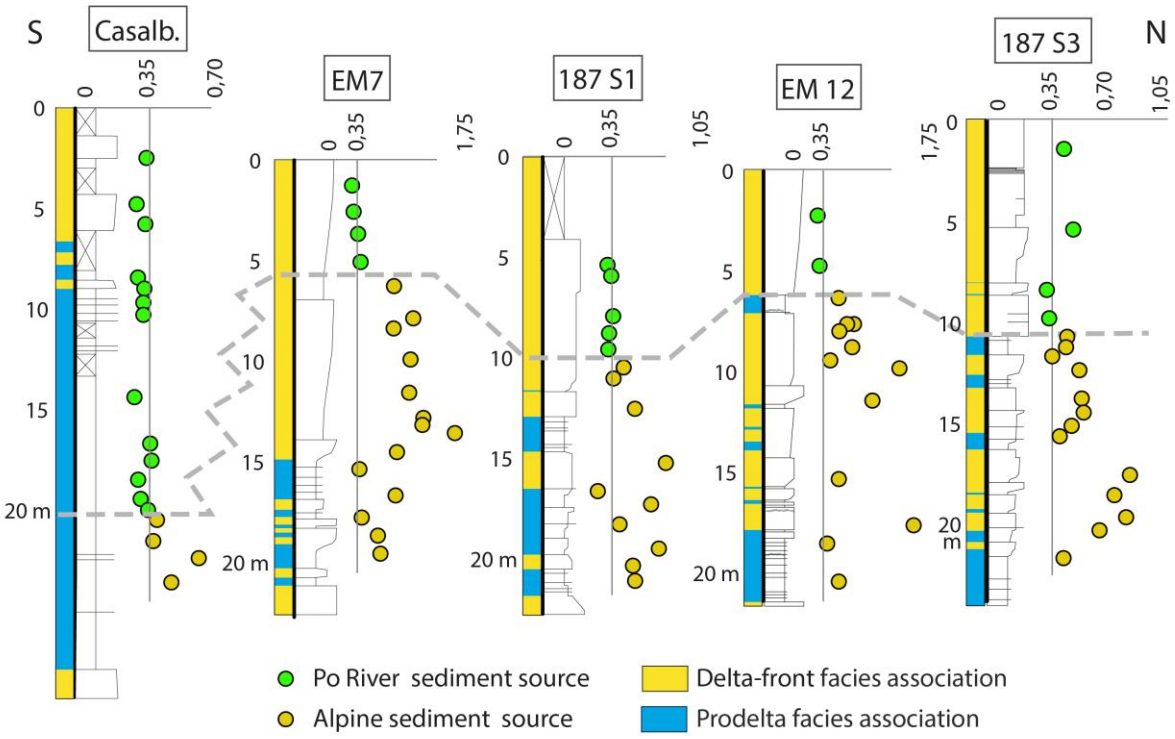

Fig. 3. Vertical profiles of MgO/Al_2O_3 in along-strike direction (core location is shown in red in Fig. 1B), showing the abrupt provenance shift from predominantly Alpine sediment sources to the Po River sediment supply (see Fig. 5). The cut-off value at 0.35 used for the differentiation of Alpine and Po sediment sources is consistent with modern river sediment composition (Fig. 2). Relatively high MgO/Al_2O_3 values in the uppermost two samples from core 187-S3 are associated with extremely high Cr/Al_2O_3 levels, and thus reflect a Po River source.

5. Foraminiferal distribution as a key to clinothem boundary identification

In prograding deltaic successions characterized by fast, relatively continuous sedimentation, clinothem boundaries are represented by hiatal stratigraphic surfaces of short duration and small areal extent. As these surfaces commonly occur within relatively homogeneous lithosomes, clinothem geometries may locally have poor physical expression. In such instances, based on comparison with the modern Po Delta area, foraminiferal distribution can be used to delineate clinothem boundaries that are independent of lithology.

Modern deltaic sediments are typified by low-diversity benthic assemblages indicative of highly-stressed and unstable environments (Jorissen, 1988). Notably, high concentrations (> 40%) of *Ammonia tepida* and *Ammonia parkinsoniana* were observed to reflect remarkable sediment discharge related to flood events, in relatively shallow waters (< 20 m depth), in front of modern Po river mouths (Barbieri et al., 2017). In contrast, relatively high amounts of *Aubignyna perlucida*, *Cribroelphidium granosum*, and *Nonionella turgida* (ca 20% considered together) are typically abundant far from river outlets. In distal prodelta environments, these taxa are commonly associated with inner shelf species, such as *Textularia* spp. and miliolids (e.g. Campo et al., 2017, Barbieri et al., 2017).

The possible use of paleocologic criteria for the delineation of clinothem boundaries is exemplified by the vertical distribution of benthic foraminifers in core 187S7 (Fig. 4 - see Barbieri et al., 2017, for details). At this location, the middle-late Holocene HST consists almost entirely of mud deposits (Fig. 1B), which makes stratigraphic correlations and parasequence boundary identification very difficult. Paleoenvironmental changes in this homogeneous muddy interval can be tracked using changes in benthic foraminiferal distribution as indicators of proximity to/distance from the river mouth. Notably, the upward increase in *A. tepida* and *A. parkinsoniana* is taken as an indication of upward shoaling, and hence, it is interpreted to reflect delta lobe progradation (Fig. 4). This trend is predictably paralleled by the decrease of subordinate species, such as *A. perlucida*, *C. granosum*, and *N. turgida*. Localized, sharp declines in the dominant species (*A. tepida* and *A. parkinsoniana*) concurrent with the occurrence of inner shelf species are, instead, indicative of lower riverine influence and sudden drops in fluvial discharge, likely related to distributary channel avulsion and delta lobe switching (Fig. 4).

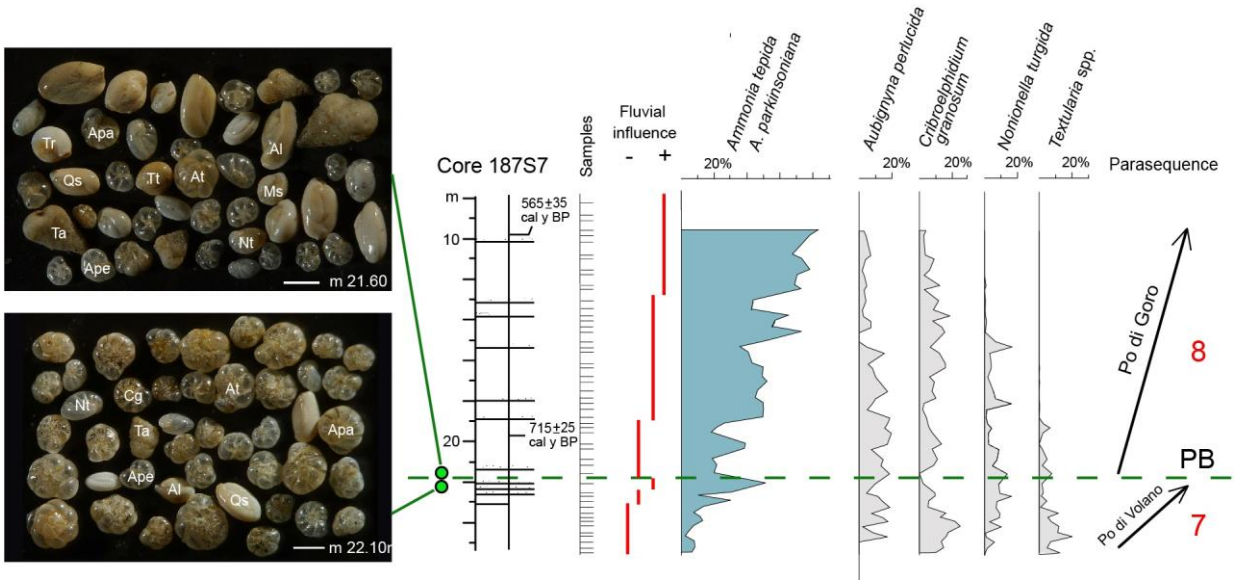

Fig. 4. Abrupt change in foraminiferal assemblage at the boundary (PB) between *Po di Volano* and *Po di Goro* delta lobes (= boundary between parasequences 7 and 8 in core 187-S7 - Figs. 1B and 5). Sample at 22.10 m depth is dominated by *Ammonia tepida* (At) and *A. parkinsoniana* (Apa), whereas sample at 21.60 m depth, just above PB, shows a significantly more diversified assemblage, involving *Aubignyna perlucida* (Ape), *Nonionella turgida* (Nt), *Textularia agglutinans* (Ta), *Cribroelphidium granosum* (Cg), and miliolids (Al: *Adelosina longirostra*; Qs: *Quinqueloculina seminulum*; Ms: *Miliolinella subrotunda*; Tr: *Triloculina rotunda*; Tt: *T. trigonula*). Scale bar: 200 µm.

6. Insight into delta evolution from the geochemical and paleoecological record

The integration and mutual calibration of two independent data sets (bulk-sediment geochemistry and benthic foraminiferal analysis), in addition to lithologic and facies descriptions can be used to generate a model of deltaic and coastal evolution in the Po coastal plain, over the last ca. 6 cal ky BP (parasequences 4 to 8 in Fig. 5). Cyclic depositional patterns are interpreted as driven by autogenic processes (Amorosi et al., 2017), and compensation stacking of mouth bars is proposed as the origin of these packages (Enge et al., 2010).

The geochemical characterization of the HST in the Po Delta system reflects remarkable along-strike variability of dispersal patterns. As a whole, provenance signals proved to be poorly affected by lithologic variation, and are consistent on a depositional system scale, being detectable across both delta front sands and prodelta muds. In general, the prograding Po Delta acted as the major source of sediment to the Adriatic coastal system. However, the proportional contribution of Alpine sources to the coastal region varied continuously as the Po River mouths approached or moved away from the study area. Generally high MgO/Al_2O_3 levels and concurrent low Cr/Al_2O_3 values along the relatively flat, distal segments of older clinothems (parasequences 4 and5 along profile AA' in Fig. 5) suggest that between about 6.0-3.0 cal ky BP Alpine, dolostone-rich river catchments represented a key sediment delivery system for wave-influenced deltas in the Adriatic area via

south-directed longshore drift. During this phase, the Adriatic coastal system experienced weak progradation, and E-dipping clinothems fed by the Po River (parasequences 4 and 5 along transversal profiles in Fig. 5) were restricted to proximal, southern locations.

Parasequence 6 documents contrasting geochemical signatures in the southern and northern regions along profile AA' (Figs. 3 and 5). Comparatively low MgO/Al_2O_3 values and high Cr/Al_2O_3 levels south of transect DD' exhibit strong affinity with modern Po River sediment composition (Fig. 3) and arguably reflect Po Delta initiation in that area. The southern branch of the Po River (*Po di Spina*) likely represented the fluvial feeder system of these southern clinothems (Correggiari et al., 2005a), as documented by the closer affinity of cored samples with the Cr-rich compositions typical of sediment derived from the Po River catchment (Fig. 2). At more northward locations, geochemical data from both sands and muds suggest mixed, fluvial-wave dispersal, with a dominant Alpine contribution and a subordinate, Po supplied component (Figs. 3 and 5).

Given the counter-clockwise oceanic circulation pattern of the Northern Adriatic Sea (Cattaneo et al., 2003), it is likely that sand of Alpine provenance was transported by S-directed, longshore currents, whereas mud was probably resuspended by storms and wave action above storm wave base, and advected alongshore by geostrophic currents for long distances along the paleoshelf. During deposition of parasequence 6, the (river-dominated) *Po di Spina* delta system was more protrusive than its wave-dominated counterparts in the north, and likely represented a barrier to southerly directed longshore transport (Fig. 5).

The prominent shift in sediment composition from Alpine feeding sources to a dominant Po River contribution (Fig. 3), which marks the boundary between parasequences 6 and 7 (Fig. 5), reflects activation of the *Po di Volano* branch, north of the *Po di Primaro* river mouth, and denotes the replacement of S-directed (Alpine) sediment supply with sediment from prograding Po Delta lobes. The change in bulk-sediment composition also reflects the switch from wave-dominated (Cr-poor and Mg-rich) to river-dominated (Cr-rich and Mg-poor) depositional systems, which occurred in response to delta outbuilding. From ~2 cal ky BP onwards, sediment composition of parasequences 7 and 8 (Fig. 1B) largely reflects deltaic sedimentation supplied by the Po River, whereas southern regions denote a geochemical signature from Apennines entry points (Fig. 5).

The mid 12th century (ca. 800 yr BP) natural avulsion (*Rotta di Ficarolo*) that shifted the main trunk of the Po River towards its present position (Correggiari et al., 2005a) is marked by the boundary between parasequences 7 and 8 (*Po di Goro* delta system in Fig. 5). This stratigraphic surface has no geochemical expression, as it separates two delta lobes of different age, but with a similar sediment composition. In this case, shifts in river mouth and delta lobe abandonment were detected by abrupt shifts in benthic foraminiferal distribution (Fig. 4).

The combined geochemical and paleoecologic approach adopted in this work is highly reproducible in ancient sedimentary basins with multiple entry points, provided that sediment source composition and paleogeographic setting are reliably constrained. It is best suited, in particular, to subsurface stratigraphic analysis, where this approach may enable new insights into the interpretation of clinothem stacking patterns, avoiding arbitrary or unrealistic correlation of sparse core data. In hydrocarbon exploration, this technique may guide the delineation of sediment bodies with distinct sediment composition, predictable lateral extent and well-defined petrophysical properties.

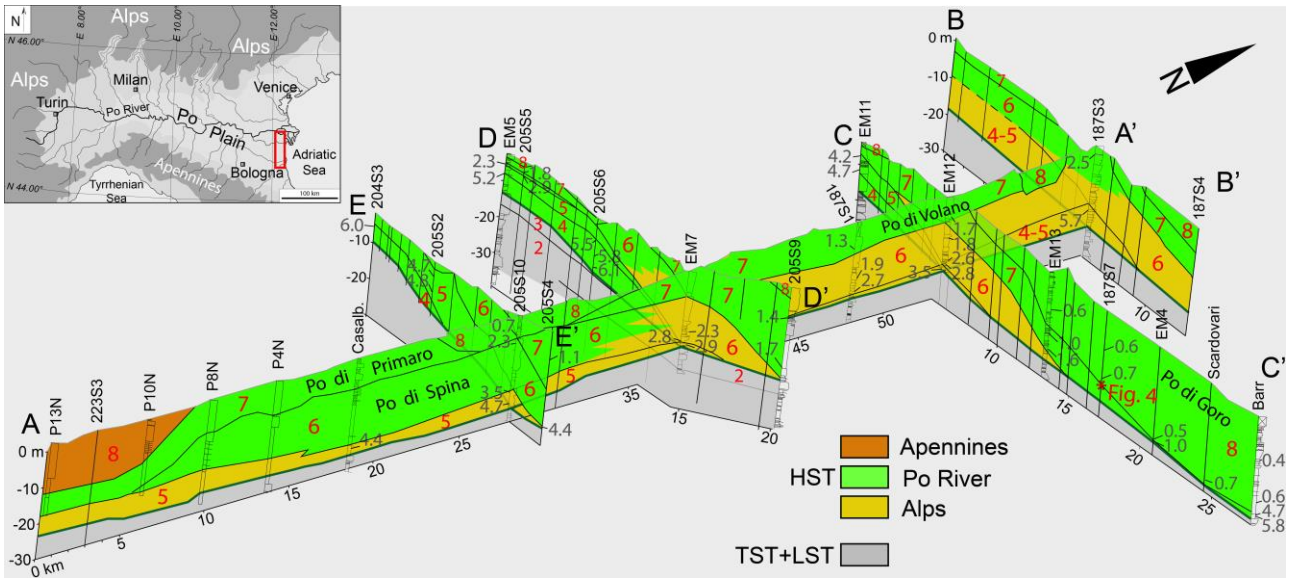

Fig. 5. Strike-oriented fence diagram (similar to Fig. 1B), which allows the visualization of the different sediment-source units and to infer sediment transport as a function of parasequence architecture and of its evolution through time. The red asterisk indicates the stratigraphic location of Figure 4. Numbers refer to 46 radiocarbon dates (cal ky BP) reported as supplementary material. LST: lowstand systems tract, TST: transgressive systems tract, HST: highstand systems tract.

7. Conclusions

Prograding clinothem sets are difficult to separate, especially in mud-prone delta systems, and can be easily missed on a sub-seismic investigation scale. Sharp changes in sediment composition and benthic foraminifera communities can provide the key criteria for deciphering subtle heterogeneities and lithologically cryptic stratigraphic patterns at the parasequence scale, allowing for accurate control of three-dimensional stratigraphic complexity.

This study shows that methods for source discrimination based on bulk-sediment geochemistry can be effective for a sound assessment of the routing system and can ultimately allow

quantification of sediment fluxes below the resolution of seismic data. In multi-sourced sediment-supply systems, unique source rocks control the spatial variation of elemental tracers at the basin scale and carry distinct geochemical fingerprints that may propagate to deltaic, coastal, and shallow marine depositional systems, and that can be applied with equal success to sand, silt and clay fractions.

The chemostratigraphic analysis of the middle-late Holocene prograding succession of the Po coastal plain documents that sediment composition in the coastal system varied significantly along strike and that its spatial distribution reflects mixing of Po, Alps and Apennines sediment sources as a function of sediment dispersal through longshore currents and punctuated delta lobe avulsions. Major and trace element composition of cored samples was matched against geochemical features of samples from the modern river network. Notably, changes in sediment dispersal pathways were detected using key element ratios, such as Cr/Al_2O_3 and MgO/Al_2O_3, where the former is a proxy for the mafic/ultramafic contribution, and the latter is discriminant for dolostone-derived detritus.

Through combined sedimentologic, paleontologic and geochemical investigations, chronologically constrained by a wealth of radiocarbon dates, this study demonstrates that tracing clinoformal geometries within stratigraphic units characterized by relatively continuous sediment accumulation is possible even without seismic data. Mixing of distinct sediment sources is likely to occur in wave-influenced coastal systems, but it is also expected in deltas characterized by strong tidal reworking. Changes in sediment composition and/or foraminiferal distribution can represent primary defining features of clinothem boundaries and are diagnostic to the identification of these surfaces. This approach can be applied successfully to analogous Quaternary subsurface successions, and has a strong potential in outcrop studies, where clinothem boundaries may have no obvious lithologic expression and dipping geometries can be too gentle to be mapped.

At the parasequence-set scale of investigation illustrated in this paper, this innovative approach provides insight into the potential complexities of sediment fluxes that can be useful for guiding interpretation of prograding deltaic and coastal successions in the ancient record. In particular, it can be used to constrain, correlate and map sediment packages that may otherwise be difficult to separate and quantify, and can be applied to developing shale hydrocarbon resources in mudstone-dominated systems.

Acknowledgments

We thank reviewers Cornel Olariu, Fabio Trincardi and an anonymous reviewer for insightful and constructive feedback, as well as Editor Claudio Pellegrini for the efficient handling of the manuscript.

References

Amorosi, A., Sammartino, I., 2018. Shifts in sediment provenance across a hierarchy of bounding surfaces: A sequence-stratigraphic perspective from bulk-sediment geochemistry. *Sediment. Geol.*, 375, 145–156.

Amorosi, A., Centineo, M.C., Dinelli, E., Lucchini, F., Tateo, F., 2002. Geochemical and mineralogical variations as indicators of provenance changes in Late Quaternary deposits of SE Po Plain. *Sediment. Geol.*, 151, 273–292.

Amorosi, A., Colalongo, M.L., Dinelli, E., Lucchini, F., Vaiani, S.C. 2007. Cyclic variations in sediment provenance from Late Pleistocene deposits of Eastern Po Plain, Italy. In Arribas J., Critelli S., Johnsson M.J. (Eds.) S*edimentary Provenance and Petrogenesis: Perspectives from Petrography and Geochemistry*. Geol. Soc. America – Spec. Paper 420, 13–24.

Amorosi, A., Dinelli, E., Rossi, V., Vaiani, S.C., Sacchetto M., 2008. Late Quaternary palaeoenvironmental evolution of the Adriatic coastal plain and the onset of Po River Delta. *Palaeogeogr., Palaeoclimatol., Palaeoecol.*, 268, 80–90.

Amorosi, A., Maselli, V., Trincardi, F., 2016. Onshore to offshore anatomy of a late Quaternary source-to-sink system (Po Plain–Adriatic Sea, Italy). *Earth-Sci. Rev.*, 153, 212–237.

Amorosi, A., Bruno, L., Campo, B., Morelli, A., Rossi, V., Scarponi, D., Hong, W., Bohacs, K.M., and Drexler, T.M., 2017. Global sea-level control on local parasequence architecture from the Holocene record of the Po Plain, Italy. *Mar. Petrol. Geol.*, 87, 99–111.

Barbieri G., Amorosi A., Vaiani, S.C., 2017. Benthic foraminifera as a key to delta evolution: A case study from the late Holocene succession of the Po River Delta. Micropaleontology, 63, 27–41.

Bhattacharya, J.P., Giosan, L., 2003. Wave-influenced deltas: Geomorphological implications for facies reconstruction. *Sedimentology,* 50, 187–210.

Birgenheier, L.P., Horton, B., McCauley, A.D., Johnson, C.L., Kennedy, A., 2017. A depositional model for offshore deposits of the lower Blue Gate Member, Mancos Shale, Uinta Basin, Utah, USA. *Sedimentology*, 64, 1402–1438.

Bohacs, K.M., Lazar, O.R., Demko, T.M., 2014. Parasequence types in shelfal mudstone strata—Quantitative observations of lithofacies and stacking patterns, and conceptual link to modern depositional regimes. *Geology,* 42, 131–134.

Bronk Ramsey, C., 2009. Dealing with outliers and offsets in radiocarbon dating. *Radiocarbon, 51*, 1023–1045.

Bruno, L., Bohacs, K.M., Campo, B., Drexler, T.M., Rossi, V., Sammartino, I., Scarponi, D., Hong, W., Amorosi, A., 2017. Early Holocene transgressive palaeogeography in the Po coastal plain (northern Italy). *Sedimentology,* 64, 1792–1816.

Campo, B., Amorosi, A. & Vaiani, S.C., 2017. Sequence stratigraphy and late Quaternary paleoenvironmental evolution of the Northern Adriatic coastal plain (Italy). *Palaeogeogr. Palaeoclimatol. Palaeoecol.,* 466, 265–278.

Cattaneo, A., Correggiari, A., Langone, L. and Trincardi, F., 2003. The late-Holocene Gargano subaqueous delta, Adriatic shelf: sediment pathways and supply fluctuations. *Mar. Geol.*, 193, 61–91.

Catuneanu, O., 2019. Model-independent sequence stratigraphy. *Earth-Sci Rev.*, 188, 312–388.

Correggiari, A., Cattaneo, A., Trincardi, F., 2005a. Depositional patterns in the Late-Holocene Po delta system. In: *River Deltas–Concepts, Models and Examples* (Eds. J.P. Bhattacharya and L. Giosan), *SEPM Spec. Publ.*, 83, 365–392.

Correggiari, A., Cattaneo, A., Trincardi, F., 2005b. The modern Po Delta system: lobe switching and asymmetric prodelta growth. *Mar. Geol.*, 222, 49–74.

Curzi, P.V., Dinelli, E., RICCI Lucchi, M., Vaiani, S.C., 2006. Palaeoenvironmental control on sediment composition and provenance in the late Quaternary deltaic successions: a case study from the Po delta area (Northern Italy). *Geol. J.*, 41, 591–612.

Enge, H.D., Howell, J.A., Buckley, S.J., 2010. The geometry and internal architecture of stream mouth bars in the Panther Tongue and the Ferron Sandstone Members, Utah, U.S.A. *J. Sedim. Res.*, 80, 1018–1031.

Garzanti, E., Ando', S., Vezzoli, G., 2009. Grain size dependence of sediment composition and environmental bias in provenance studies. *Earth and Planet. Sci. Lett.*, 277, 422–432.

Garzanti, E., Resentini, A., Vezzoli, G., Anso', S., Malusa', M., Padoan, M., 2012. Forward compositional modelling of Alpine orogenic sediments. *Sedimentary Geology*, 280, 149–164.

Greggio, N., Giambastiani, B.M.S., Campo, B., Dinelli, E., Amorosi, A., 2018. Sediment composition, provenance and Holocene paleoenvironmental evolution of the Southern Po River coastal plain (Italy). *Geol. J.*, 53, 914–928.

Jorissen, F.J., 1988. Benthic foraminifera from the Adriatic Sea; principles of phenotypic variation. *Utrecht Micropaleontol. Bull.*, 37, 1–176.

Lazar, O.R., Bohacs, K.M., MacQuaker, J.H.S., Schieber, J., Demko, T.M., 2015. Capturing key attributes of fine-grained sedimentary rocks in outcrops, cores and thin sections—nomenclature and description guidelines. *J. Sed. Res.*, 85, 230–246.

Macquaker, J.H.S., Bentley, S.J., Bohacs, K.M., 2010. Wave-enhanced sediment-gravity flows and mud dispersal across continental shelves: reappraising sediment transport processes operating in ancient mudstone successions. *Geology*, 38, 947–950.

Madof, A.S., Harris, A.D., Connell, S.D., 2016. Nearshore along-strike variability: Is the concept of systems tract unhinged? Geology, 44, 315–318.

Marchesini, L., Amorosi, A., Cibin, U., Zuffa, G.G., Spadafora, E., Preti, D., 2000. Sand composition and sedimentary evolution of a Late Quaternary depositional sequence, northwestern Adriatic Coast, Italy. *J. Sed. Res.*, 70, 829–838.

Maselli, V., Trincardi, F., 2013. Man made deltas. *Scientific Reports*, 3, 1–7.

Olariu, C., Steel, R.J., 2009. Influence of point-source sediment-supply on modern shelf-slope morphology: implications for interpretation of ancient shelf margins. *Basin Res*., 21, 484–501.

Olariu, C., Steel, R.J., Petter, A.L., 2010. Delta-front hyperpycnal bed geometry and implications for reservoir modeling: Cretaceous Panther Tongue Delta, Book Cliffs, Utah. Am. Assoc. Petrol. Geol. Bull., 94, 819–845.

Pellegrini, C., Maselli, V., Gamberi, F., Asioli, A., Bohacs, K.M., Drexler, T.M., Trincardi, F., 2017. How to make a 350-m-thick lowstand systems tract in 17,000 years: The Late Pleistocene Po River (Italy) lowstand wedge. *Geology*, 45, 327–330.

Pellegrini, C., Asioli, A., Bohacs, K.B., Drexler, T.M., Feldman, H.R., Sweet, M.L., Maselli, V., Rovere, M., Gamberi, F., Dalla Valle, G., Trincardi, F., 2018. The late Pleistocene Po River lowstand wedge in the Adriatic Sea: Control on architecture variability and sediment partitioning. *Mar. Petrol. Geol.*, 96,16-50.

Reimer, P.J., Bard, E., Bayliss, A., Beck, J.W., Blackwell, P.G., Bronk Ramsey, C., Buck, C.E, Cheng, H., Edwards, R.L., Friedrich, M., Grootes, P.M., Guilderson, T.P., Haflidason, H., Hajdas, I., Hatté, C., Heaton, T.J., Hoffmann, D.L., Hogg, A.G., Hughen, K.A., Kaiser, K.F., Kromer, B., Manning, S.W., Niu, M., Reimer, R.W., Richards, D.A., Scott, E.A., Southon, J.R., Staff, R.A., Turney, C.S.M., Van Der Plicht, J., 2013. IntCal13 and Marine13 radiocarbon age calibration curves, 0-50,000 years cal BP. *Radiocarbon, 55*, 1869–1887.

Rossi, V., Vaiani, S.C., 2008. Benthic foraminiferal evidence of sediment supply changes and fluvial drainage reorganization in Holocene deposits of the Po Delta. *Mar. Micropaleontol.*, 69, 106–118.

Trincardi, F., Cattaneo, A., Asioli, A., Correggiari, A., Langone, L., 1996. Stratigraphy of the Late-Quaternary deposits in the central Adriatic basin and the record of short term climatic events. *Mem. Istit. Ital. Idrobiol.*, 55, 39–70.

Trincardi, F., Cattaneo, A., Correggiari, A., 2004. Mediterranean prodelta systems: natural evolution and human impact investigated by EURODELTA. Oceanography, 17, 34–45.

5. CONCLUSIONS

Over the last decade, late Quaternary depositional systems have been studied extensively at different time scales, with the aim of developing models able to predict the sedimentary response of depositional environments to future climate change.

Recent stratigraphic studies have focused on facies characterization and reconstruction of stratigraphic architecture: the proximal segments of alluvial successions exhibit a characteristic stratigraphic architecture, made up of a complex succession of floodplain clays and fluvial-channel sand bodies, resulting from the interplay of allogenic and autogenic controlling factors; the distal portion of the late Quaternary Po Basin succession has been characterized by swampy and marine-influenced facies associations.

Previous sequence-stratigraphic work in the Po Plain has emphasized the key role of paleosols and associated sand-dominated fluvial bodies for interpreting and correlating alluvial architecture, but these studies have been carried out deliberately far from tectonically active areas, in order to assess sedimentary evolution in response to relative sea-level change. Furthermore, transgressive-regressive coastal deposits, with a wedge-shaped geometry, exhibit an internal architecture of millennial-scale sediment packages that has been predominantly conceptualized rather than documented. Additionally, in most cases stratigraphic correlations have been made with a relatively poor chronologic control.

This Ph.D. study focused on the Late Pleistocene-Holocene alluvial succession of the Po Plain, close to tectonically active areas. This period represents an interval of time where process controls are well established. In this respect, such sedimentary successions can be used for a reliable interpretation of the rock record.

The southeastern sector of the Po Plain, specifically the Argenta-Longastrin area, was analyzed in detail and high-resolution core-based stratigraphy was carried as a new technique to assess a complete and decipherable record of tectonic deformation on a range of scales and to help predict the likely spatial distribution of future damaging earthquakes in the study area (Paper 1).

Coastal successions were examined for their stratigraphic markers originally deposited in a horizontal position (nearshore and lagoon deposits). In the distal portion of the alluvial plain, the lateral traceability of stratigraphic markers and the relationship between their morphology and the location of the buried structures were investigated through the 3D reconstruction of selected Late Pleistocene and Holocene marker beds (Paper 2).

The factors controlling the natural subsidence of sediments were examined through geotechnical analysis and decompaction modelling (Paper 3).

Finally, the stratigraphic architecture of the entire prograding, middle-late Holocene Po Delta coastal succession was analyzed using geochemical and palaeoecological analysis in order to refine the stratigraphic framework (Paper 4).

The key points of this work, which analyzed about eight hundred stratigraphic data, can be summarized as follows:

- The south-eastern Po Plain may serve as a very useful location for high-resolution stratigraphic analysis of Quaternary deposits, due to the comprehensive stratigraphic, sedimentological, and paleontological database available in this region.

The coastal succession was analyzed to identify diagnostic marker horizons and track them in the subsurface. The stratigraphic framework was refined and chronologically constrained by about 200 radiocarbon dates and an optically-stimulated luminescence (OSL) dating. Beyond the limits of radiocarbon dating, age assignments were carried out by electron spin resonance (ESR) data coupled with pollen profiles. In order to enhance stratigraphic analysis, a coring survey was carried out between May and October 2018 and four continuous cores (B1-B4), 17 m to 35 m long, were recovered.

In this study, depositional facies were determined accurately, on the basis of lithology, accessory components, and their faunal content. In areas where active tectonics has a poor geomorphic expression, core stratigraphy helped predict likely locations of future damaging earthquakes.

.

- The detailed chronostratigraphic framework reconstructed in the study area was built through distinct highly effective stratigraphic markers of different type. These markers were accurately selected on the basis of their sedimentological characteristics, and were typified for their fossil content. Five stratigraphic markers of three distinct ages appeared to be deformed: (i) nearshore beach deposits, assigned to the Last Interglacial (about 120 kyr BP), (ii) two Late Pleistocene paleosols, assigned to the Marine Isotope Stage 3/2 transition (26-29 cal kyr BP), and to the Younger Dryas cold spell (11-13 cal kyr BP), respectively, and (iii) two lagoon horizons of Holocene age, dated to 8.3-8.6 and 5.6-6.2 cal kyr BP, respectively.

Late Pleistocene pedogenically modified horizons represent key markers for high-resolution stratigraphic analysis in the Po Plain, because of their basin-wide occurrence and very high correlation potential. These weakly developed paleosols exhibit distinctive A-Bk, A-Bw or A-Bk-Bw profiles (Inceptisols) that make them easily recognizable within thick floodplain successions. The main limitation on their use is that they may have complex morphology at time of formation. Therefore, only a qualitative evaluation of their post-burial deformation is possible. Holocene

coastal sands, that may span several meters in depth, can hardly be used to restore a detailed paleotopography.

By contrast, older beach deposits represent excellent sea-level marker at the basin scale, as alternating alluvial and coastal deposits are the typical expression of late Quaternary glacial/interglacial cycles. Clay-rich lagoon/outer estuary horizons are the most reliable indicators of post-burial deformation, as they represent approximately horizontal surfaces at the time of deposition. Brackish deposits, in particular, can be easily ascertained on the basis of refined paleontologic criteria and easily differentiated from adjacent freshwater (swamp/inner estuary) and coastal deposits.

In this work, we demonstrate that the areas of maximum deformation of Late Pleistocene-Middle Holocene stratigraphic markers are strikingly coincident with the epicenters of historic and instrumental seismicity dating back to the last five centuries and the offset of marker horizons across the Argenta-Longastrino ridge coincides with the location of major thrust fronts.

- In the study area, located above the Ferrara Arc, specifically in correspondence of the Longastrino thrust front, deposits of distinct ages from the subsurface of the Po Plain were observed to be displaced and involved in deformation. Holocene facies distribution is strongly influenced by the underlying tectonic structures; beach-barrier systems are abruptly replaced by thick lagoon deposits above the Longastrino ridge. This suggests a morphologic (tectonic?) control on the Early Holocene landward shift of the shoreline and its subsequent seaward migration. Late Pleistocene swamp deposits have remarkably lenticular geometries that thicken in the synclines and wedge out onto the structural highs. This indicates that swamp environments occupied the lowest position in the landscape, as an effect of possibly growing, active structures.

The deformation of the Last Interglacial nearshore sand body, of Late Pleistocene paleosols and of Holocene lagoon horizons suggests that the Argenta-Longastrino area, where the last significant earthquakes were recorded five centuries ago, may have a near-identical, or even higher potential for seismic hazard than the near Mirandola area, which experienced two damaging earthquakes in 2012.

- The morphology of three stratigraphic markers (LGM paleosol, YD paleosol, and a brackish horizon dated to about 6.1 cal kyr BP) was reconstructed through correlation of about four hundred data in a dense network of cross-sections generated and analyzed with the software package Petrel 2014.

The maximum elevation of these surfaces is encountered above the buried thrust front and decreases north-eastwards, which means that the deformation grows through time. Three-dimensional maps of deformed stratigraphic markers demonstrate that there is a relationship between the morphological culminations observed in the cross-sections and the location of the buried tectonic structures.

This study shows that tectonic activity along these thrusts played a significant role in the deformation of the paleosols and of other stratigraphic markers.

- The identification of major unconformities and their correlative conformities from the Argenta-Longastrino area was carried out through the analysis and interpretation of seismic profiles from the Eni s.p.a. database.

Three basin-scale unconformity-bounded units were identified and classified, based on their geometry and on seismic-reflector terminations, through the identification of two major unconformities: (i) an intensely deformed and faulted pre-tectonic unit; (ii) an intermediate wedge-shaped syntectonic unit made up of marine turbidites with seismic reflectors converging towards the culmination of the thrust-related anticlines; (iii) an upper undeformed post-tectonic unit, sealing the main structures and draping the whole succession. Minor unconformities within the post-tectonic unit allowed its subdivision into four lower-rank units.

According to the ENI stratigraphy, the post-tectonic unit includes two formations: Carola Formation, of Calabrian age, and Ravenna Formation, of Middle Pleistocene-Holocene age. Undeformed reflectors with planar onlap terminations onto the lower bounding unconformity are recurrent features in the post-tectonic Carola Formation, at comparatively southern locations. In contrast, SW to the structural culminations, onlapping reflectors from the upper Carola and Ravenna formations show distinctive inclined geometries that thin out towards the crest, suggesting they were tilted by the growth of the Longastrino structural high.

Detailed analysis of seismic-reflector terminations showed clear evidence of syn-tectonic deformation (onlap deformation, decreasing thickness and converging reflectors towards growing anticlines) close to Longastrino fault.

- The high-resolution study of drill cores of Late Pleistocene-Holocene age from the shallow subsurface, coupled with the seismic stratigraphic analysis of the basin fill can represent a technique to assess a decipherable record of near-surface tectonic deformation. Delineating a geologic scenario of Late Pleistocene-Holocene tectonic deformation through a combined stratigraphic and sedimentological approach may represent the missing link between the analysis of long-term (basin-

scale), steady-state tectonics, acting on 10^6-10^7 yrs time periods and short-term deformation, primarily developed on 10^0-10^2 yrs time scales.

The large overlap between deformation of the Last Interglacial nearshore sand body and of a series of prominent stratigraphic markers of Late Pleistocene-Holocene age across structural lineaments of the southern Po Plain, deformation of older stratigraphic markers, and earthquake location provides some support for the hypothesis that the Argenta-Longastrino ridge could host active seismogenic faults.

- In the Po coastal plain the stratigraphy of the uppermost 140 m is characterized by two thin laterally extensive lagoon horizons: (i) a thin (0.5-3 m) lagoon horizon that drapes coastal sands assigned to the MIS 5e; and (ii) a thin lagoon horizon, mostly sandwiched between freshwater deposits, dated to ~ 5.6 cal ky BP. These stratigraphic markers were used as reference key beds to assess subsidence rates for the last 5.6 and 120 ky within a chronologically constrained stratigraphic framework.

Subsidence rates (SR) in the Po coastal plain appear to be strongly influenced by the buried tectonic structures. Particularly, subsidence rates averaged over the last 5.6 and 120 ky decrease towards the anticline culmination of the Argenta-Longastrino area. In syncline areas, subsidence may have been enhanced by high sedimentation rates and by the preferential accumulation of highly compressible prodelta, delta plain and swamp deposits. Subsidence rates in the last 5.6 ky are in the range of 0.8-2.0 mm y^{-1}, about twice the values measured for the last 120 ky (0.4-0.8 mm y^{-1}).

The Holocene stratigraphic architecture influenced lateral changes in subsidence rates over the last 5.6 ky. Subsidence rates are higher in areas where the 5.6 ky BP horizon overlies soft estuarine muds, and lower where the same marker bed lies onto the less compressible, 7 m-thick coastal sand body.

Subsidence rates in the last 120 ky appear to have been controlled mainly by the location of the buried Apennines thrust-related folds, which in turn influenced sedimentation rates and distribution of the highly compressible depositional facies.

The contribution of sediment compaction to natural subsidence was assessed through a finite-element 1D decompaction model, applied to core B4 from the Argenta area. The mechanical characterization of the main lithofacies associations, based on oedometer tests, bulk-density, loss-on-ignition tests and numerical modelling, shows that higher compaction values are associated with the presence of peat horizons (about 50% of deformation). Compaction of Late Pleistocene and Holocene sediments strongly impacted subsidence rates in the last 5.6 ky, where subsidence at this

location is almost entirely accommodated by the compaction of the uppermost 30 m-thick sediment package.

- The middle-late Holocene deposits of the Po coastal plain form a typical transgressive-regressive sedimentary wedge made up of coastal to shallow-marine facies assemblages that overlie Pleistocene alluvial deposits; an aggradational to progradational parasequence set reveals the complex interaction of W–E Po Delta progradation, S-directed longshore currents (from Alpine rivers) and Apennines rivers supply.

This study enhances our knowledge about the use of an integrated geochemical and palaeoecological approach to delineate three distinct sources (Po, Alps and Apennines) that contributed to coastal progradation. Well-established geochemical markers of sediment provenance (Cr and Mg) were used to assess distinctive detrital signatures.

It was demonstrated that tracing clinoformal geometries within stratigraphic units characterized by relatively continuous sediment accumulation is possible even in absence of seismic data. The stratigraphic framework of the Po coastal Plain was refined through combined sedimentologic, palaeontological and geochemical investigations, chronologically constrained by a wealth of radiocarbon dates.

This approach can be applied successfully to analogous Quaternary subsurface successions, and has a strong potential in outcrop studies, where clinothem boundaries may have no obvious lithological expression to be mapped. At the parasequence-set scale of investigation this innovative approach provides information about the potential complexities of sediment fluxes that can be useful for building interpretation of prograding deltaic and coastal successions in the ancient record. This approach can be used to correlate and map sediment packages that may otherwise be difficult to separate and quantify, as a function of sediment provenance.

REFERENCES

AGIP Mineraria, 1959. Campi gassiferi padani, in Atti del Convegno su Giacimenti Gassiferi dell'Europa Occidentale (Milano, 30 September–5 October 1957): Accademia Nazionale dei Lincei ed Ente Nazionale Idrocarburi, Milano (ENI), 2, 45–497.

AGIP, 1977. Temperature Sotterranee: Inventario dei Dati Raccolti dall'AGIP durante la Ricerca e la Produzione di Idrocarburi in Italia: Milano, Edizioni AGIP, 1930.

Aquater-ENEL, 1981. Elementi di neotettonica del territorio italiano: Volume Speciale, Roma.

Amorosi, A., 2008. Delineating aquifer geometry within a sequence stratigraphic framework: Evidence from the quaternary of the Po river Basin, Northern Italy, in A. Amorosi, B.U. Haq, and L. Sabato, eds., Advances in Application of Sequence Stratigraphy in Italy: GeoActa Spcial Pubblication 1, 1-14.

Amorosi, A., 2012. Chromium and nickel as indicators of source-to-sink sediment transfer in a Holocene alluvial and coastal system (Po Plain, Italy): Sedimentary Geology 280, 260-269.

Amorosi, A., and Marchi, N, 1999. High-resolution sequence stratigraphy from piezocone tests: an example from the Late Quaternary deposits of the southeastern Po Plain: Sedimentary Geology, 128, 67-81.

Amorosi, A., and Milli, S., 2001. Late Quaternary depositional architecture of Po and Tevere river deltas (Italy) and worldwide comparison with coeval deltaic successions: Sedimentary Geology, 144, 357–375.

Amorosi, A., and Colalongo, M. L., 2005. The linkage between alluvial and coeval nearshore marine successions: evidence from the Late Quaternary record of the Po River Plain, Italy, in M. D. Blum, S.B. Marriott, and S.F. Leclair, eds., Fluvial Sedimentology VII: International Association of Sedimentologists Special Publication 35, 257-275.

Amorosi, A., and Sammartino, I., 2018. Shifts in sediment provenance across a hierarchy of bounding surfaces: A sequence-stratigraphic perspective from bulk-sediment geochemistry: Sedimentary Geology, 375, 145-156. https://doi.org/10.1016/j.sedgeo.2017.09.017.

Amorosi, A., Farina, M., Severi, P., Preti, D., Caporale, L., and Di Dio, G., 1996. Genetically related alluvial deposits across active fault zones: an example of alluvial fan-terrace correlation from the upper Quaternary of the southern Po Basin, Italy: Sedimentary Geology 102, 275-295.

Amorosi, A., Colalongo, M.L., Pasini, G., and Preti, D., 1999a. Sedimentary response to late Quaternary sea-level changes in the Romagna coastal plain (northern Italy): Sedimentology 46, 99-121.

Amorosi, A., Colalongo, M. L., Fusco, F., Pasini, G., and Fiorini, F., 1999b. Glacio-eustatic control of continental shallow marine cyclicity from Late Quaternary deposits of the south-eastern Po Plain (Northern Italy): Quaternary Research 52, 1-13.

Amorosi, A., Centineo, M. C., Dinelli, E., Lucchini, F., and Tateo, F., 2002. Geochemical and mineralogical variations as indicators of provenance changes in Late Quaternary deposits of SE Po Plain: Sedimentary Geology 151, 273-292.

Amorosi, A., Centineo, M.C., Colalongo, M.L., Pasini G., and Sarti, G., 2003. Facies architecture and Latest Pleistocene-Holocene depositional history of the Po Delta (Comacchio Area, Italy): The Journal of Geology 111, 39-56.

Amorosi, A., Colalongo, M.L., Fiorini F., Fusco, F., Pasini, G., Vaiani, S. C., and Sarti, G, 2004. Palaeogeographic and palaeoclimatic evolution of the Po Plain from 150-ky core records: Global and Planetary Change 40, 55-78.

Amorosi, A., Centineo, M.C., Colalongo M.L., and Fiorini, F., 2005. Millennial-scale depositional cycles from the Holocene of the Po Plain, Italy: Marine Geology 222-223, 7-18. https://doi.org/10.1016/j.margeo.2005.06.041.

Amorosi, A., Colalongo, M. L., Dinelli, E., Lucchini, F. and Vaiani, S. C., 2007. Cyclic variations in sediment provenance from late Pleistocene deposits of the eastern Po Plain, Italy, in: Arribas, J., Critelli, S. and Johnsson, M. J., Eds., Sedimentary provenance and petrogenesis: perspectives from petrography and geochemistry, 13–24. Boulder: Geological Society of America. Special Paper 420.

Amorosi, A., Pavesi, M., Ricci Lucchi, M., Sarti, G., and Piccin, A, 2008a. Climatic signature of cyclic fluvial architecture from the Quaternary of the central Po Plain, Italy: Sedimentary Geology 209, 58-68.

Amorosi, A., Dinelli, E., Rossi, V., Vaiani, S.C. and Sacchetto, M., 2008b. Late Quaternary palaeoenvironmental evolution of the Adriatc coastal plain and the onset of the Po River Delta: Palaeogeography, Palaeoclimatology, Palaeoecology, 268, 80-90.

Amorosi, A., Bruno, L., Rossi, V., Severi, P., and Hajdas, I, 2014. Paleosol architecture of a late Quaternary basin–margin sequence and its implications for high-resolution, non-marine sequence stratigraphy: Global and Planetary Change 112, 12-25. https://doi.org/10.1016/j.gloplacha.2013.10.007.

Amorosi, A., Bruno, L., Campo, B., Morelli, A., 2015. The value of pocket penetration tests for the high-resolution palaeosol stratigraphy of late Quaternary deposits: Geological Journal 50, 670-682. doi 10.1002/gj.2585.

Amorosi, A., Bruno L., Facciorusso, J., Piccin, A., and Sammartino, I., 2016a. Stratigraphic control on earthquake-induced liquefaction: A case study from the Central Po Plain (Italy): Sedimentary Geology, 345, 42-53. https://doi.org/10.1016/j.sedgeo.2016.09.002.

Amorosi, A., Maselli, V., Trincardi, F., 2016b. Onshore to offshore anatomy of a late Quaternary source-to-sink system (Po Plain-Adriatic Sea, Italy): Earth Sci. Rev. 153:212–237.http://doi.org/10.1016/j.earscirev.2015.10.010.

Amorosi, A., Bruno, L., Campo, B., Morelli, A., Rossi, V., Scarponi, D., Hong, W., Bohacs, K.M., and Drexler, T.M., 2017a. Global sea-level control on local parasequence architecture from the Holocene record of the Po plain, Italy: Marine and Petroleum Geology, 87, 99–111.

Amorosi, A., Bruno, L., Cleveland, D.M., Morelli, A., and Hong, W., 2017b. Paleosols and associated channel-belt sand bodies from a continuously subsiding late Quaternary system (Po Basin, Italy): New insights into continental sequence stratigraphy: Geological Society of America Bulletin, 129(3-4), 449-463. https://doi.org/10.1130/B31575.1.

Amorosi, A., Bruno, L., Campo, B., Costagli, B., Dinelli, E., Hong, W., Sammartino, I., Vaiani, S.C., 2019. Tracing clinothem geometry and sediment pathways in the prograding Holocene Po Delta system through integrated core stratigraphy: Basin Research. https://doi.org/10.1111/bre.12360.

Antonioli, F., Ferranti, L., Fontana, A., Amorosi, A., Bondesan, A., Braitenberg,C., Dutton, A., Fontolan, G., Furlani, S., Lambeck, K., Mastronuzzi, G., Monaco, C., Spada, G., and Stocchi, P., 2009. Holocene relative sea-level changes and vertical movements along the Italian and Istrian coastlines: Quaternary International 206, 102-133.

Anzidei, M., Maramai, A., and Montone, P., 2012. The Emilia (Northern Italy) seismic equence of May–June, 2012: Preliminary data and results: Annals of Geophysics, 55, 515–842.

Argnani, A., and Frugoni, F., 1997. Foreland deformation in the Central Adriatic and its bearing on the evolution of the Northern Apennines: Annali Di Geofisica, 40(3), 771–780.

Astori, A., Castaldini, G., Burrato, P., and Valensise, G., 2002. Where the Alps meets the Apennines, active tectonics and seismicity of Central Po Plain: SAFE Project, semester meeting, Mantova, 20-23.

Bartolini, C., Bernini, M., Carloni, G.C., Costantini, A., Federici, P.R., Gasperi, G., Lazzarotto, A., marchetti, G., Mazzanti, R., Papani, G., Pranzini, G., Rau, A., Sandrelli, F., Vercesi, P.L., Castaldini, D., and Francavilla, F., 1982. Carta neotettonica dell'Appennino Settentrionale, Note Illustrative: Bollettino della Società Geologica Italiana 101, 523-549.

Bellotti, P., Chiocci, F.L., Milli, S., Tortora, P., Valeri, P., 1994. Sequence stratigraphy and depositional setting of the Tiber delta: integration of high resolution seismics, well logs and archaeological data: Journal of Sedimentary Research, B64, 3, 416-432.

Bellotti, P., Milli, S., Tortora, P., Valeri, P., 1995. Physical stratigraphy and sedimentology of the Late Pleistocene-Holocene Tiber Delta depositional sequence: Sedimentology, 42(4), 617-634. https://doi.org/10.1111/j.1365-3091.1995.tb00396.x.

Bender, O., H.J. Boehmer, D. Jens, and K.P. Schumacher, 2005. Using GIS to analyze long-term cultural land-scape change in Southern Germany: Landscape and Urban Planning, 70, 111-125.

Berendsen, H. J., and Stouthamer, E., 2000. Late Weichselian and Holocene palaeogeography of the Rhine-Meuse delta, the Netherlands: Palaeogeography, Palaeoclimatology, Palaeoecology, 161(3–4), 311–335. https://doi.org/10.1016/S0031-0182(00)00073-0.

Berger, G.W., Pillans, B.J., Bruce, J.G., and McIntosh, P.D., 2002. Luminescence chronology of loess-paleosol sequences from southern South Island, New Zealand: Quaternary Science Reviews, 21 (16–17), 1899–191. https://doi: 10 .1016 /S0277 -3791 (02)00021 -5.

Bestland, E.A., 1997. Alluvial terraces and Paleosols as indicators of early Oligocene climate change (John Day Formation, Oregon): Journal of Sedimentary Research 67, 840-855.

Bignami, C., Burrato, P., Cannelli, V., Chini, M., Falcucci, E., Ferretti, A., Gori, S., Kyriakopoulos, C., Melini, D., Moro, M., Novali, F., Saroli, M., Stramondo, S., Valensise, G., Vannoli, P., 2012. Coseismic deformation pattern of the Emilia 2012 seismic sequence imaged by Radarsat-1 interferometry: Annales Geophysicae, 55(4), 788–795.

Blum, M.D., Martin, J., Milliken, K., and Garvin, M., 2013. Paleovalley systems: Insights from Quaternary analogs and experiments: Earth-Science Reviews, 116, 128–169. https://doi: 10 .1016 /j.earscirev .2012 .09 .003.

Boccaletti, M., Coli, M., Eva, C., Ferrari, G., Giglia, G., Lazzarotto, A., Merlanti, F., Nicolich, R., Papani, G., and Postpischl, D., 1985. Considerations on the seismotectonics of the Northern Apennines: Tectonophysics, 117, 7-38.

Boccaletti, M., Martinelli, P., Cerrina Ferroni, A., Mannori, M.R., and Sani, F., 1987. Neogene tectonic phases of the Northern Apennines-South Alpine system; their significance in relation to the foredeep sedimentation: Acta Naturalia de l'Ateneo Parmense, 23, 253-264.

Bonini, L., Toscani, G., and Seno, S., 2014. Three-dimensional segmentation and different rupture behavior during the 2012 Emilia seismic sequence (Northern Italy): Tectonophysics, 630, 33-42.

Bondesan, M., Favero, V., and Viñals, M. J., 1995. New evidence on the evolution of the Po delta coastal plain during the Holocene: Quaternary International 29-30, 105-110.

Bown, T.M., and Kraus, M.J., 1987. Integration of channel and floodplain suites; I, Developmental sequence and lateral relations of alluvial Paleosols: Journal of Sedimentary Research, 57(4), 587-601. https://doi.org/10.1306/212F8BB1-2B24-11D7-8648000102C1865D.

Bronk Ramsey, C., and Lee, S., 2013. Recent and planned development of the program OxCal: Radiocarbon, 55, 720–730.

Bruno, L., Amorosi, A., Severi, P., and Costagli, B., 2017a. Late Quaternary aggradation rates and stratigraphic architecture of the southern Po Plain, Italy: Basin Research. https://doi 10.1111/bre.12174.

Bruno, L., Bohacs, K. M., Campo, B., Drexler, T. M., Rossi, V., Sammartino, I., and Amorosi, A., 2017b. Early Holocene transgressive paleogeography in the Po coastal plain (Northern Italy): Sedimentology, 64(7), 1792–1816. https://doi: 10.1111/sed.12374.

Bruno, L., Campo, B., Di Martino, A., Hong, W., and Alessandro, A. 2019. Peat layer accumulation and post-burial deformation during the mid-late Holocene in the Po coastal plain (Northern Italy): Basin Research. https://doi 10.1111/bre.12339.

Burrato, P., Ciucci, F., and Valensise, G., 2003. An inventory of river anomalies in the Po Plain, Northern Italy: Evidence for active blind thrust faulting: Annals of Geophysics 46, 865–882.

Campo, B., Amorosi, A., and Bruno, L., 2016. Contrasting alluvial architecture of Late Pleistocene and Holocene deposits along a 120-km transect from the central Po Plain (northern Italy): Sedimentary Geology 341, 265-275. https://doi 10.1016/j.sedgeo.2016.04.013.

Campo, B., Amorosi, A., VAiani, S.C., 2017. Sequence stratigraphy and late Quaternary paleoenvironmental evolution of the Northern Adriatic coastal plain (Italy): Paleogeography, Paleoclimatology, Paleoecology 466, 265-278.

Caputo, R., Iordanidou, K., Minarelli, L., Papathanassiou, G., Poli, M.E., Rapti-Caputo, D., Sboras, S., Stefani, M., and Zanferrari, A., 2012. Geological evidence of pre-2012 seismic events, Emilia-Romagna, Italy: Annals of Geopgysics 55, 743-749.

Caputo, R., Pellegrinelli, A., Bignami, C., Bondesan, A., Mantovani, A., Stramondo, S., and Russo, P., 2015. High-precision levelling, DInSAR and geomorphological effects in the Emilia 2012 epicentral area: Geomorphology, 235, 106–117. https://doi.org/10.1016/j. geomorph.2015.02.002.

Carannante, S., Argnani, A., Massa, M., D'Alema, E., Lovati, S., Moretti, M., and Augliera, P., 2015. The May 20 (MW 6.1) and 29 (MW 6.0), 2012, Emilia (Po Plain, northern Italy) earthquakes: New seismotectonic implications from subsurface geology and highquality hypocenter location: Tectonophysics, 655, 107–123. https://doi.org/10.1016/j.tecto.2015.05.015.

Carminati, E., Doglioni, C., and Scrocca, D., 2005. Magnitude and causes of long-term subsidence of the Po Plain and the Venetian region, in C.A. Fletcher, and T. Spencer, eds., with J. Da Mosto and P. Campostrini, Flooding and Environmental changes for Venice and its Lagoon: State of Knowledge, Cambridge University Press, p. 23-28.

Carminati, E. and Vadacca, L., 2010. Two- and three-dimensional numerical simulations of the stress field at the thrust front of the Northern Apennines, Italy: Journal of Geophysical Research. https://doi 10.1029/2002GC000481.

Carminati, E., and Doglioni, C., 2012. Alps vs. Apennines: The paradigm of a tectonically asymmetric Earth: Earth-Science Reviews, 112(1-2), 67-96.

Castellarin, A., 2001. Alps-Apennines and Po Plain-frontal Apennines relations.Anatomy of an Orogen: the Apennines and Adjacent Mediterranean Basins, 13, 177-195.

Castellarin, A., Eva, C., Giglia, G., Vai, G.B., Rabbi, E., Pini, G.A., and Crestana, G., 1985. Analisi strutturale del Fronte Appenninico Padano: Giornale di Geologia 47, 47-75.

Castellarin, A., Cantelli, L., Fesce, A.M., Mercier, J.L., Picotti, V., Pin, G.A., Prosser, G., and Selli, L., 1992. Alpine compressional tectonics in the Southern Alps. Relationships with the N-Apennines: Annales Tectoncae, 6(1), 62-94.

Castellarin, A., Eva, C., and Capozzi, R., 1994. Tomografie sismiche e interpretazione geologica profonda dell'Appennino Settentrionale Nord-occidentale: Studi geologici Camerti, Volume Speciale 1992/2, 85-98.

Cattaneo, A., and Trincardi, F., 1999. The Late Quaternary transgressive record in the Adriatic Epicontinental sea: Basin widening and facies partitioning: Society for Sedimentary Geology, 127-146.

Cattaneo, A., Correggiari, A., Langone, L., and Trincardi, F., 2003. The late-Holocene Gargano subaqueous delta, Adriatic shelf: Sediment pathways and supply fluctuations: Marine Geology, 193 (1–2), 61-91.

Cattaneo, A., Trincardi, F., Asioli, A., and Correggiari, A., 2007. The Western Adriatic shelf clinoform: energy-limited bottomset: Continental Shelf Research, 27(3-4), 506-525. https://doi.org/10.1016/j.csr.2006.11.013.

Chamberlain, E.L., Törnqvist, T. E., Shen, Z., Mauz, B., Wallinga, J., 2018. Anatomy of Mississippi Delta growth and its implications for coastal restoration: Science Advances, 4(4). https://doi: 10.1126/sciadv.aar4740.

Chiarabba, C., De Gori, P., Improta, L., Lucente, F.P., Moretti, M., Govoni, A., Di Bona, M., Margheriti, L., Marchetti, A., and Nardi, A., 2014. Frontal compression along the Apennines thrust

system: The Emilia 2012 example from seismicity to crustal structure: Journal of Geodynamics, 82, 98-109.

Cohen, K. M., Stouthamer, E., and Berendsen, H. J. A., 2002. Fluvial deposits as a record for Late Quaternary neotectonic activity in the Rhine-Meuse delta, the Netherlands: Netherlands Journal of Geosciences - Geologie en Mijnbouw, 81(3–4), 389–405. https://doi.org/10.1017/S0016774600022678.

Cohen, K. M., Gouw, M. J. P., and Holten, J. P., 2003. Fluvio-deltaic floodbasin deposits recording differential subsidence within a coastal prism (Central Rhine-Meuse Delta, the Netherlands), In M. D. Blum, S. B. Marriott, & S. F. Leclair (Eds), Fluvial sedimentology VII. Special Publication 35, International Association of Sedimentologists. Cambridge, MA: Blackwell Scientific.

Correggiari, A., Roveri, M., Trincardi, F., 1992. Regressioni «forzate», regressioni «deposizionali» e fenomeni di instabilità 1n unità progradazionali tardo-quaternarie (Adriatico centrale). Giornale di Geologia, 54(1), 19-36.

Correggiari, A., Trincardi, F., Langone, L., and Roveri, M., 2001. Styles of failure in late Holocene highstand prodelta wedges on the Adriatic shelf: Journal of Sedimentary Research, 71(2), 218-236.

Correggiari, A., Cattaneo, A., and Trincardi, F., 2005a. Depositional patterns in the Late-Holocene Po delta system. In J. P. Bhattacharya, and L. Giosan (Eds.), River deltas-concepts, models and examples, Society for Sedimentary Geology, Special Publications 83, 365–392.

Correggiari, A., Cattaneo, A., and Trincardi, F., 2005b. The modern Po Delta system: Lobe switching and asymmetric prodelta growth: Marine Geology, 222, 49–74. https://doi.org/10.1016/j.margeo.2005.06.039.

Cremonini, G., and Ricci Lucchi, F., 1982. Guida alla Geologia del margine appenninicopadano: Società Geologica Italiana, Guide geologiche regionali, Pitagora Tecnoprint, Bologna.

Curzi, P. V., Dinelli, E., Ricci Lucchi, M., and Vaiani, S. C., 2006. Palaeoenvironmental control on sediment composition and provenance in the late Quaternary deltaic successions: A case study from the Po delta area (Northern Italy): Geological Journal, 41, 591–612. https://doi.org/10.1002/gj.1060.

Demarest, I.I.J.M. and Kraft, J.C., 1987. Stratigraphic record of Quaternary sea levels: implications formore ancient strata, in D. Nummedal, O.H. Pilkey and J.D. Howard (eds.), Sea-Level Fluctuation and Coastal Evolution: Society for Sedimentary Geology, Special Publication, 41, 223-239.

Doglioni, C., 1993. Some remarks on the origin of foredeeps: Tectonophysics 228, 1-20.

Doglioni, C., Harabaglia, P., Merlini, S., Mongelli, F., Peccerillo, A., and Piromallo, C., 1999, Orogens and slab vs their direction of subduction: Earth Science Reviews, 45, 167-208.

Dondi, L., and D'Andrea, M.G., 1986. La Pianura Padana e Veneta dall'Oligocene superiore al Pleistocene: Giornale di geologia, 48(01-02), 197-225.

Eppes, M.C., Bierma, R., Vinson, D., and Pazzaglia, F., 2008. A soil chronosequence study of the Reno valley, Italy: Insights into the relative role of climate versus anthropogenic forcing on hillslope processes during the mid-Holocene: Geoderma, 147, 97-107.

Feng, Z.D., and Wang, H.B., 2005. Pedostratigraphy and carbonate accumulation in the last interglacial pedocomplex of the Chinese Loess Plateau: Soil Science Society of America Journal, 69 (4), 1094–1101. https://doi: 10 .2136 /sssaj2004 .0078.

Ferranti, L., Antonioli, F., Mauz, B., Amorosi, A., Dai Pra, G., Mastronuzzi, G., Monaco, C., Orru, P., Pappalardo, M., Radtke, U., Renda, P., Romano, P., Sansò, P., and Verrubbi, V., 2006. Markers of the last interglacial sea-level high stand along the coast of Italy: Tectonic implications: Quaternary International, 145–146, 30–54. https://doi.org/10.1016/j.quaint.2005.07.009.

Fiorini, F., 2004. Benthic foraminiferal associations from Upper Quaternary deposits of southeastern Po Plain, Italy: Micropaleontology 50, 45-58.

Gambolati, G., Giunta, G. and Teatini, P., 1998. Numerical modeling of natural land subsidence over sedimentary basins undergoing large compaction, in: Gambolati, G. (Ed.), CENAS - Coastiline Evolution of the Upper Adriatic Sea due to Sea Level Rise and Natural and Anthropogenic Land Subsidence: Klwer Acedemic Publ., 28(4), 77–102.

Gasperi, G., Gelati, R., and Papani, G., 1986. Neogene evolution of the Northern Apennines on the Po Valley side: Giornale di geologia, 48(01-02), 187-195.

Govoni, A., Marchetti, A., De Gori, P., Di Bona, M., Lucente, F.P., Improta, L., Chiarabba, C., Nardi, A., Margheriti, L., Piana Agostinetti, N., Di Giovambattista, R., Latorre, D., Anselmi, M., Ciaccio M.G., Moretti, M., Castellano, C., and Piccinini, D., 2014. The 2012 Emilia seismic sequence (Northern Italy): Imaging the thrust fault system by accurate aftershock location: Tectonophysics, 622, 44-55.

Greggio, N., Giambastiani, B. M. S., Campo, B., Dinelli, E., and Amorosi, A., 2018. Sediment composition, provenance and Holocene paleoenvironmental evolution of the Southern Po River coastal plain (Italy): Geological Journal, 53, 914–928. https://doi.org/10.1002/gj.2934.

Hijma, M., Engelhart, S.E., Tornqvist, T.E., Horton, B.P., Hu, P. and Hill, D., 2015. A protocol for a Geological Sea-level Database, in: Shennan, I., Long, A. and Horton, B.P. (Eds.), Handbook of Sea Level Research: Wiley, 536–553. https://doi:10.1002/9781118452547.ch34.

Hoang, T.M., van Lap, N., Oanh, T.T.K., and Takemura, J., 2016. The influence of delta formation mechanism on geotechnical property sequence of the late Pleistocene–Holocene sediments in the Mekong River Delta: Heliyon, 2(11). https://doi.org/10.1016/j.heliyon.2016.e00165

Hori, K., Saito, Y., Zhao, Q., and Wang, P., 2002. Evolution of the coastal depositional systems of the Changjiang (Yangtze) River in response to late Pleistocene-Holocene sea-level changes: Journal of Sedimentary Research, 72, 884–897.

Iside Working Group, 2010. Italian seismological instrumental and parametric database. Retrieved from http://iside.rm.ingv.it.

Landva, A. 2006. Characterization of Escuminac peat and construction on peatland, in: Tan, T.S., Phoon, K.K. et al. (eds) Second International Workshop on Characterisation and Engineering Properties of Natural Soils, 3: Taylor & Francis, Oxford, 2135–2192.

Lowrie, A., and Hamiter, R., 1995. Fifth and Sixth Order Eustatic Events During Holocene (Fourth Order) Highstand Influencing Mississippi Delta-Lobe Switching. Journal of Coastal Research, 1, 225-229.

Kamola, D.L., and Van Wagoner, J.C., 1995. Stratigraphy and facies architecture of parasequences with examples from the Spring Canyon Maber, Blackhawk Formation, Utah, in J.C. Van Wagoner and G.T. Bertram, eds., Sequence Stratigraphy Foreland Basin Deposits: American Association of Petroleum Geologists Memoirs, 64, 27-54.

Kearey, P., and Vine, F.J., 1990. Geoscience Texts: Global Tectonics.

Kemp, R.A., Derbyshire, E., Xingmin, M., Fahu, C., and Baotian, P., 1995. Pedosedimentary reconstruction of a thick loess–palaeosol sequence near Lanhzou in North-Central China: Quaternary Research, 43, 30-45.

Kemp, R.A., Zárate, M., Toms, P., King, M., Sanabria, J., and Arguello, G., 2006. Late Quaternary paleosols, stratigraphy and landscape evolution in the northern Pampa, Argentina: Quaternary Research, 66(1), 119–132. https://doi: 10 .1016 /j .yqres .2006 .01 .001.

Koster, K., De Lange, G., Harting, R., De Heer, E., and Middelkoop, H., 2018a. Characterization void ratio and compressibility oh Holocene peat with CPT for assessing coastal-deltaic subsidence: Quarterly Journal of Engineering Geology and Hydrogeology, 51, 210-218. https://doi.org/10.1144/qjegh2017-120.

Koster, K., Stafleu, J., Cohen, K.M., Stouthemer, E., Busschers, F.S., and Middelkoop, H., 2018b. Three-dimensional distribution of organic matter in coastal-deltaic peat: Implications for subsidence and carbon dioxide emissions by human-induced peat oxidation: Anthropocene 22, 1-9. https://doi.org/10.1016/j.ancene.2018.03.001.

Kraus, M.J., 1999. Paleosols in clastic sedimentary rocks: Their geologic applications: Earth-Science Reviews, 47(1–2), 41–70. https://doi: 10 .1016 /S0012 -8252 (99)00026 -4.

Mahaney, W.C., Andres, W., and Barendregt, R.W., 1993. Quaternary paleosol stratigraphy and paleomagnetic record near Dreihausen, central Germany: Catena, 20(1–2), 161–177. https://doi: 10.1016 /0341 -8162 (93)90035 -N.

Marcucci, D.J., 2000. Landscape history as a planning tool: Landscape and Urban Planning, 49, 67-81. https://doi.org/10.1016/S0169-2046(00)00054-2.

Maselli, V., Trincardi, F., Cattaneo, A., Ridente, D., and Asioli, A., 2010. Subsidence pattern in the central Adriatic and its influence on sediment architecture during the last 400 kyr. Journal of Geophiysical Research, 115. https://doi.org/10.1029/2010JB007687.

Maselli, V., Hutton, E.W., Kettner, A.J., Syvitski, J.P.M., and Trincardi, F., 2011. High-frequency sea level and sediment supply fluctuations during Termination I: An integrated sequence-stratigraphy and modeling approach from the Adriatic Sea (central Mediterranean): Marine Geology, 287(1–4), 54–70. https://doi: 10 .1016 /j.margeo .2011 .06 .012.

Maselli, V., and Trincardi, F., 2013. Man made deltas: Scientific Reports, 3, 1–7. https://doi.org/10.1038/srep01926.

Marchesini, L., Amorosi, A., Cibin, U., Zuffa, G. G., Spadafora, E., and Preti, D., 2000. Sand composition and sedimentary evolution of a Late Quaternary depositional sequence, northwestern Adriatic Coast, Italy: Journal of Sedimentary Research, 70, 829–838.

Mazzoli, S., Santini, S., Macchiavelli, C., and Ascione, A., 2015. Active tectonics of the outer northern Apennines: Adriatic vs Po Plain seismicity and stress fields: Journal of Geodynamics 84, 62-76.

Milli, S, D'Ambrogi, C., Bellotti, P., Calderoni, G., Carboni, M.G., Celant, A., Di Bella, L., Di Rita, F., Frezza, V., Magri, D., Pichezzi, R.M., Ricci, V., 2013. The transition from wave-dominated estuary to wave-dominates delta: The Late Quaternary stratigraphic architecture of Tiber River deltaic succession (Italy): Sedimentary Geology, 284-285, 159-180. https://doi.org/10.1016/j.sedgeo.2012.12.003.

Milli, S., Mancini, M., Moscatelli, M., Stigliano, F., Mattia, M., Cavinato, G.P., 2016. From river to shelf, anatomy of a high-frequency depositional sequence: The Late Pleistocene to Holocene Tiber depositional sequence: Sedimentology, 63, 1886-1928. http://doi: 10.1111/sed.12277.

Molinari, F.C., Boldrini, G., Severi, P., Dugoni, G., Rapti Caputo, D., and Martinelli, G., 2007. Risorse idriche sotterranee della Provincia di Ferrara, in G. Dugoni and Pignone R. (eds.): Risorse idriche sotterranee della Provincia di Ferrara, 7-61.

Morelli, A., Bruno, L., Cleveland, D.M., Drexler, T.M., and Amorosi, A., 2017. Reconstructing Last Glacial Maximum and Younger Dryas paleolandscapes through subsurface paleosol stratigraphy: An example from the Po coastal plain, Italy: Geomorphology, 295, 790–800.

Morrison, R.B., 1976. Quaternary soil stratigraphy - concepts, methods, and problems, in Mahaney, W.C., ed., Quaternary soils: 3rd Symposium on Quaternary Research, York University: Geoabstracts, Norwich, 77-108.

Morton, R.A., and Suter, J.R., 1996. Sequence stratigraphy and composition of Late Quaternary shelf-margin deltas, northern Gulf of Mexico: American Association of Petroleum Geologists Bulletin, 80, 505-530.

Muttoni, G., Carcano, C., Garzanti, E., Ghielmi, M., Piccin, A., Pini, R., Rogledi, S., and Sciunnach, D., 2003. Onset of major Pleistocene glaciations in the Alps: Geology, 31, 989–992. https://doi.org/10.1130/G19445.1.

Nummedal, D. and Swift, D.J.P., 1987. Transgressive stratigraphy at sequence-bounding unconformities: some principles derived from Holocene and Cretaceous examples, in D. Nummedal, O.H. Pilkey and J.D. Howard, eds., Sea-Level Fluctuation and Coastal Evolution: Society of Sedimentary Geology, Special Publication, 41, 241-260.

Ori, G.G., 1993. Continental depositional systems of the Quaternary of the Po Plain (northern Italy): Sedimentary Geology 83, 1-14.

Pellegrini, C., Maselli, V., Cattaneo, A., Piva, A., Ceregato, A. and Trincardi, F., 2015. Anatomy of a compound delta from the post-glacial transgressive record in the Adriatic Sea: Marine Geology, 362, 43–59.

Pellegrini, C., Maselli, V., and Trincardi, F., 2016. Pliocene–Quaternary contourite depositional system along the south-western Adriatic margin: changes in sedimentary stacking pattern and associated bottom currents: Geo-Marine Letters, 36(1), 67-79.

Pellegrini, C., Maselli, V., Gamberi, F., Asioli, A., Bohacs, K. M., Drexler, T. M., and Trincardi, F., 2017. How to make a 350-m-thick lowstand systems tract in 17,000 years: The Late Pleistocene Po River (Italy) lowstand wedge: Geology, 45, 327–330. https://doi. org/10.1130/g38848.1.

Pellegrini, C., Asioli, A., Bohacs, K. B., Drexler, T. M., Feldman, H. R., Sweet, M. L., and Trincardi, F., 2018. The late Pleistocene Po River lowstand wedge in the Adriatic Sea: Control on architecture variability and sediment partitioning: Marine and Petroleum Geology, 96, 16–50. https://doi.org/10.1016/j.marpetgeo.2018.03.002

Picotti, V., and Pazzaglia, F.J., 2008. A new active tectonic model for the construction of the Northern Apennines mountain front near Bologna (Italy): Journal of Geophysical Research: Solid Earth 113. https://doi 10.1029/2007JB005307.

Picotti, V., Ponza, A., and Pazzaglia, F.J., 2009. Topographic expression of active faults in the foothills of the Northern Apennines: Tectonophysics, 474(1-2), 285-294.

Pieri, M., and G. Groppi, 1975. The structure of the base of the Pliocene-Quaternary sequence in the subsurface of the Po and Veneto Plains, the Pedeapennine Basin and the Adriatic Sea: Quad. Ric. Sci., 90, 409–415.

Pieri, M., and Groppi, G., 1981. Subsurface geological structure of the Po Plain, Italy: Progetto Finalizzato Geodinamica, CNR Pubblication, 414, pp. 23.

Pini, G.A., 1999. Tectonosomes and olistostromes in the argille scagliose of the Northern Apennines, Italy: The Geological Society of America, Special Paper, 335.

Pini, R., Carcano, C., Garzanti, E., Ghielmi, E., Muttoni, G., Piccin, A., Rogledi, S., and Sciunnach, D., 2004. Stratigraphic evidence for a major climate change during MIS2: the Pianego core (Po Plain, Northern Italy): 32nd International Geological Congress, Firenze, 1, 392.

Posamentier, H.W., and Allen, HG.WP., 1999. Siliciclastic sequence stratigraphy-concepts and applications: SEPM Concepts in Sedimentology and Paleontology 7 (7). https://doi.org/10.2110/csp.99.07.

Proskea, U., Hanebuth, T. J.J., Gröger, J., and PhátDiệm, B., 2011. Late Holocene sedimentary and environmental development of the northern Mekong River Delta, Vietnam: Quaternary International, 230, 57-66.

Regione Emilia-Romagna & ENI-AGIP, 1998. Riserve idriche sotterranee della Regione Emilia-Romagna. A cura di G. Di Dio. Selca, Firenze.

Regione Lombardia & ENI DIVISIONE AGIP, 2002. Geologia degli acquiferi Padani della Regione Lombardia. Selca, Firenze.

Reimer, P. J., Bard, E., Bayliss, A., Beck, J. W., Blackwell, P. G., Ramsey, C. B., Buck, C.E., Cheng, H., Edwards, R.L., Friedrich, M., Grootes, P.M., Guilderson, T.P., Haflidason, H., Hajdas, I., Hatté, C., Heaton, T.J., Hoffmann, D.L., Hogg, A.G., Hughen, K.A., Kaiser, K.F., Kromer, B., Manning, S.W., Niu, M., Reimer, R.W., Richards, D.A., Scott, E.M., Southon, J.R., Staff, R.A., Turney, C.S.M., and van der Plicht, J. (2013). IntCal13 and Marine13 radiocarbon age calibration curves, 0–50,000 years cal BP. Radiocarbon, 55, 1869–1887. https://doi.org/10.2458/azu_js_rc.55.16947.

Ricci Lucchi, F., Colella, A., Ori, G.G., Ogliani, F., and Colalongo, M.L., 1981. Pliocene fan deltas of the Intra-Apenninic basin, Bologna: International Association of Sedimentologists, 2nd European Regional Meeting, Excursion Guidebook, 81-164 .

Ricci Lucchi, F., Colalongo, M.L., Cremonini, G., Gasperi, G., Iaccarino, G., Papani, G., Raffi, S., and Rio, D., 1982. Evoluzione sedimentaria e paleogeografica nel margine appenninico, in:

Cremonini, G., and Ricci Lucchi, F., (Eds.), Guida alla Geologia del margine appenninico-padano: Guide Geologiche Regionali della Società Geologica Italiana, 17-46.

Ricci Lucchi, F., 1986. Oligocene to recent foreland basins of Northern Apennines, in Allen, P., and Homewood, P. (eds.), Foreland Basins: International Association of Sedimentologists Special Publication 8, 105–139. https://doi: 10 .1002 /9781444303810.ch6.

Ridente, D., and Trincardi, F., 2002. Eustatic and tectonic control on deposition and lateral variability of Quaternary regressive sequences in the Adriatic basin (Italy). Marine Geology, 184(3), 273-293.

Ridente, D., and Trincardi, F., 2005. Pleistocene "muddy" forced-regression deposits on the Adriatic shelf: A comparison with prodelta deposits of the late Holocene highstand mud wedge: Marine Geology, 222-223, 213-233.

Ridente, D., and Trincardi, F., 2006. Active foreland deformation evidenced by shallow folds and faults affecting late Quaternary shelf-slope deposits (Adriatic Sea, Italy): Basin Research, 18(2), 171-188.

Ridente, D., Trincardi, F., Piva, A., Asioli, A., and Cattaneo, A., 2008. Sedimentary response to climate and sea level changes during the past ~400 ka from borehole PRAD1–2 (Adriatic margin): Geochemistry, Geophysics, Geosystems, 9 (9). https://doi:10.1029/2007GC001783.

Ridente, D., Trincardi, F., Piva, A., and Asioli, A., 2009. The combined effect of sea level and supply during Milankovitch cyclicity: Evidence from shallow-marine $\delta^{18}O$ records and sequence architecture (Adriatic margin): Geology, 37(11), 1003-1006. https://doi.org/10.1130/G25730A.1.

Rizzini, A., 1974. Holocene sedimentary cycle and heavy mineral distribution, Romagna–Marche coastal plain, Italy: Sedimentary Geology 11, 17-37.

Roveri M., Correggiari A., Asioli A., and Trincardi F., 2001. Ultra high-resolution marine record of paleoenvironmental changes in the last 5000 years: Archivio di Oceanografia e Limnologia, 22, 223-234.

Rovida, A., Camassi, R., Gasperini, P., and Stucchi, M., 2011. Version of the Parametric Catalogue of Italian Earthquakes, Milano, Bologna. Retrieved from http://emidius.mi.ingv.it/CPTI/.

Saito, Y., Katayama, H., Ikehara, K., Kato, Y., Matsumoto, E., Oguri, K., Oda, M., and Yumoto, M., 1998. Transgressive and highstand systems tracts and post-glacial transgression, the East China sea: Sedimentary Geology 122, 217–232.

Salvi, S., Tolomei, C., Merryman Boncori, J. P., Pezzo, G., Atzori, S., Antonioli, A., Trasatti, E., Merryman Boncori, J.P., Pezzo, G., Coletta, A., and Zoffoli, S., 2012. Activation of the SIGRIS monitoring system for ground deformation mapping during the Emilia 2012 seismic sequence, using COSMO-SkyMed InSAR data. Annales Geophysicae, 55(4), 796–802.

Scarponi, D., Kowalewski, M., 2004. Stratigraphic paleoecology: Bathymetric signatures and sequence overprint of mollusk associations from upper Quaternary sequences of the Po Plain, Italy: Geology 32(11), 989-992. https://doi.org/10.1130/G20808.1.

Scarponi, D., Kaufman, D., Amorosi, A. and Kowalewski, M., 2013. Sequence stratigraphy and the resolution of the fossil record: Geology, 41, 239–242.

Serpelloni, E., Vannucci, G., Pondrelli, S., Argnani, A., Casula, G., Anzidei, M., Baldi, P., and Gasperini, P., 2007. Kinematics of the Western Africa-Eurasia plate boundary from focal mechanism and GPS data: Geophysical Journal International 169, 1180-1200.

Sheldon, N.D., and Tabor, N.J., 2009. Quantitative paleoenvironmental and paleoclimatic reconstruction using paleosols: Earth-Science Reviews, 95, 1–52. https://doi:10 .1016 /j .earscirev.2009.03 .004.

Schellenberger, A., and Veit, H., 2006. Pedostratigraphy and pedological and geochemical characterization of Las Carreras loess-paleosol sequence, Valle de Tafí, NW-Argentina: Quaternary Science Reviews, 25(7–8), 811–831 https://doi: 10 .1016 /j .quascirev .2005 .07.011.

Scardia, G., Muttoni, G., and Sciunnach, D., 2006. Subsurface magnetostratigraphy of Pleistocene sediments from the Po Plain (Italy): Constraints on rates of sedimentation and rock uplift: Geological Society of America Bulletin, 118(11–12), 1299–1312. https://doi: 10.1130 /B25869 .1.

Somoza, L., Barnolas, A., Arasa, A., Maestro, A., Rees, J. G., and Hernandez-Molina, F. J., 1998. Architectural stacking patterns of the Ebro delta controlled by Holocene high-frequency eustatic fluctuations, delta-lobe switching and subsidence processes: Sedimentary Geology, 117, 11–32.

Srivastava, P., Rajak, M.K., Sinha, R., Pal, D.K., and Bhattacharyya, T., 2010. A high-resolution micromorphological record of the late Quaternary paleosols from Ganga-Yamuna interfluve: Stratigraphic and paleoclimatic implications: Quaternary International, 227(2), 127–142. https://doi: 10 .1016 /j .quaint .2010 .02 .019.

Stanley, D.J., and Warne, A.G., 1994. Worldwide Initiation of Holocene Marine Deltas by Deceleration of Sea-Level Rise: Science, 265, 228-231. https://doi: 10.1126/science.265.5169.22.

Stefani, M., and Vincenzi, S., 2005. The interplay of eustasy, climate and human activity in the late Quaternary depositional evolution and sedimentary architecture of the Po Delta system: Marine Geology, 222–223, 19–48. https://doi.org/10.1016/j.margeo.2005.06.029.

Stouthamer, E., Cohen, K.M., and Gouw, M.J.P., 2011. Avulsion and its Impactions for Fluvial-Deltaic Architecture: Insights from the Holocene Rhine-Meuse Delta: Society of Sedimentary Geology 978-1, 215-231.

Styllas, M., 2014. A simple approach for defining Holocene sequence stratigraphy using borehole and cone penetration test data: Sedimentology 61, 444-460.

Tamura, T., Saito, Y., Sieng, S., Ben, B., Kong, M., Sim, I., Choup, S., and Akiba, F., 2009. Initiation of Mekong Riverdelta at 8 ka: evidence from the sedimentary succession in the Cambodian lowland: Quaternary Science Reviews, 28, 327-344.

Tamura, T., Saito, Y., Nguyen, V.L., Oanh Ta, T.K., Bateman, M.D., Matsumoto, D., and Yamashita, S., 2012. Origin evolution of interdistributary delta plains; insights from Mekong River delta: Geology, 40, 303-306.

Tanabe, S., Hori, K., Saito, Y., Haruyama, S., Vu, V.P., and Kitamura, A., 2003. Song Hong (Red River) delta evolution related to millennium-scale Holocene sea-level change: Quaternary Science Reviews 22, 2345-2361.

Tjallingii R., Stattegger, K., Wetzel, A., and Phach, P.V., 2010. Infilling and flooding of Mekong River incised valley during deglacial sea-level rise: Quaternary Science Reviews 29, 1432-1444.

Trendell, A.M., Atchley, S.C., and Nordt, L.C., 2012. Depositional and diagenetic controls on reservoir attributes within a fluvial outcrop analog: Upper Triassic Sonsela member of the Chinle Formation, Petrified Forest National Park, Arizona: American Association of Petroleum Geologists Bulletin, 96 (4), 679–707. https://doi:10 .1306 /08101111025.

Törnqvist, T. E., Bick, S. J., van der Borg, K., and de Jong, A. F. M., 2006. How stable is the Mississippi Delta?: Geology, 34, 697–700.

Törnqvist, T. E., Wallace, D. J., Storms, J. E., Wallinga, J., van Dam, R. L., Blaauw, M., and Snijders, E. M., 2008. Mississippi Delta subsidence primarily caused by compaction of Holocene strata: Nature Geoscience, 1, 173–176.

Trincardi, F., and Field, M.E., 1991. Geometry, lateral variation, and preservation of downlapping regressive shelf deposits; eastern Tyrrhenian Sea margin, Italy: Journal of Sedimentary Researc, 61 (5), 775-790. https://doi.org/10.1306/D42677D0-2B26-11D7-8648000102C1865D.

Trincardi, F., and Correggiari A., 2000. Quaternary forced regression deposits in the Adriatic basin and the record of composite sea-level cycles: Special Publication-Geological Society of London, 172, 245-270.

Trincardi, F., Correggiari, A., and Roveri, M., 1994. Late Quaternary transgressive erosion and deposition in a modern epicontinental shelf: The Adriatic semienclosed basin: Geo-Marine Letters, 14(1), 41-51.

Trincardi, F., Cattaneo, A., Asioli, A., Correggiari, A., and Langone, L., 1996. Stratigraphy of the Late-Quaternary deposits in the central Adriatic basin and the record of short term climatic events: Memorie Dell'istituto Italiano Di Idrobiologia, 55, 39–70.

Trincardi, F., Cattaneo, A., and Correggiari, A., 2004. Mediterranean prodelta systems: Natural evolution and human impact investigated by EURODELTA: Oceanography 17(4), 34–45. https://doi.org/10.5670/oceanog.2004.02.

Tsatskin, A., Sandler, A., and Avnaim-Katav, S., 2015. Quaternary subsurface paleosols in Haifa Bay, Israel: A new perspective on stratigraphic correlations in coastal settings: Palaeogeography, Palaeoclimatology, Palaeoecology 426, 285-296.

Ufnar, D.F., 2007. Clay coatings from a modern soil chronosequence: A tool for estimating the relative age of well-drained paleosols: Geoderma, 141(3-4), 181-200.

Vai, G.B., and Castellarin, A., 1992. Correlazione sinottica delle unità stratigrafiche nell'appennino settentrionale, in: "Studi preliminari all'acquisizione dati del profilo CROP 1-1A La Spezia-Alpi orientali": Studi Geologici Camerti, 2, 171-185.

Vai, G.B., and Martini, I.P., 2001. Anatomy of an orogen: the Apennines and adjacent Mediterranean basins: Kluwer Academic Publishers, Springer, 632, 1-4.

Van Asselen, S., 2011. The contribution of peat compaction to total basin subsidence: implications for the provision of accommodation space in organic-rich deltas: Basin Research 23, 239-255.

Van Asselen, S., and Roosendaal, C., 2009. A new method for determining the bulk density of uncompacted peat from field settings: Journal of Sedimentary Research 79, 918-922.

van Asselen, S., Stouthamer, E., and van Asch, T. W. J., 2009. Effects of peat compaction on delta evolution: A review on processes, responses, measuring and modeling: Earth-Science Reviews, 92, 35–51.

van Asselen, S., Erkens, G., Stouthamer, E., Woolderink, H. A. G., Geeraert, R. E. E., and Hefting, M. M., 2018. The relative contribution of peat compaction and oxidation to subsidence in builtup areas in the Rhine-Meuse delta, The Netherlands: Science of the Total Environment, 636, 177–191. https://doi.org/10.1016/j. scitotenv.2018.04.141

Van Wagoner, J.C., Mitchum, R.M., Campion, K.M., and Rahmanian, V.D., 1990. Siliciclastic sequence stratigraphy in well logs, cores and outcrops: concepts for high resolution correlations of time and facies: American Association of Petroleum Geologists, Tulsa, U.S.A, Methods in Exploration 7, 55 p.

Vannoli, P., Burrato, P., and Valensise, G., 2015. The seismotectonics of the Po Plain (northern Italy): tectonic diversity in a blind faulting domain: Pure and Applied Geophysics 172, 1105-1142.

Wallinga, J., Törnqvist, T.E., Busschers, F.S., and Weerts, H.J.T., 2004. Allogenic forcing of the late Quaternary Rhine-Meuse fluvial record: The interplay of sea-level change, climate change and crustal movements: Basin Research, 16(4), 535–547. https://doi: 10 .1111 /j .1365-2117 .2003 .00248 .x.

Wright, V.P., and Marriott, S.B., 1993. The sequence stratigraphy of fluvial depositional systems: The role of floodplain sediment storage: Sedimentary Geology, 86(3–4), 203–210. https://doi: 10.1016 /0037 -0738(93)90022 -W.

Zoccarato, C., Minderhoud, P.S.J., Teatini, P., 2018. The role of sedimentation and natural compaction in a prograding delta: insights from the mega Mekong delta, Vietnam: Scientific Reports 8. https://doi: 10 .1038 /s41598-018-29734-7.

Zhisheng, A., and Porter, S.C., 1997. Millennial-scale climatic oscillations during the last interglaciation in central China: Geology, 25(7), 603–606. https://doi:10 .1130 /0091 -7613 (1997)025 <0603: MSCODT>2 .3.CO;2.